Status of High-Momentum Transfer Form Factor Program at JLab and EIC

Prof. Andrew Puckett
University of Connecticut
EINN2023, Paphos, Cyprus
November 1, 2023

UCONN

Acknowledgements

- Supported by US DOE Office of Science, Office of Nuclear Physics, Award DE-SC0021200
- Additional support from Jefferson Lab and UConn
- SBS and Hall A Collaborations
- EINN 2023 organizers and hosts

Elastic Electron-Nucleon Scattering and Form Factors

- The Dirac (F_1) and Pauli (F_2) form factors describe the most general form of the virtual photon-nucleon vertex function consistent with the symmetries of QED; namely, Lorentz invariance, parity conservation and gauge invariance/current conservation
- They are real-valued functions of the (space-like) squared four-momentum transfer $q^2 = (k - k')^2 < 0$.
- Experimental observables sensitive to form factors include differential cross sections and double-spin asymmetries involving polarized e^- beams and/or targets

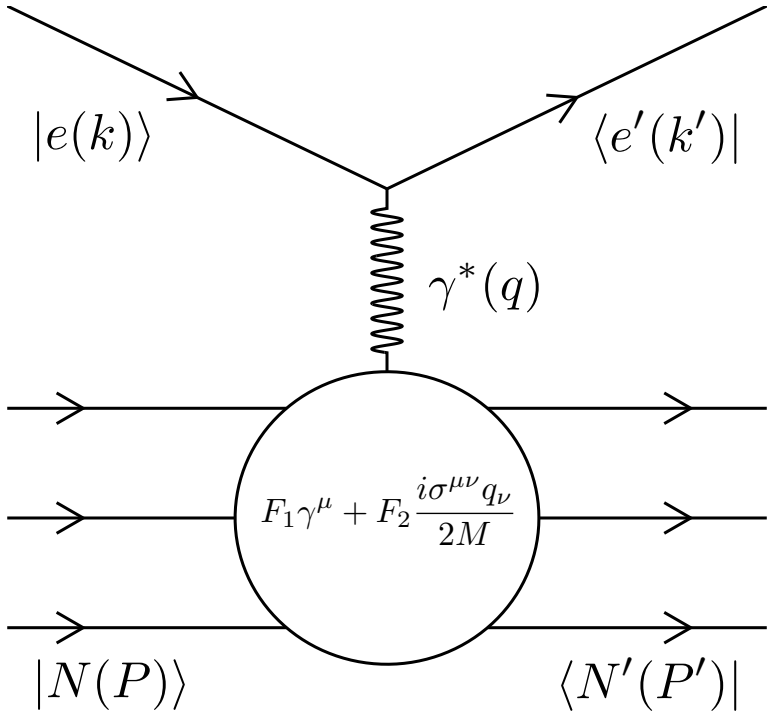

Feynman Diagram for elastic $eN \to eN$ scattering in OPE approximation

$$\text{Invariant amplitude: } \mathcal{M} = 4\pi\alpha\bar{u}(k')\gamma^\mu u(k)\left(\frac{g_{\mu\nu}}{q^2}\right)\bar{u}(P')\Gamma^\nu u(P)$$

$$\gamma^* N \text{ vertex function: } \Gamma^\mu = F_1(q^2)\gamma^\mu + \frac{i\sigma^{\mu\nu}q_\nu}{2M}F_2(q^2)$$

$$\text{Sachs FF: } G_E = F_1 - \tau F_2$$

$$G_M = F_1 + F_2$$

$$\text{Rosenbluth Formula: } \frac{d\sigma}{d\Omega_e} = \left(\frac{d\sigma}{d\Omega_e}\right)_{\text{Mott}} \frac{\epsilon G_E^2 + \tau G_M^2}{\epsilon(1+\tau)}$$

$$\tau \equiv \frac{Q^2}{4M^2}$$

$$\epsilon \equiv \left[1 + 2(1+\tau)\tan^2\left(\frac{\theta_e}{2}\right)\right]^{-1}$$

Proton Form Factors From Rosenbluth Separations

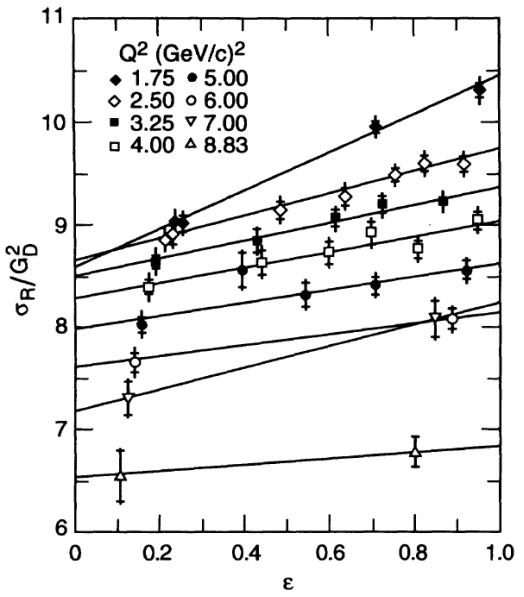

FIG. 22. Reduced cross sections divided by the square of the dipole fit plotted versus ϵ for each value of Q^2. The 1.6 GeV data points correspond to the leftmost point on each line, and the E136 data point is the rightmost point on the $Q^2 = 8.83$ (GeV/c)^2 line. The inner error bars show the statistical error, while the outer error bars show the total point-to-point uncertainty, given by the quadrature sum of the statistical and point-to-point systematic errors. An overall normalization uncertainty of ±1.77% has not been included.

NE11 L/T separations from Andivahis *et al.*, Phys. Rev. D 50, 5491 (1994)

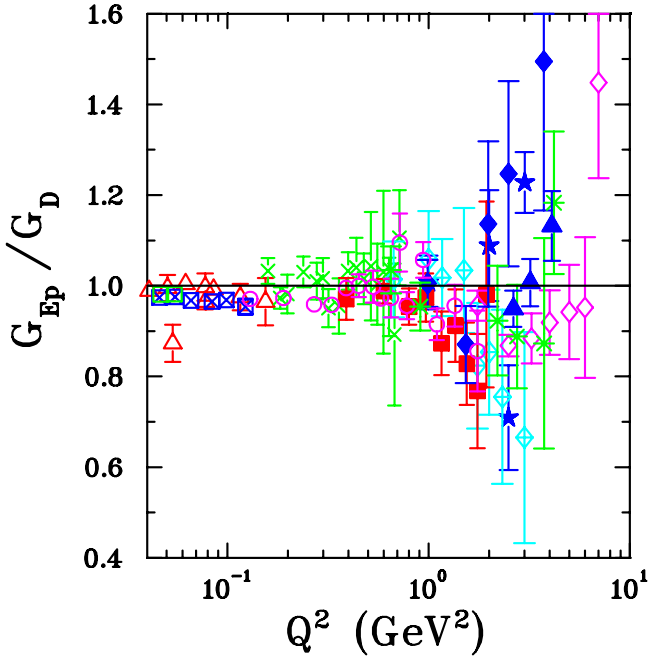

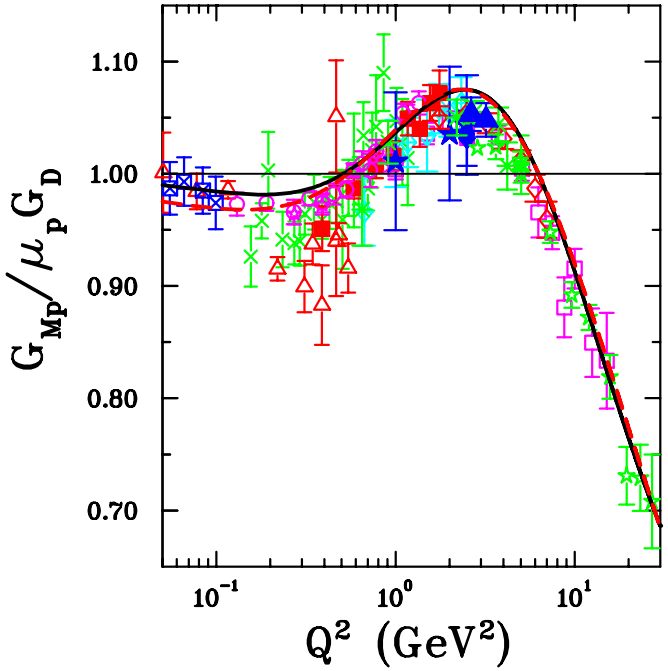

- **Above figures from Puckett *et al.* PRC 96, 055203 (2017)**
- Most proton electric and magnetic FF Rosenbluth extractions can be described to within ~10-20% over the entire measured Q^2 range by the so-called "dipole" form factor:

$$G_E^p \approx G_M^p/\mu_p \approx G_D \equiv \left(1+\frac{Q^2}{\Lambda^2}\right)^{-2}$$

$$\Lambda^2 = 0.71\ (\mathrm{GeV/c})^2$$

Polarization Observables in Elastic $eN \rightarrow eN$ Scattering

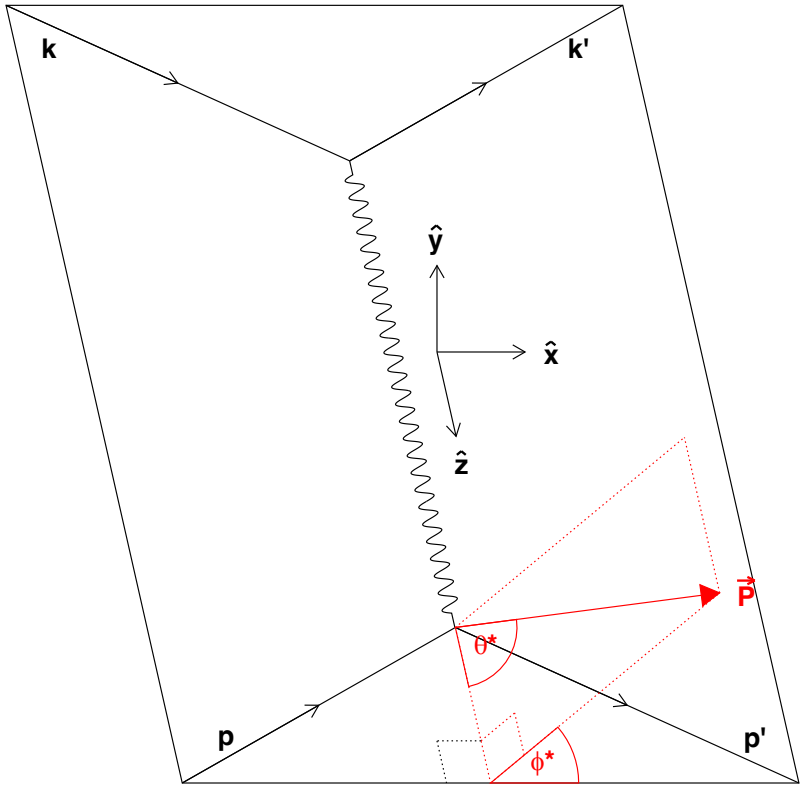

Standard coordinate system and angle definitions for nucleon polarization components in $eN \rightarrow eN$

$$A_{eN} \equiv \frac{\sigma_+ - \sigma_-}{\sigma_+ + \sigma_-} = P_{\text{beam}} P_{\text{targ}} \left[A_t \sin\theta^* \cos\phi^* + A_\ell \cos\theta^* \right]$$

$$A_t = -\sqrt{\frac{2\epsilon(1-\epsilon)}{\tau}} \frac{r}{1 + \frac{\epsilon}{\tau} r^2}$$

$$A_\ell = -\frac{\sqrt{1-\epsilon^2}}{1 + \frac{\epsilon}{\tau} r^2}$$

$$r \equiv \frac{G_E}{G_M}$$

$$P_t = P_{beam} A_t$$

$$P_\ell = -P_{beam} A_\ell$$

$$\frac{G_E}{G_M} = -\frac{P_t}{P_\ell} \sqrt{\frac{\tau(1+\epsilon)}{2\epsilon}} = -\frac{P_t}{P_\ell} \frac{E_e + E'_e}{2M} \tan\left(\frac{\theta_e}{2}\right)$$

- Polarized beam-polarized target double-spin asymmetry or polarization transfer observables in OPE are sensitive to the electric/magnetic form factor *ratio*, giving enhanced sensitivity to $G_E (G_M)$ for large (small) values of Q^2, as compared to the Rosenbluth method

Polarization Results for $\mu_p G_E^p / G_M^p$ and the 2017 Bonner Prize

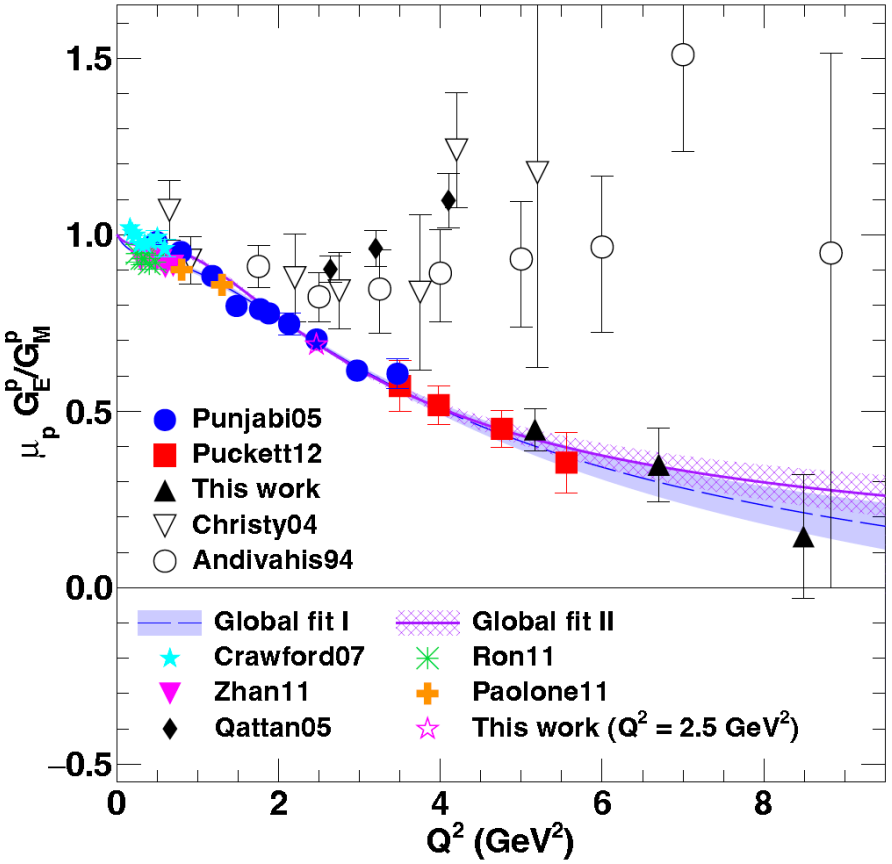

Figure from PRC 96, 055203 (2017)

References:

- GEp-I:
  - Jones, PRL 84, 1398 (2000)
  - Punjabi, PRC 71, 055202 (2005)
- GEp-II:
  - Gayou, PRL 88, 092301 (2002)
  - Puckett, PRC 85, 045203 (2012)
- GEp-III/GEp-2γ:
  - Puckett, PRL 104, 242301 (2010)
  - Meziane, PRL 106, 132501 (2011)
  - Puckett, PRC 96, 055203 (2017)

- (Arguably) most famous results in the history of JLab, inarguably among the most cited

APS physics

2017 Tom W. Bonner Prize in Nuclear Physics Recipient

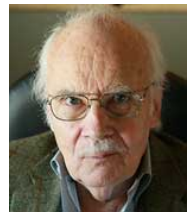

Charles F. Perdrisat
College of William and Mary

Citation:

"*For groundbreaking measurements of nucleon structure, and discovering the unexpected behavior of the magnetic and electric nucleon form factors with changing momentum transfer.*"

Background:

Charles F. Perdrisat, Ph.D., was a professor at the College of William and Mary (Williamsburg, Va.) for the last 50 years having retired earlier this year. Throughout his career, Dr. Perdrisat's research focus included nuclear reactions with proton and deuteron beams, both polarized and unpolarized. He conducted research at SATURNE in Saclay, France, TRIUMF in Vancouver, B.C., LAMPF in Los Alamos, New Mexico, Brookhaven National Laboratory in Upton, N.Y., and JINR in Dubna, Russia. During the last half of his career, he was committed to the investigation of the structure of the proton at Jefferson Laboratory, concentrating in obtaining polarization transfer data in the scattering of polarized electrons on unpolarized protons. These data, from 3 distinct experiments organized in close collaboration with Vina Punjabi, Ph.D., Mark K. Jones, Ph.D., Edward J. Brash, Ph.D., and Lubomir Pentchev, Ph.D., have resulted in a significant change of paradigm in the understanding of the structure of the nucleon. After completing his undergraduate training in physics and mathematics at the University of Geneva in 1956, Dr. Perdrisat became an assistant in the physics department at the Swiss Federal Institute of Technology in Zurich) in Switzerland, under Prof. Paul Scherrer; he received his Ph.D. in 1962. He completed a three-year postdoctoral fellowship at the University of Illinois Urbana-Champaign, before heading to William and Mary in 1966.

Selection Committee:

2017 Selection Committee Members: Rocco Schiavilla (Chair), D. Hertzog, P. Jacobs, Kate Jones, I-Y. Lee

Proton Form Factors World Data Summary: G_E^p and G_M^p

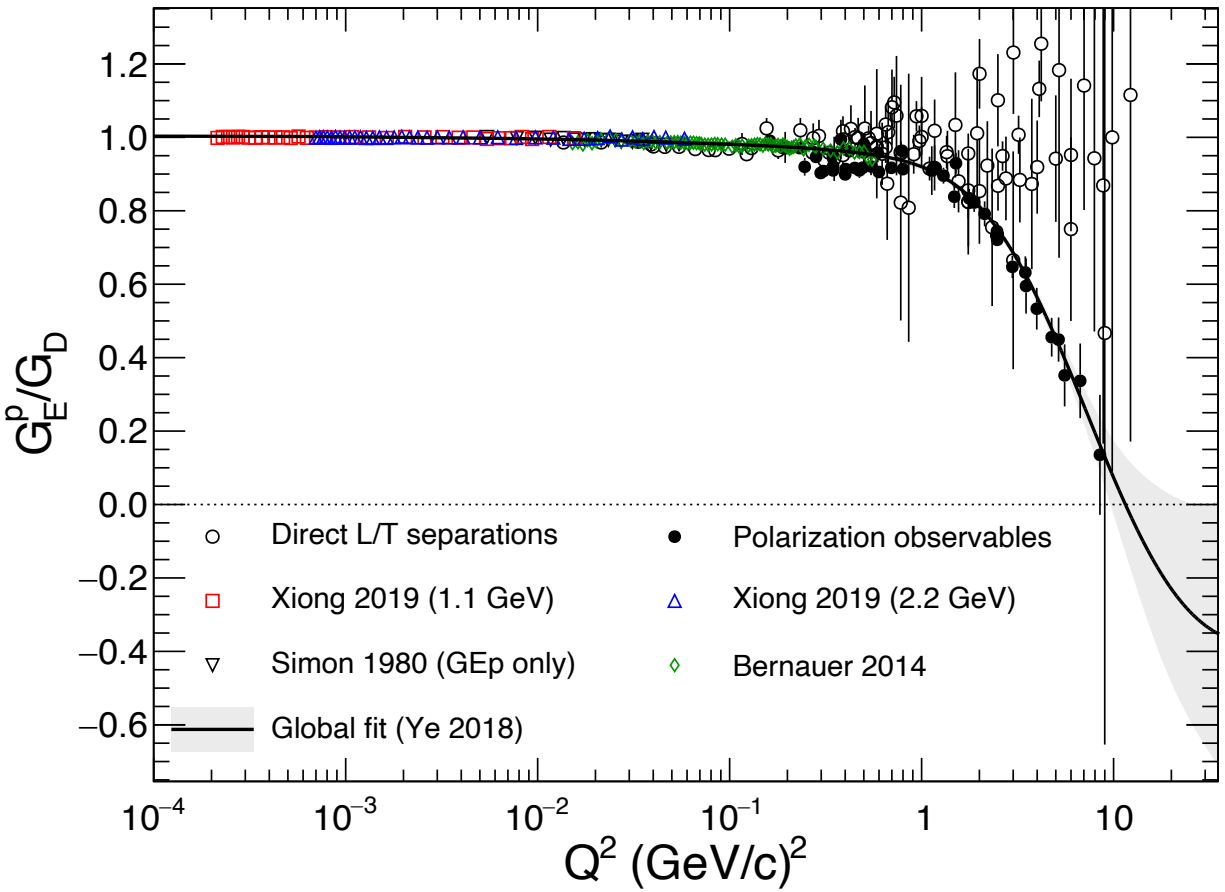

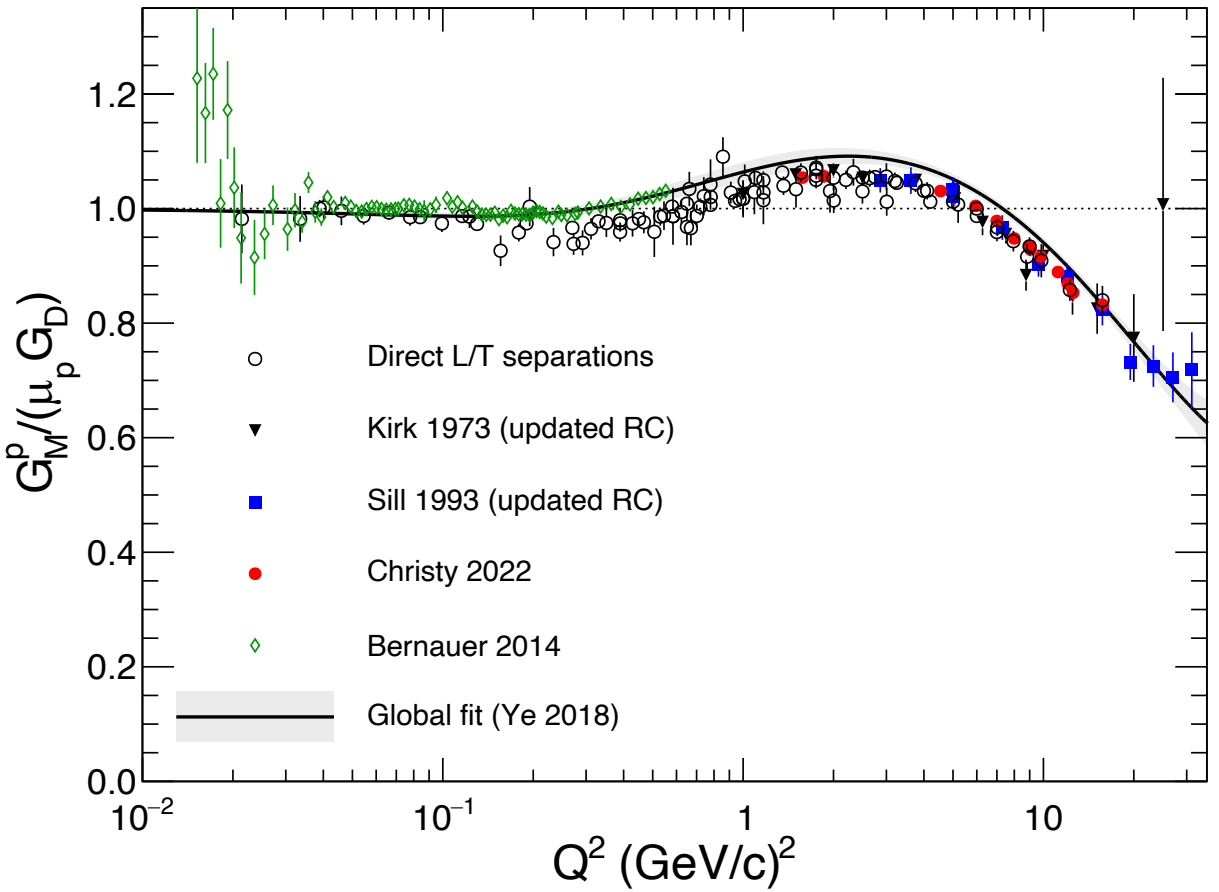

- Left: $\frac{G_E^p}{G_M^p}$. Right: $\frac{G_M^p}{\mu_p G_D}$. Figures, references, explanations from section 10.1 of "50 years of QCD": https://arxiv.org/abs/2212.11107 (Eur. Phys. Journal C, in press)

Neutron Form Factors at the start of the JLab12/SBS era

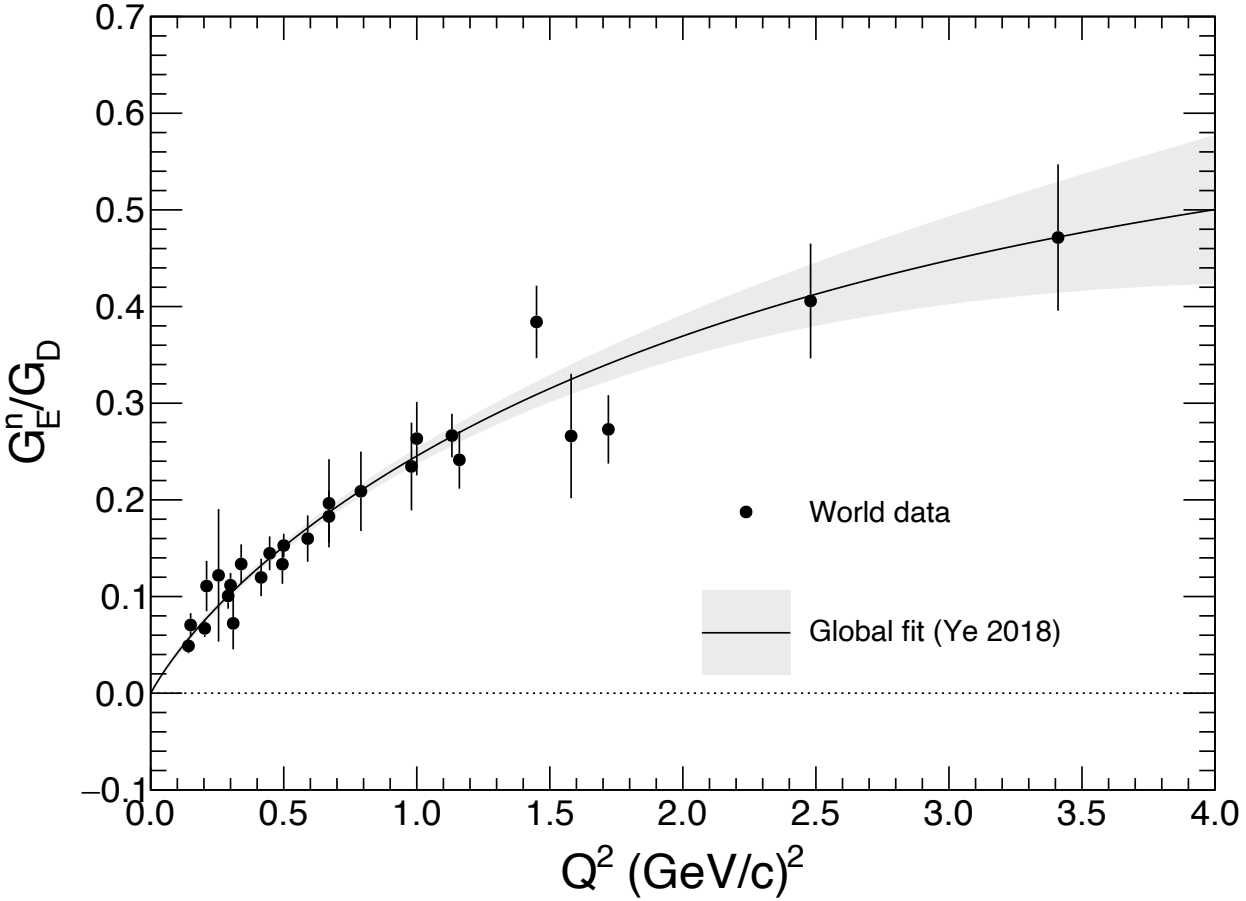

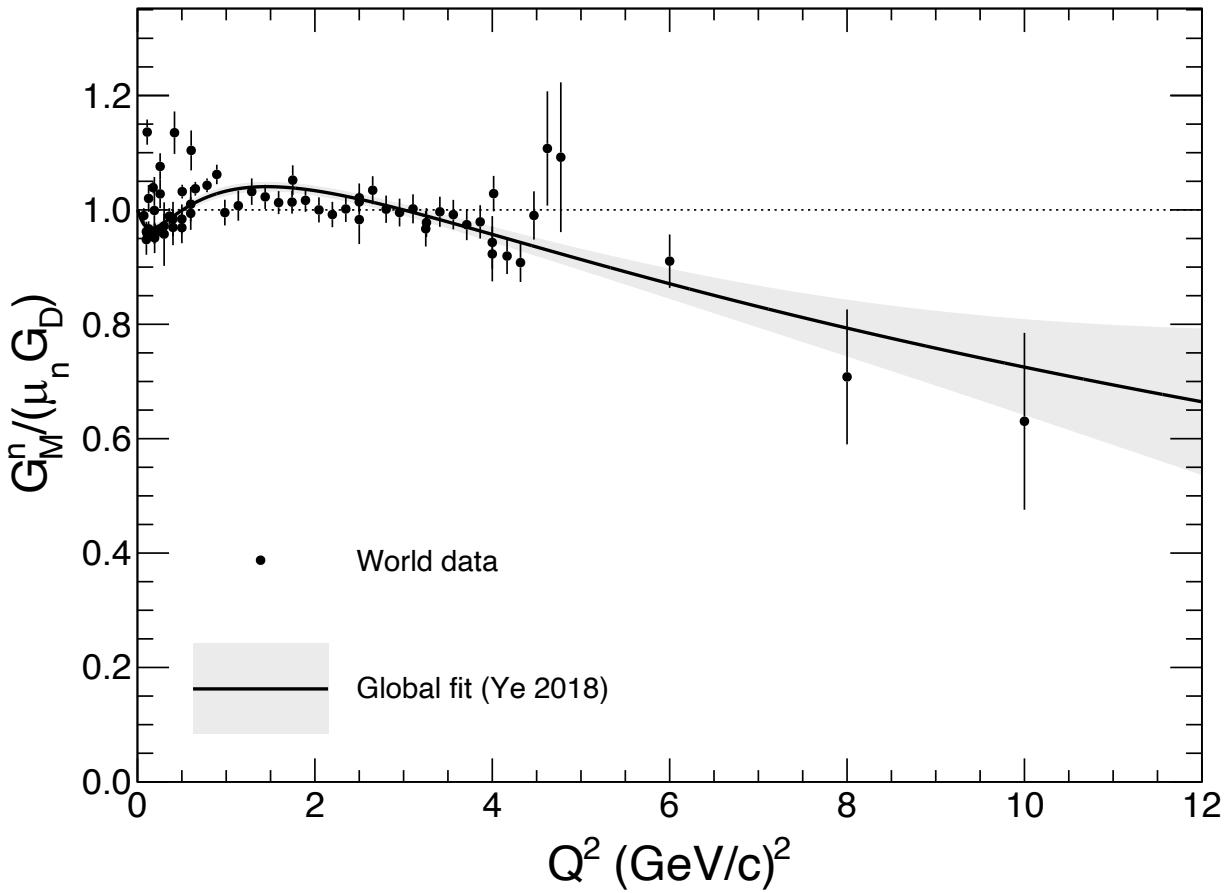

- Left: $\frac{G_E^n}{G_M^n}$. Right: $\frac{G_M^n}{\mu_n G_D}$. Figures, references, explanations from section 10.1 of "50 years of QCD": https://arxiv.org/abs/2212.11107 (Eur. Phys. Journal C, in press)

Hall A G_M^p experiment: New precise elastic *ep* cross sections to $Q^2 \approx 16\ GeV^2$

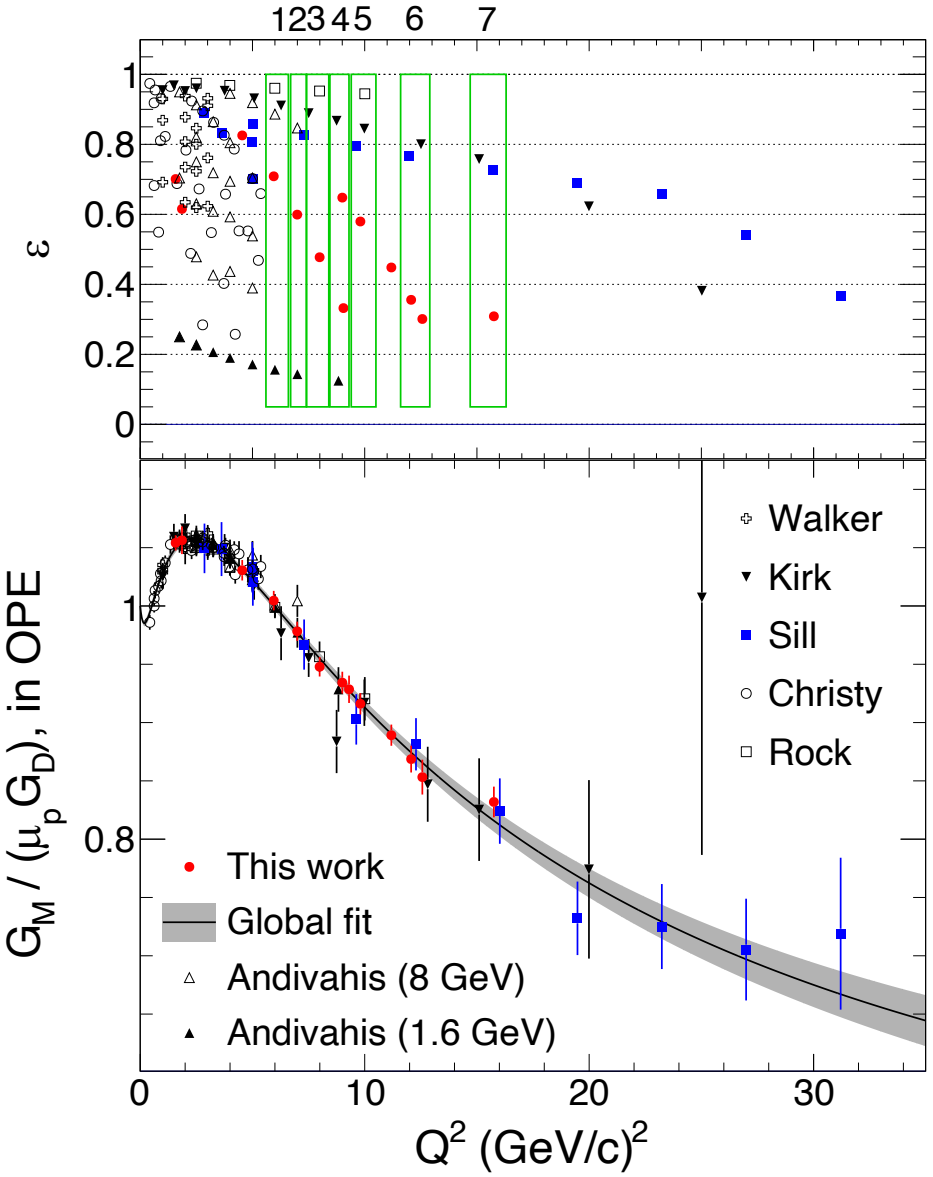

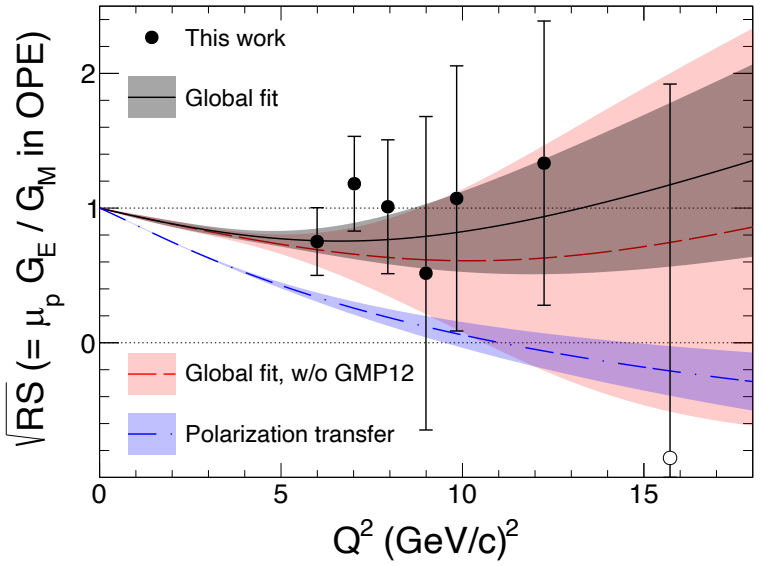

- Above: new L/T separation results including Hall A GMP12 data
- Left: new G_M^p data and (Q^2, ϵ) coverage; groupings of data for new L/T separations
- Published as: Christy et al., PRL 128, 102002 (2022)

- Precision elastic *ep* cross section measurements in Hall A carried out in fall 2016 up to $Q^2 \approx 16$ GeV^2
- Significantly improved precision for $Q^2 \geq 6$ GeV^2
- ϵ coverage of new data allows new L/T separations out to ~16 GeV^2
- Significant tension between L/T separations and polarization transfer now firmly established to higher Q^2

Continued relevance of high-Q^2 FF measurements

- For Q ~ few GeV and higher we are probing the theoretically challenging region of transition between non-perturbative QCD, strong-coupling, and confinement to weak-coupling, asymptotic freedom, and pQCD.
- Precise FF knowledge is required both to directly constrain GPD moments and to interpret DVCS experiments
- Quark flavor separation to very large momentum reveals role of diquark correlations: PPNP 116, 103835 (2021), https://doi.org/10.1016/j.ppnp.2020.103835

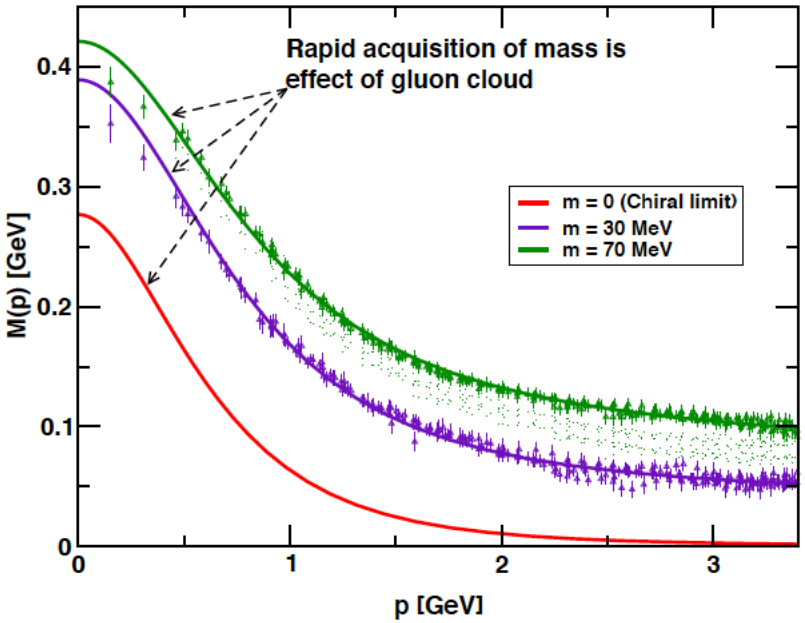

- Comparison of continuum and Lattice results for M(p)

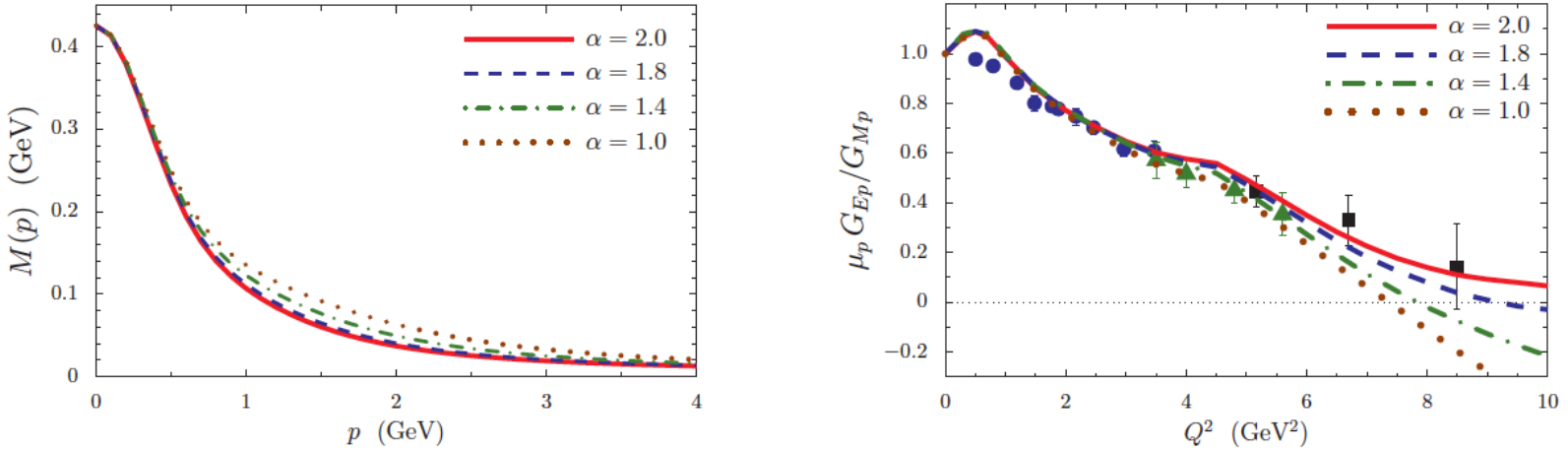

Figure 7.1: *Left panel.* Dressed-quark mass function employed in Ref. [89]. $\alpha = 1$ specifies the reference form and increasing α diminishes the domain upon which DCSB is active. *Right panel.* Response of $\mu_p G_E/G_M$ to increasing α; i.e., to an increasingly rapid transition between constituent- and parton-like behaviour of the dressed-quarks. Data are from Refs. [301, 312–316].

- High-Q^2 form factor behavior highly sensitive to M(p) in Dyson-Schwinger Equation (DSE) framework
- Cloet and Roberts, PPNP 77, 1 (2014)

The SBS high-Q^2 Form Factor Program in Hall A

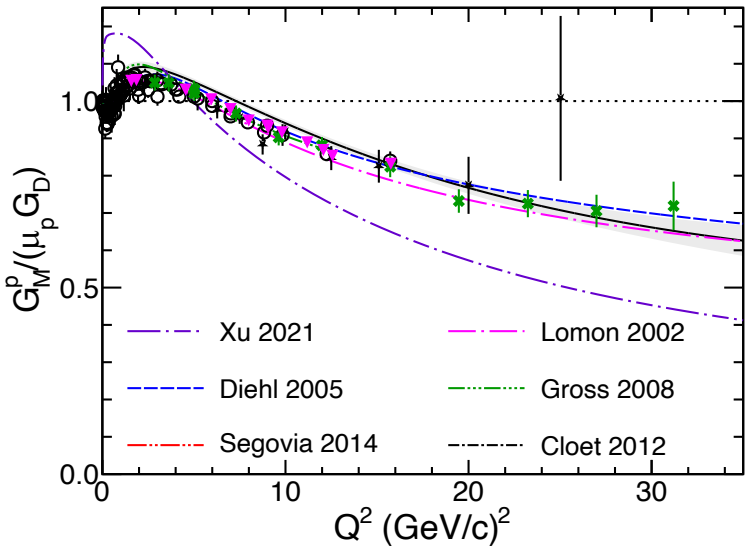

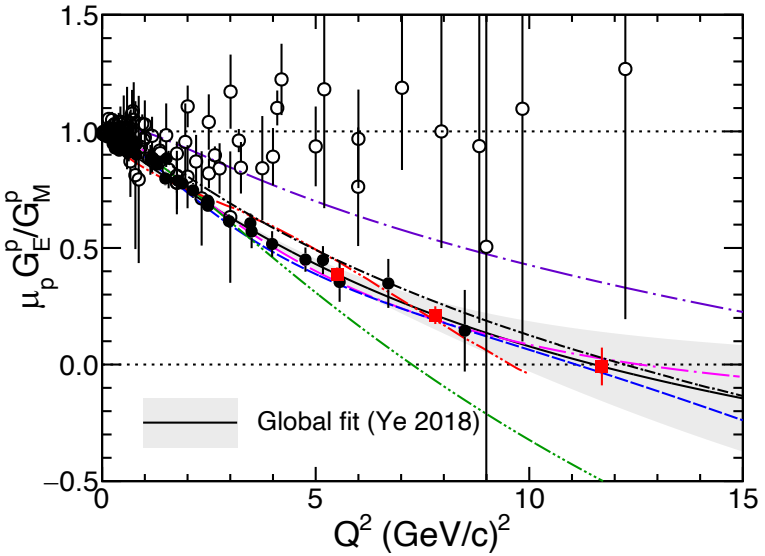

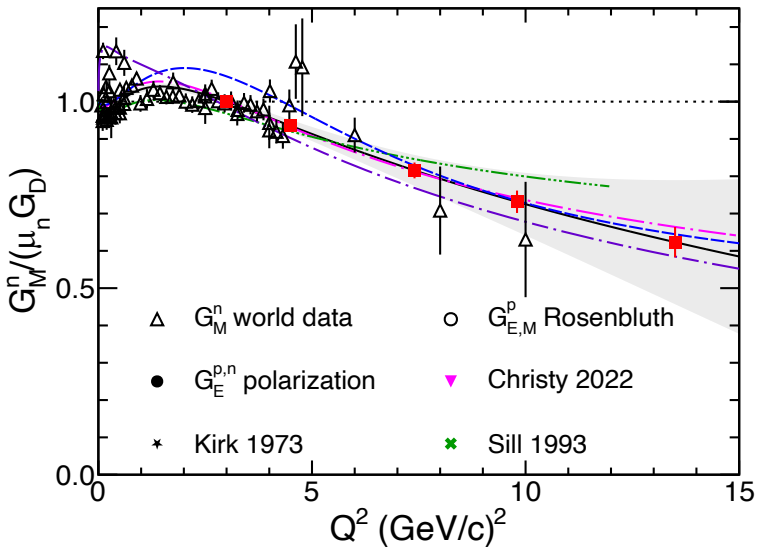

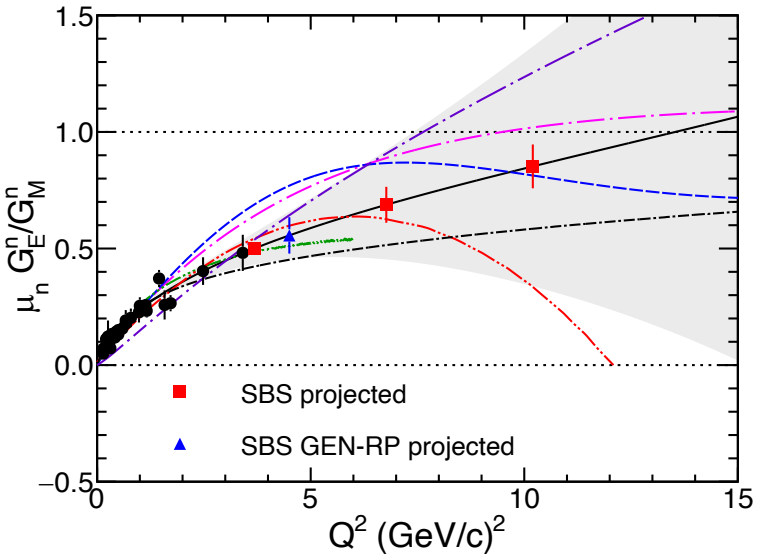

- Figure from "50 Years of QCD" (EPJ C, in press): https://arxiv.org/abs/2212.11107
- GMN/nTPE (E12-09-019/E12-20-010) using "ratio" method on deuterium: **Completed Oct. 2021-Feb. 2022**
- GEN Helium-3: **Data-taking finished three days ago (Oct. 29, 2023)**
- GEN-RP: Projected run spring 2024
- GEP: Projected run 2024-2025
- Except for G_M^n, all SBS form factor measurements are based on polarization observables.
  - Small elastic cross sections and asymmetries require as large as possible FOM (= Luminosity × Polarization^2 × Acceptance)

Statistical requirements: asymmetries vs. cross section measurements

Cross sections:

$$\sigma \propto N$$

$$\Longrightarrow \frac{\Delta\sigma}{\sigma} = \frac{1}{\sqrt{N}}$$

To measure a cross section with a relative statistical precision of 1%, you need 10,000 events.

Asymmetries:

$$\Delta A = \sqrt{\frac{1-A^2}{N}}$$

$$\frac{\Delta A}{A} = \sqrt{\frac{1-A^2}{NA^2}}$$

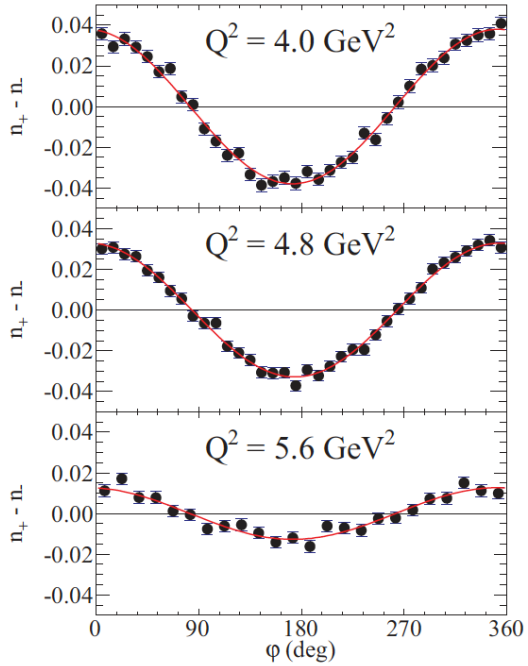

FIG. 6. (Color online) Focal-plane helicity-difference asymmetry $n_+ - n_- \equiv (N_{\text{bins}}/2)[N^+(\varphi)/N_0^+ - N^-(\varphi)/N_0^-]$, where N_{bins} is the number of φ bins and $N^{\pm}(\varphi)$, $N_0^{\pm}$ are defined as in Eq. (4), for the three highest Q^2 points from GEp-II. Curves are fits to the data. See text for details.

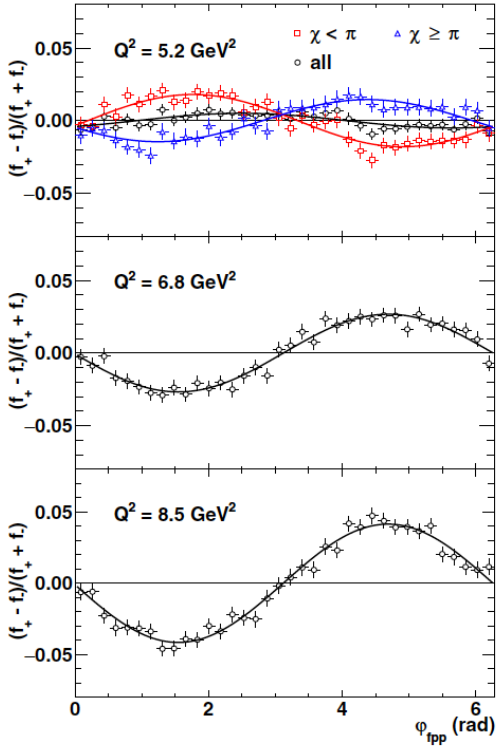

FIG. 10. Focal plane helicity difference/sum ratio asymmetry $(f_+ - f_-)/(f_+ + f_-)$, defined as in Eq. (20), for the GEp-III kinematics, for FPP1 and FPP2 data combined, for single-track events selected according to the criteria discussed in Sec. III B 2. Asymmetry fit results are shown in Table V. The asymmetry at $Q^2 = 5.2$ GeV^2 is also shown separately for events with precession angles $\chi < \pi$ and $\chi \geq \pi$, illustrating the expected sign change of the $\sin(\varphi)$ term.

- Typical asymmetry magnitude in a recoil proton polarimeter at ”high” momentum is ~few percent.
- For example: to measure a 5% asymmetry with a relative precision of 1%, one needs $N = 10{,}000 \times \frac{1-A^2}{A^2} \approx 4 \times 10^6$ events!

→ Asymmetry measurement must maximize beam and/or target polarization, and luminosity × acceptance! Original motivation for SBS concept!

The Neutron Magnetic FF

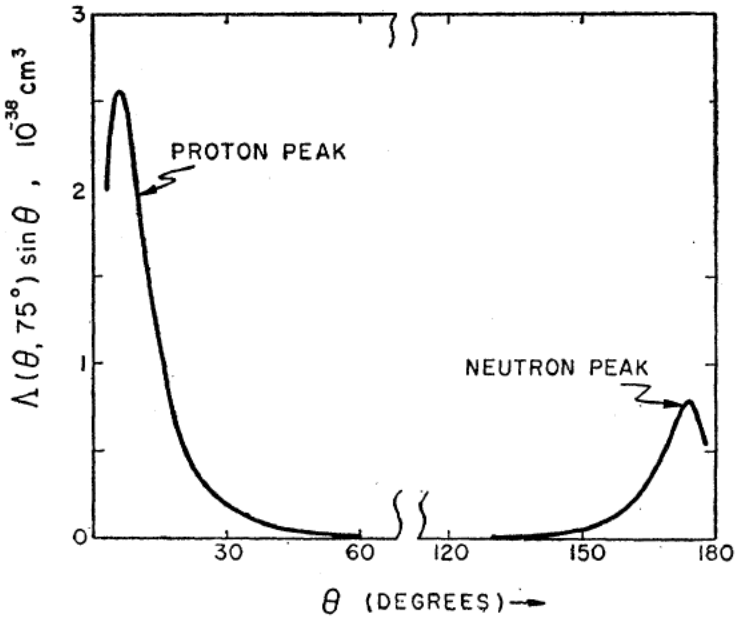

FIG. 1. The angular distribution function $\Lambda(\theta,\vartheta)\sin\theta$ in the absence of final-state interactions is plotted as a function of the proton scattering angle in the nucleon center-of-mass system $[\cos\theta=\hat{p}\cdot\hat{q}]$ for the scattering of 500-Mev electrons through an angle $\vartheta=75°$ with a momentum transfer giving $p=\frac{1}{2}q=1.3\times10^{13}$ cm^{-1}. $\Lambda(\theta,\vartheta)$ is defined in Eq. (11.2); the function $F(\theta)$ entering the definition was evaluated using a Hulthén wave function for the deuteron. The cross section $d^3\sigma/(d\theta d\Omega_e dE_e')$ is given by $(4.71\times10^5$ cm^{-1} rad^{-1} sterad^{-1} Mev$^{-1})$ $\Lambda(\theta,\vartheta)\sin\theta$. No nucleon form factors have been introduced into the results.

Ratio method: Durand, Phys. Rev. 115, 1020 (1959)

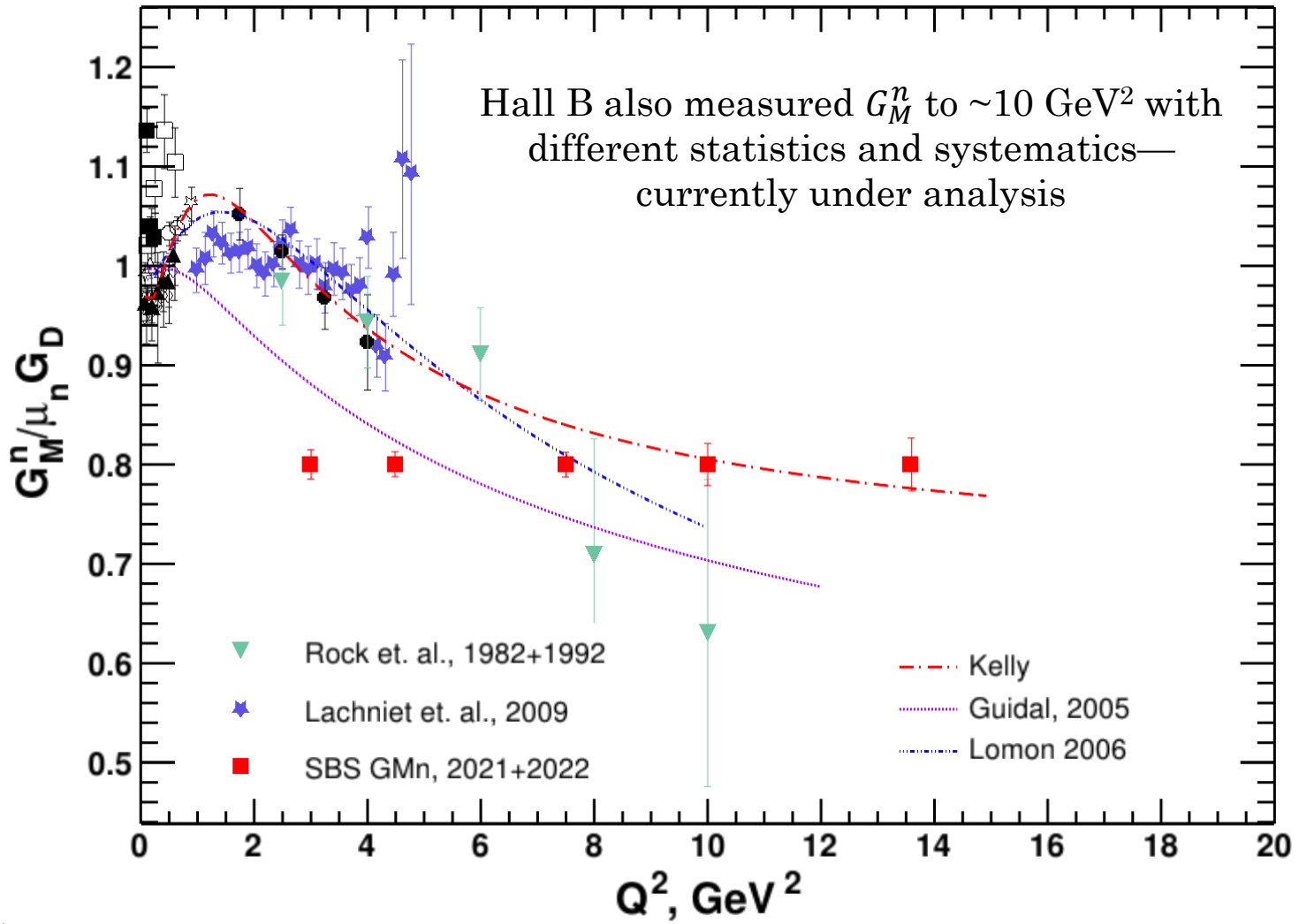

- Existing GMN data with projected SBS Q^2 points and uncertainties **(Plot credit: Provakar Datta (UConn))**

BigBite and SBS on the floor of Hall A—First physics run completed Oct. 2021-Feb. 2022!

UConn Physics in Hall A, SBS GMN installation, July 2021

SBS GMN/nTPE Overview (Figure Credits: Provakar Datta (UConn))

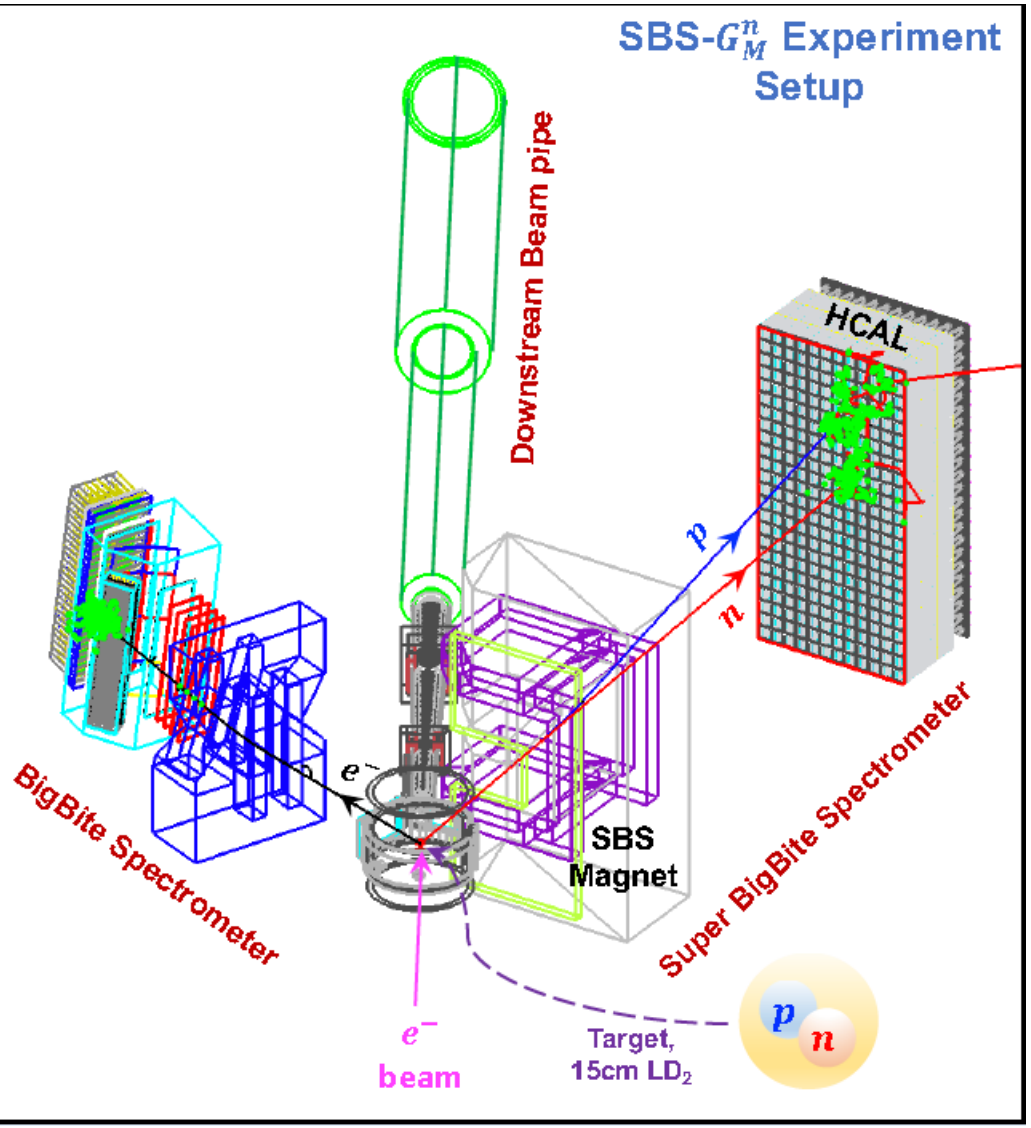

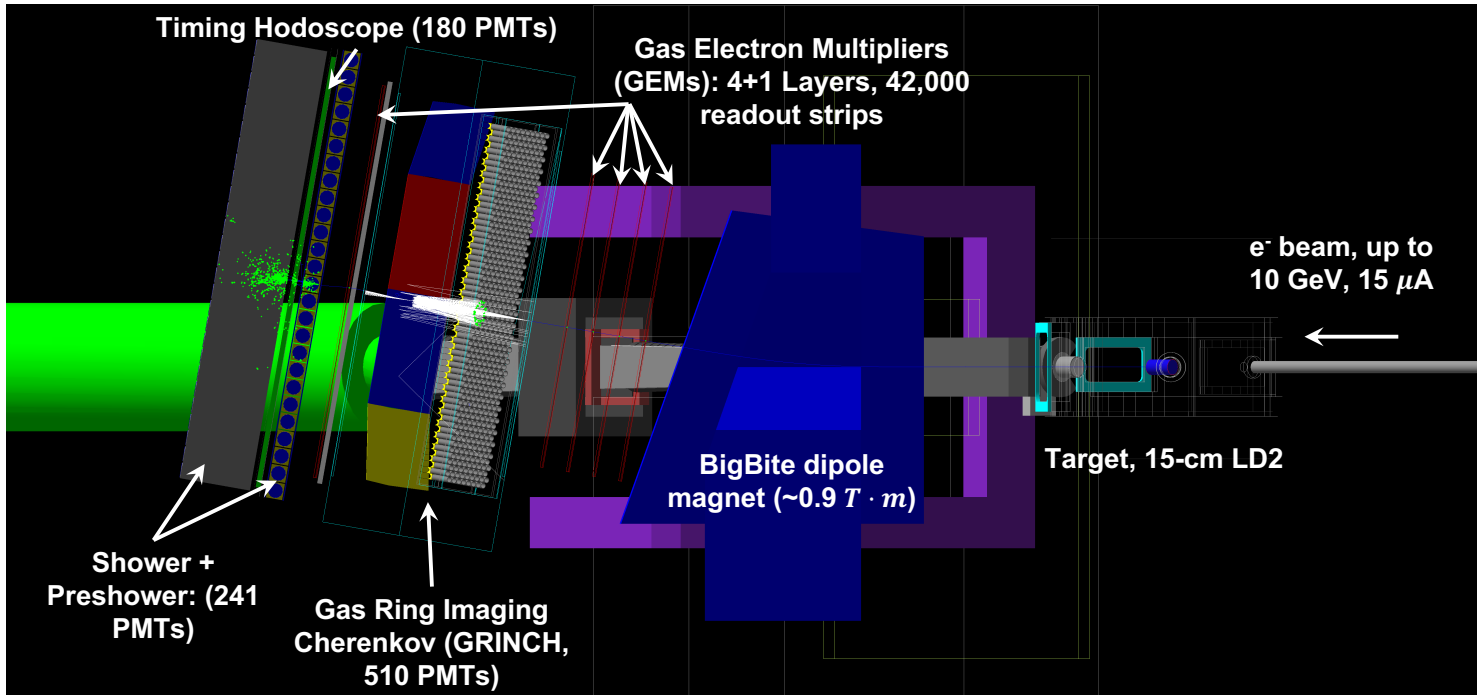

- Measure cross section ratio d(e,e'n)/d(e,e'p) on liquid deuterium.
- e^- arm: BigBite with upgraded detectors for high-luminosity running
- n/p arm: SBS with HCAL
- Ran Oct. 2021-Feb. 2022

Neutron/proton separation in SBS G_M^n

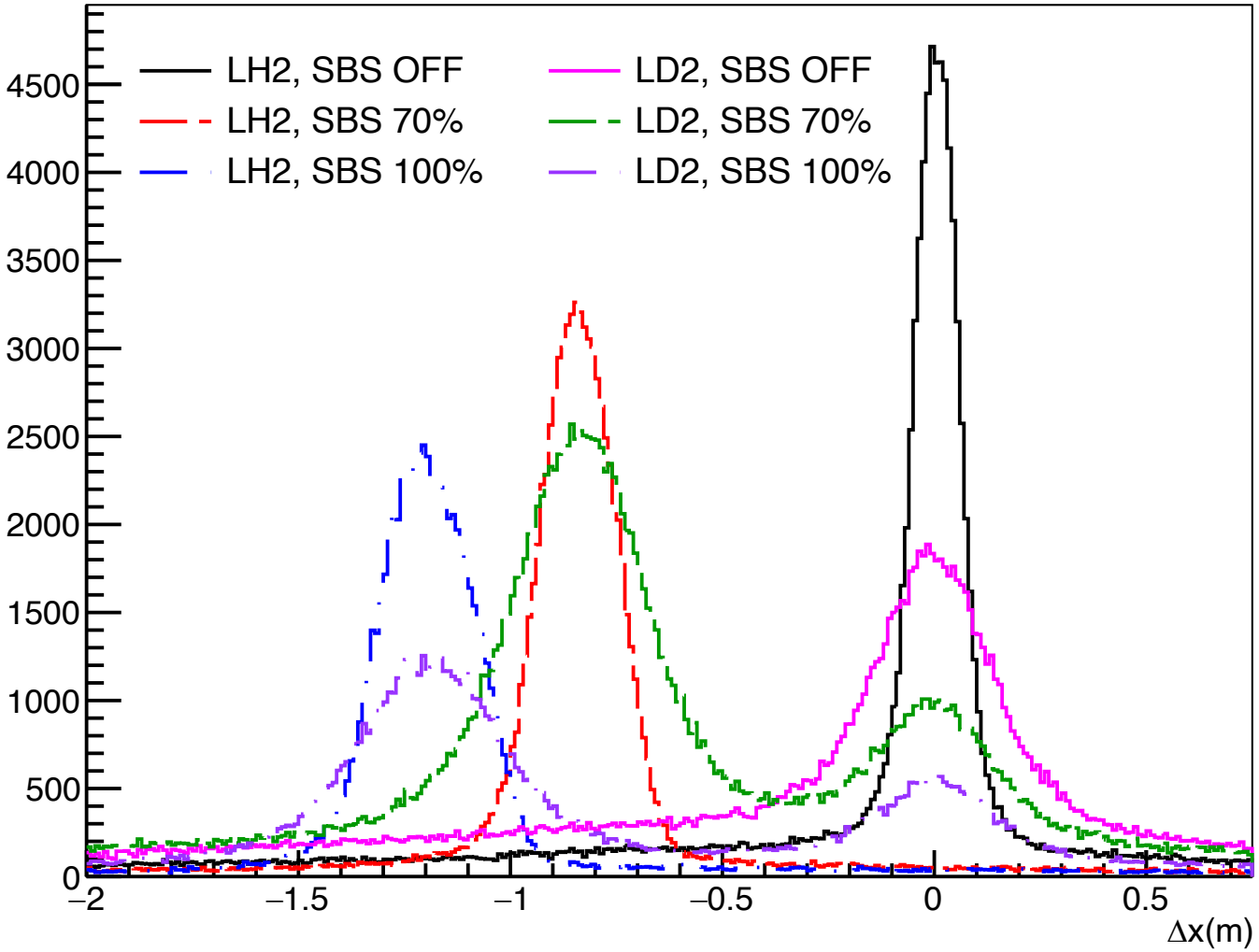

- Nucleon charge ID is accomplished by a small vertical deflection of protons in SBS magnet
- Optimal deflection is that which gives ”clean” n/p separation while minimizing acceptance/efficiency difference between neutrons and protons
- “Fiducial cut” is calculated based on reconstructed *electron* kinematics—requires that both proton and neutron in quasi-elastic kinematics would hit HCAL active area with a safety margin equivalent to ~100 MeV Fermi smearing

Elastic event selection, $Q^2 = 4.5, \epsilon = 0.5$

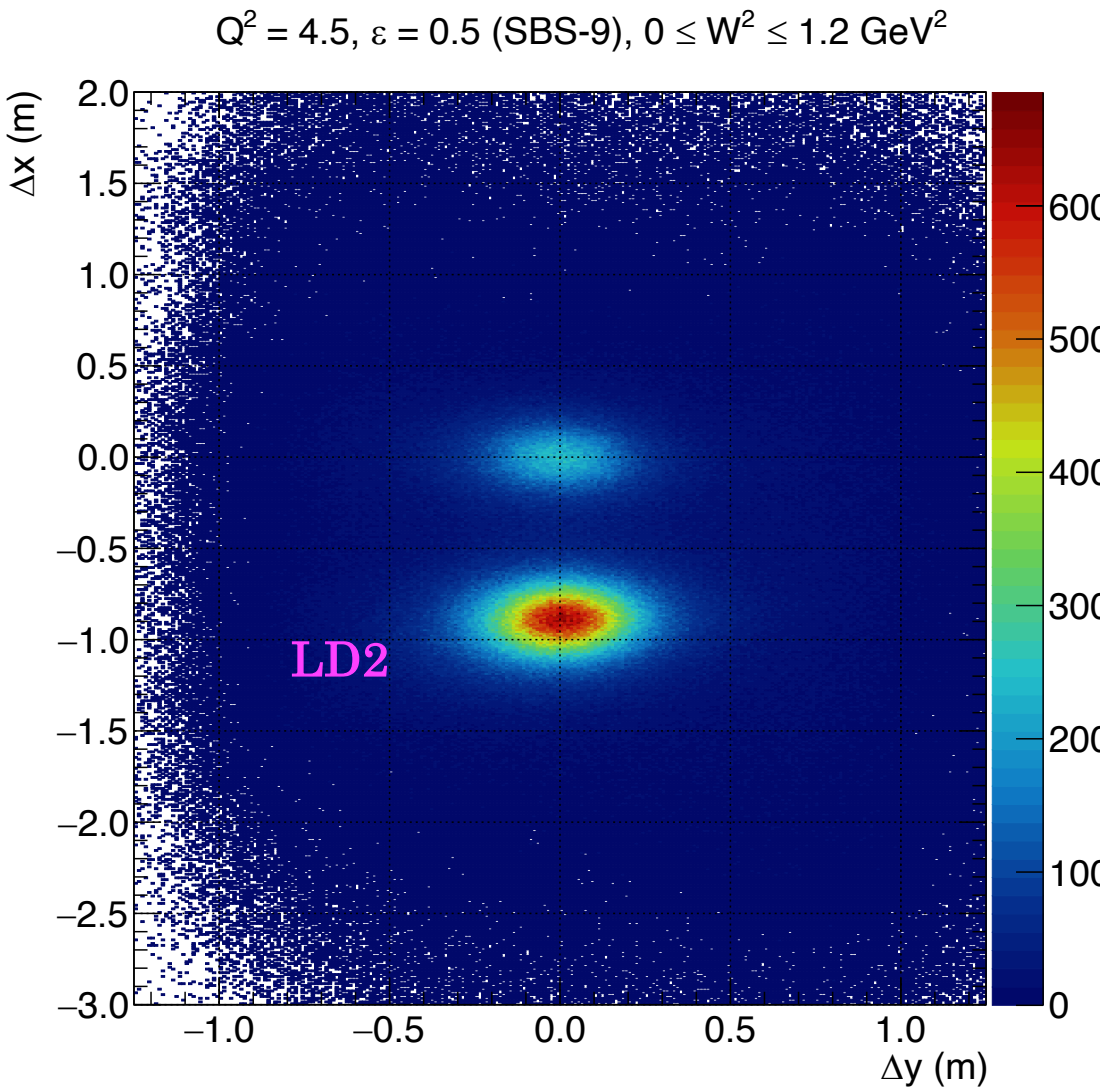

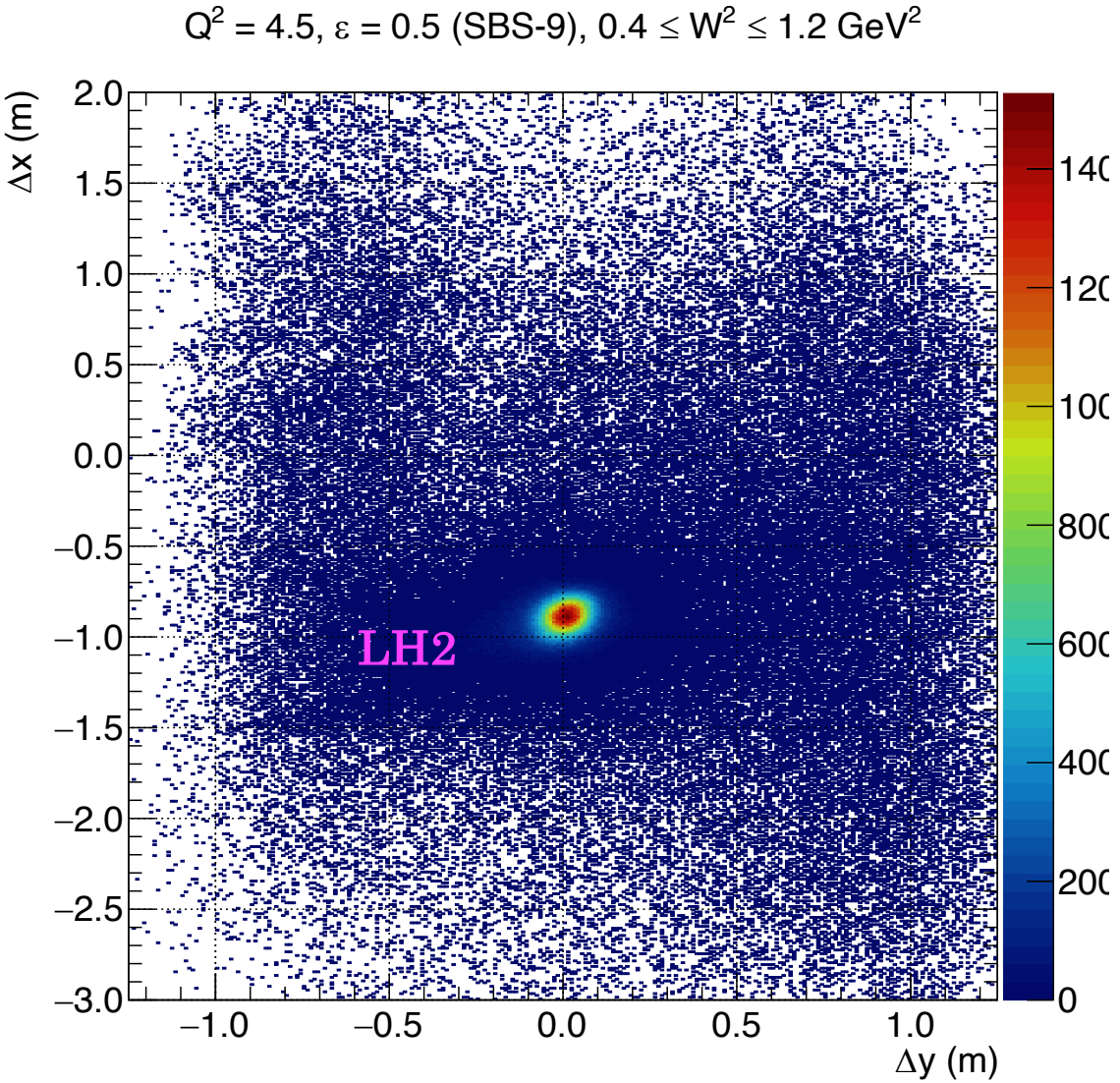

Elastic Event Selection, $Q^2 = 13.5$ GeV^2

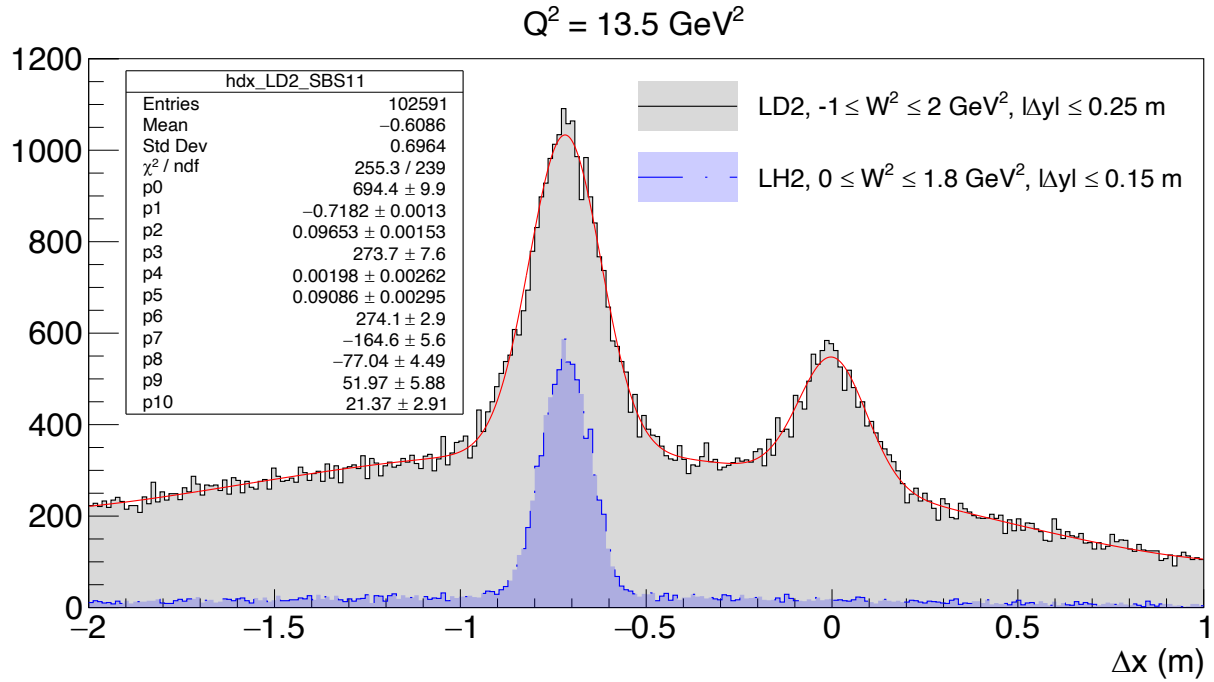

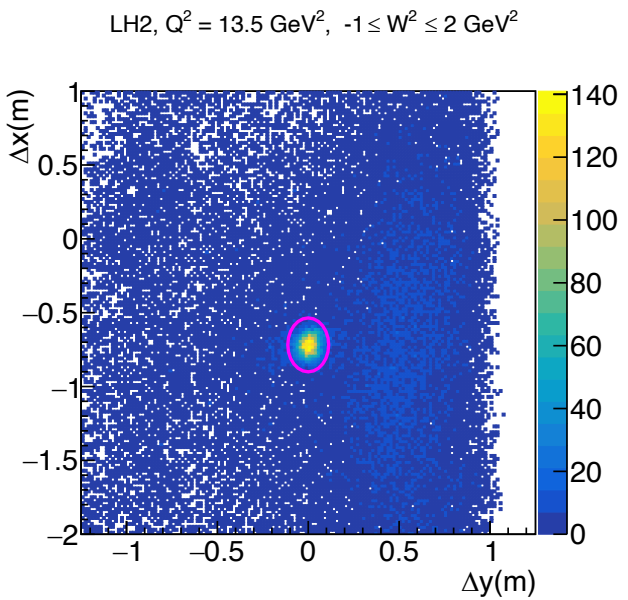

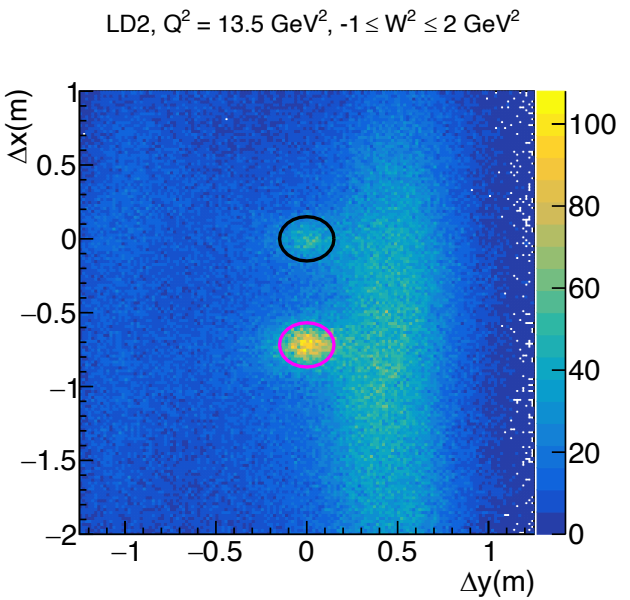

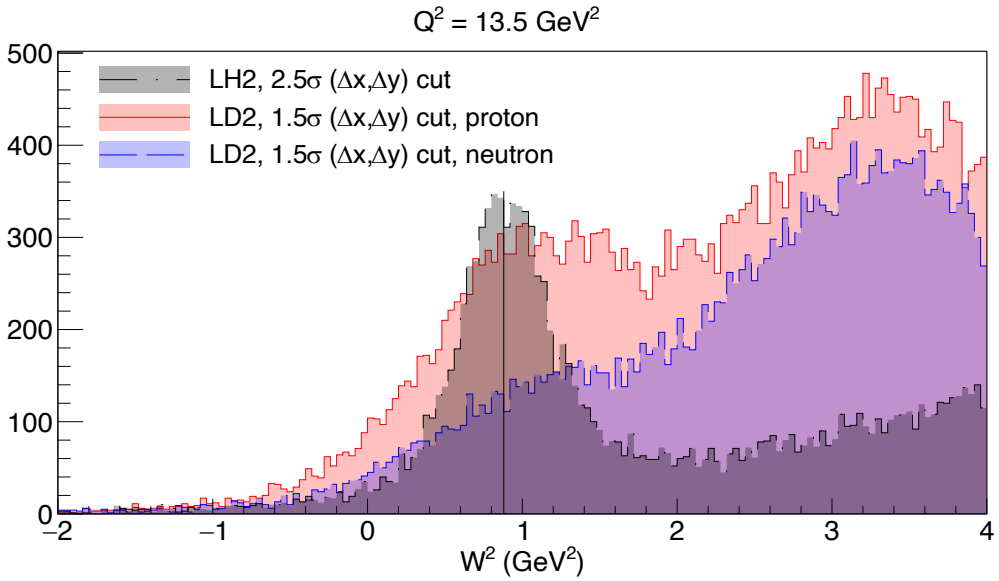

- Above, left: Δx distributions for LH2, LD2
- Above, right: $(\Delta x, \Delta y)$ distribution for LH2 and LD2
- Bottom, right: W^2 distributions for LH2, LD2 with proton, neutron cuts

SBS-GMN: raw n/p yield ratios

SBS-GMN PRELIMINARY (stat. ⊕ estimated syst. error)

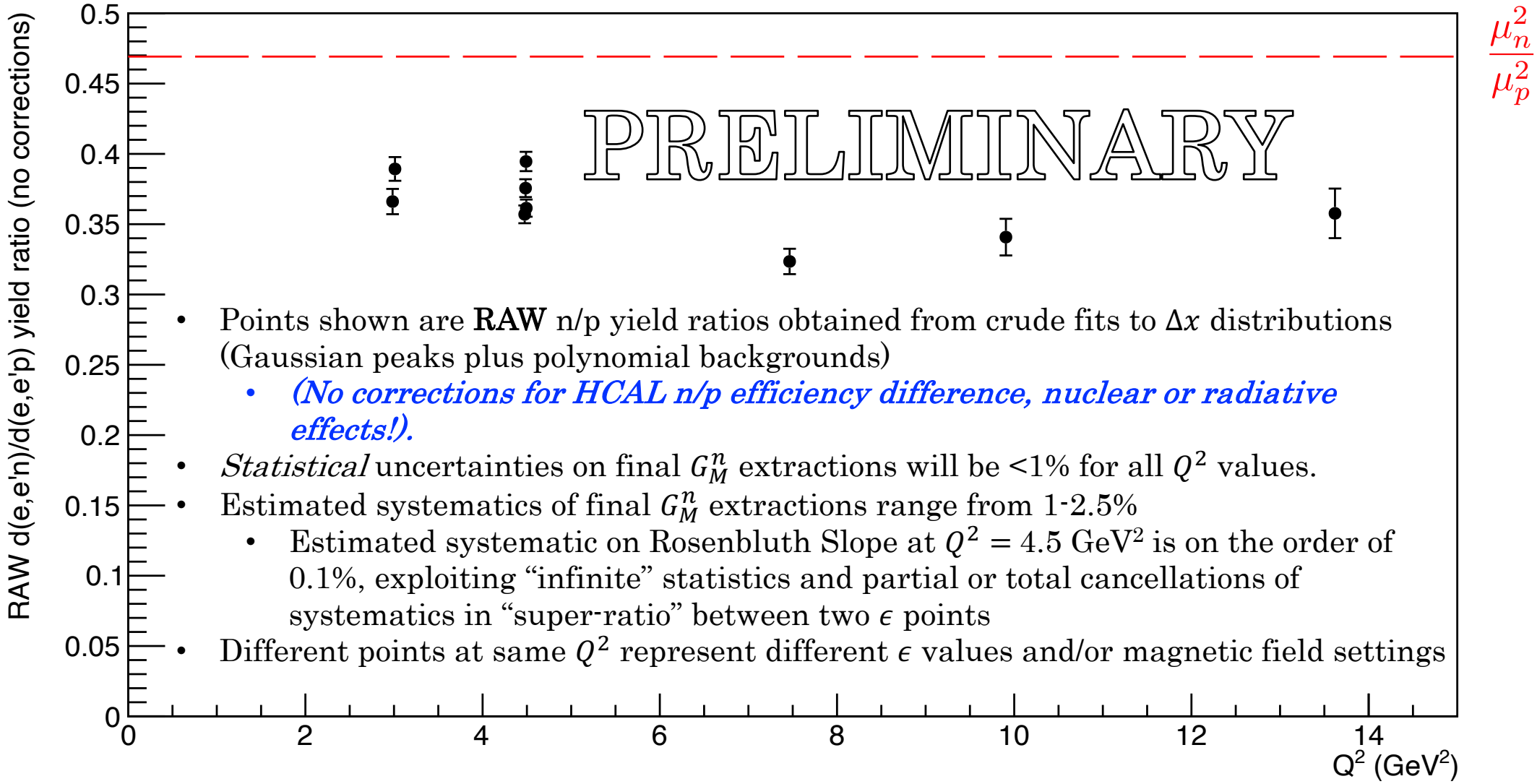

- Points shown are **RAW** n/p yield ratios obtained from crude fits to Δx distributions (Gaussian peaks plus polynomial backgrounds)
  - *(No corrections for HCAL n/p efficiency difference, nuclear or radiative effects!).*
- *Statistical* uncertainties on final G_M^n extractions will be <1% for all Q^2 values.
- Estimated systematics of final G_M^n extractions range from 1-2.5%
  - Estimated systematic on Rosenbluth Slope at $Q^2 = 4.5$ GeV^2 is on the order of 0.1%, exploiting "infinite" statistics and partial or total cancellations of systematics in "super-ratio" between two ϵ points
- Different points at same Q^2 represent different ϵ values and/or magnetic field settings

Projected SBS Uncertainties for $\frac{G_M^n}{\mu_n G_D}$ and Rosenbluth Slope

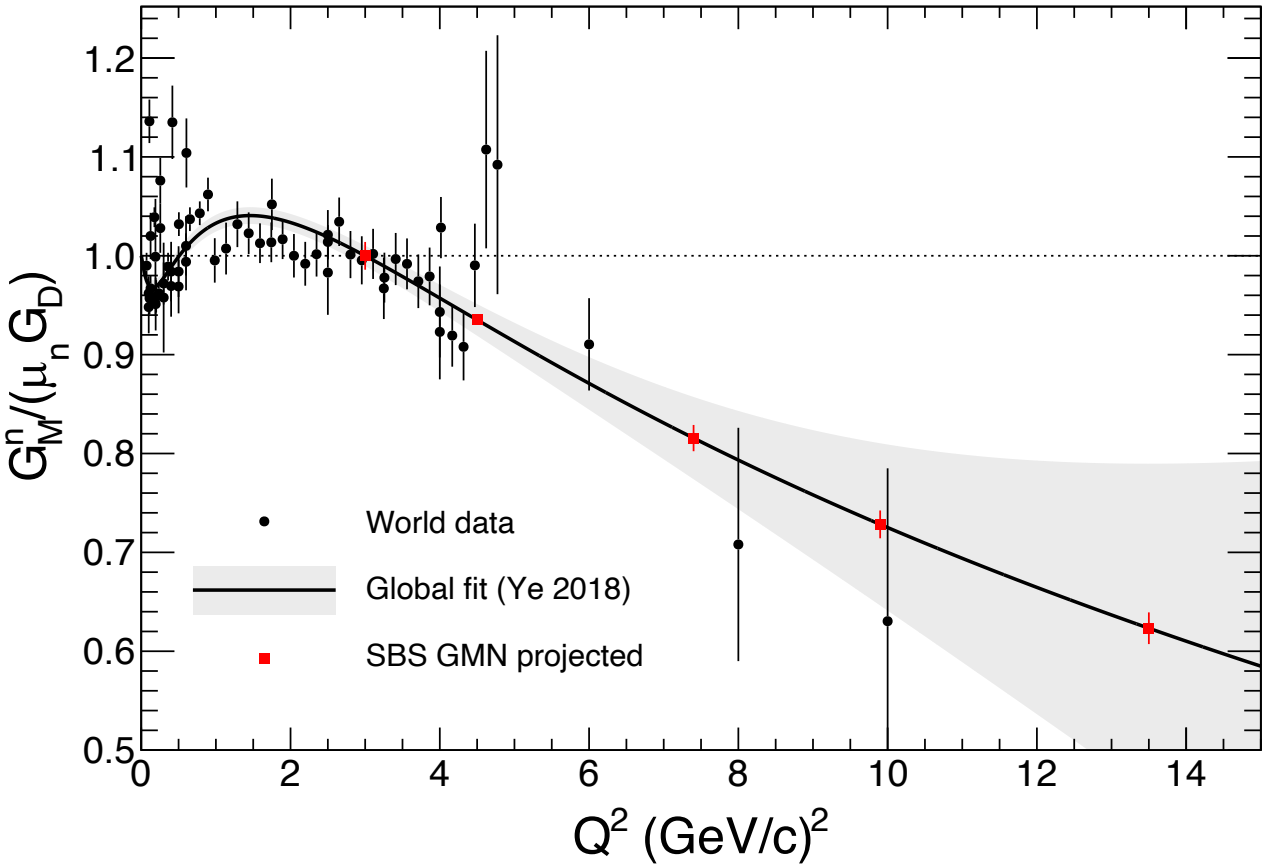

World data for $G_M^n/\mu_n G_D$ plotted on the global fit curve with **projected SBS accuracy** ***based on completed data taking 2021-2022***

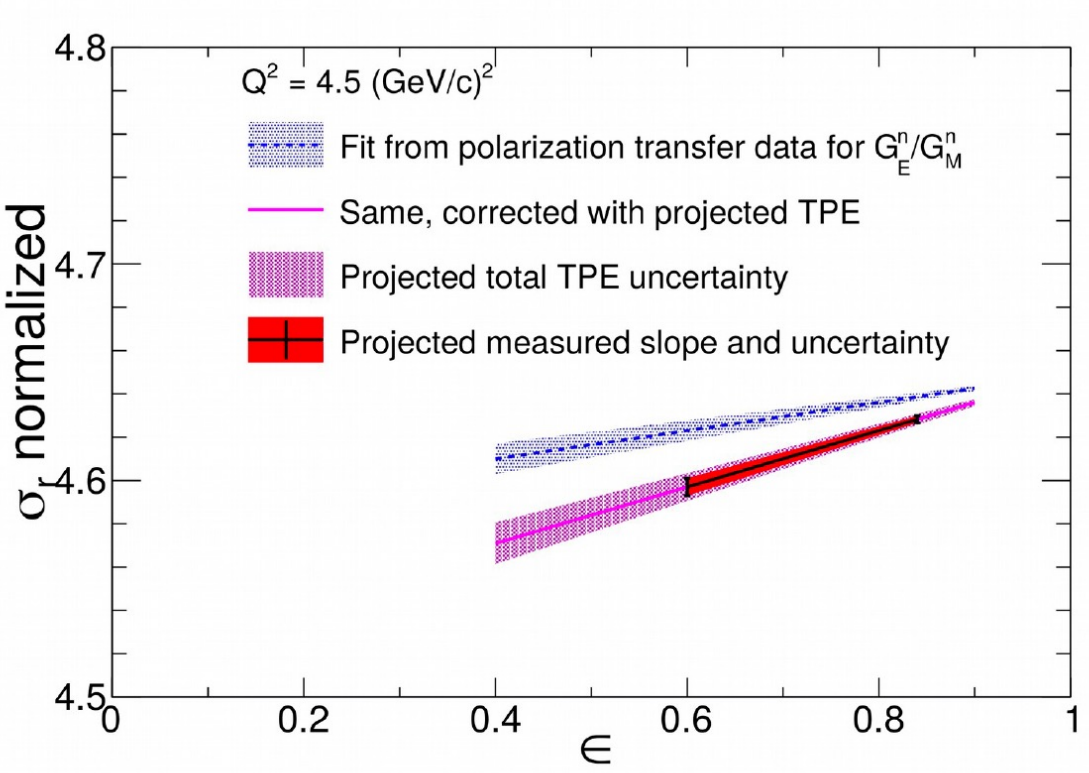

Projected accuracy of Rosenbluth Slope at $Q^2 = 4.5$ GeV^2

- Actual data has somewhat greater lever arm in ϵ: $\Delta\epsilon \approx 0.29$ (actual) compared to $\Delta\epsilon = 0.24$ (proposal)

Neutron FFs—GEN

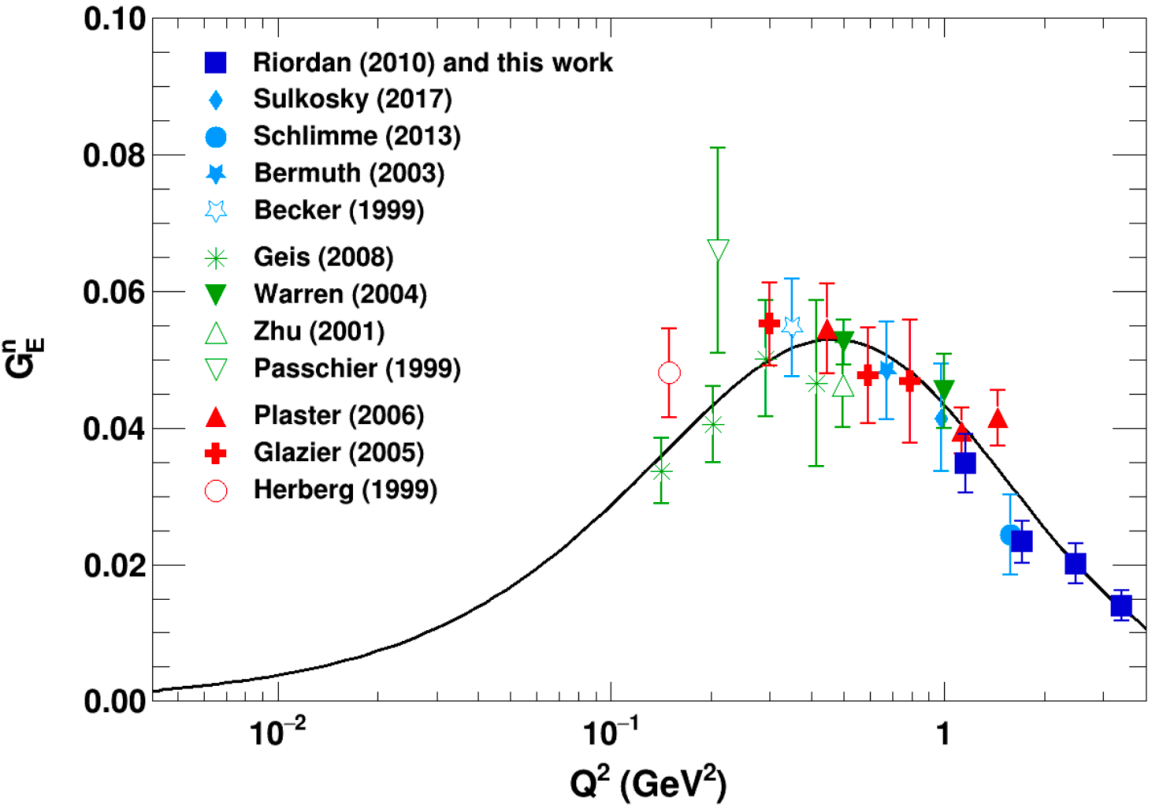

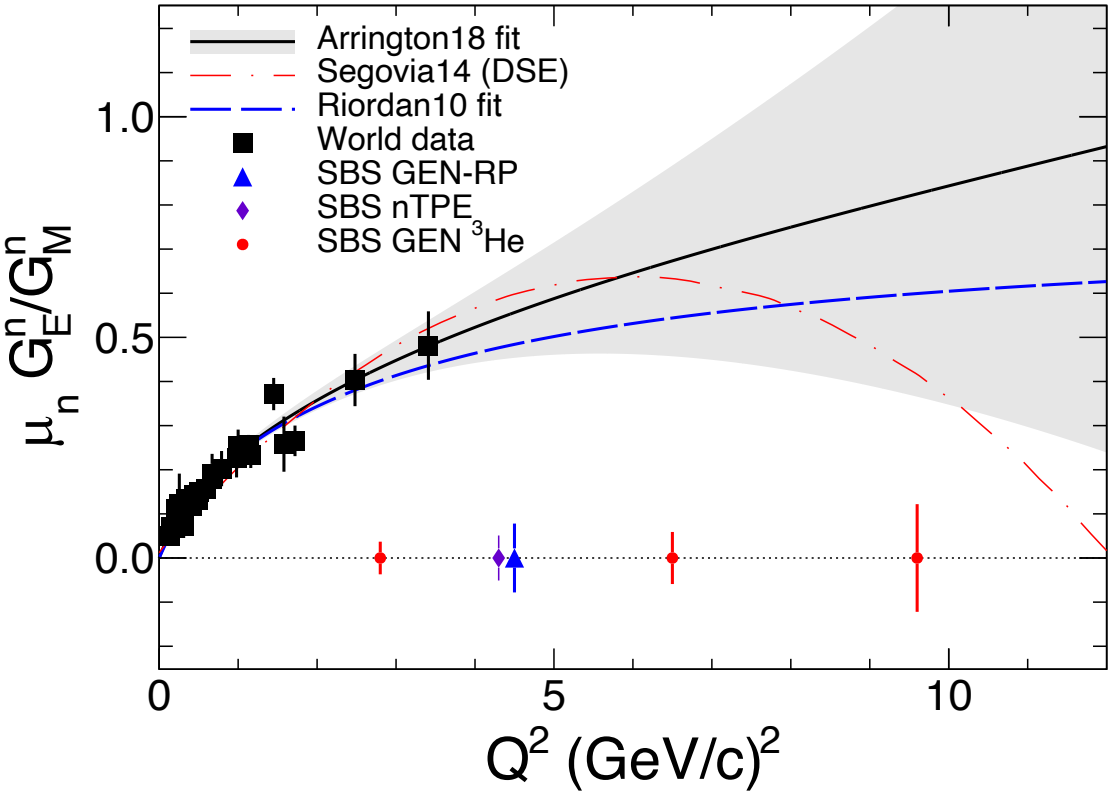

- Left (from Obrecht *et al.*, in preparation): G_E^n from polarization observables (color-coded by observable): **Polarized Helium-3 target asymmetry, Deuteron recoil polarimetry, Polarized deuterium target asymmetry.**
  - See Freddy Obrecht Ph.D. thesis: https://opencommons.uconn.edu/dissertations/2045/
- Right: GEN world data with projected SBS results (based on actually collected data for Helium-3!).

E12-09-016: G_E^n/G_M^n to 10 GeV^2 using polarized ^{3}He(e,e'n)pp

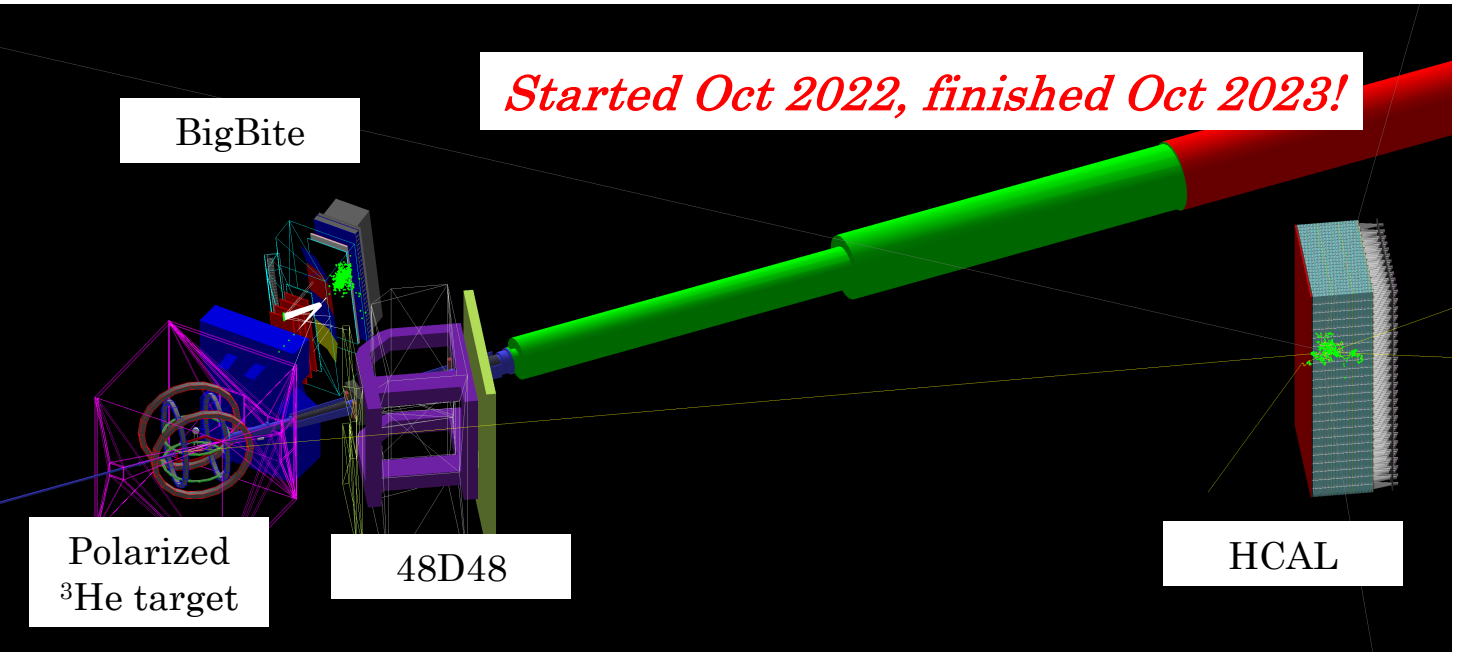

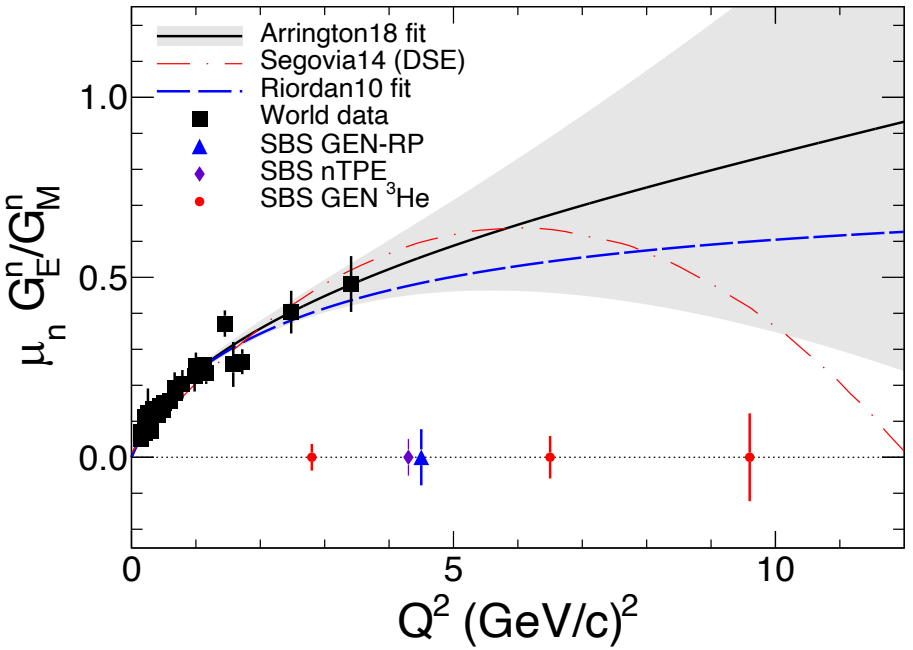

- Same detector configuration as GMN (E12-09-019)
- High-luminosity polarized ^{3}He target with convection-driven circulation of polarized gas.
- Measurement to 10 GeV^2 has enormous discrimination power among theoretical models
- **Data-taking completed Oct. 29, 2023!**

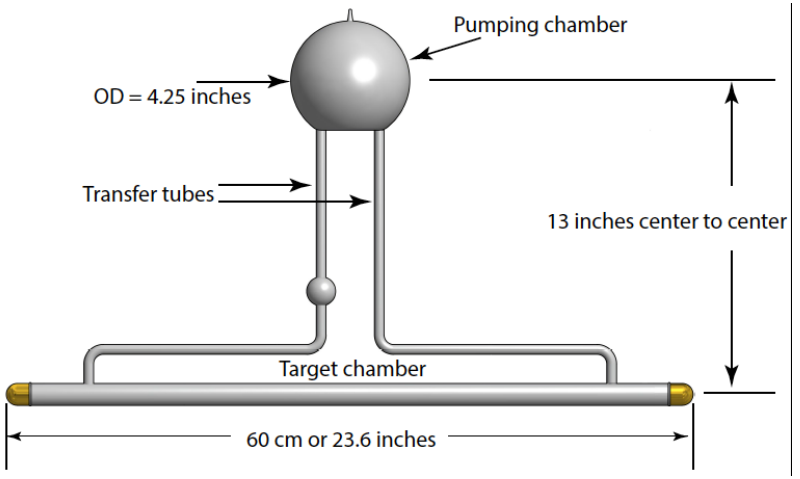

Polarized Helium-3 Target in Hall A, Oct. 2022

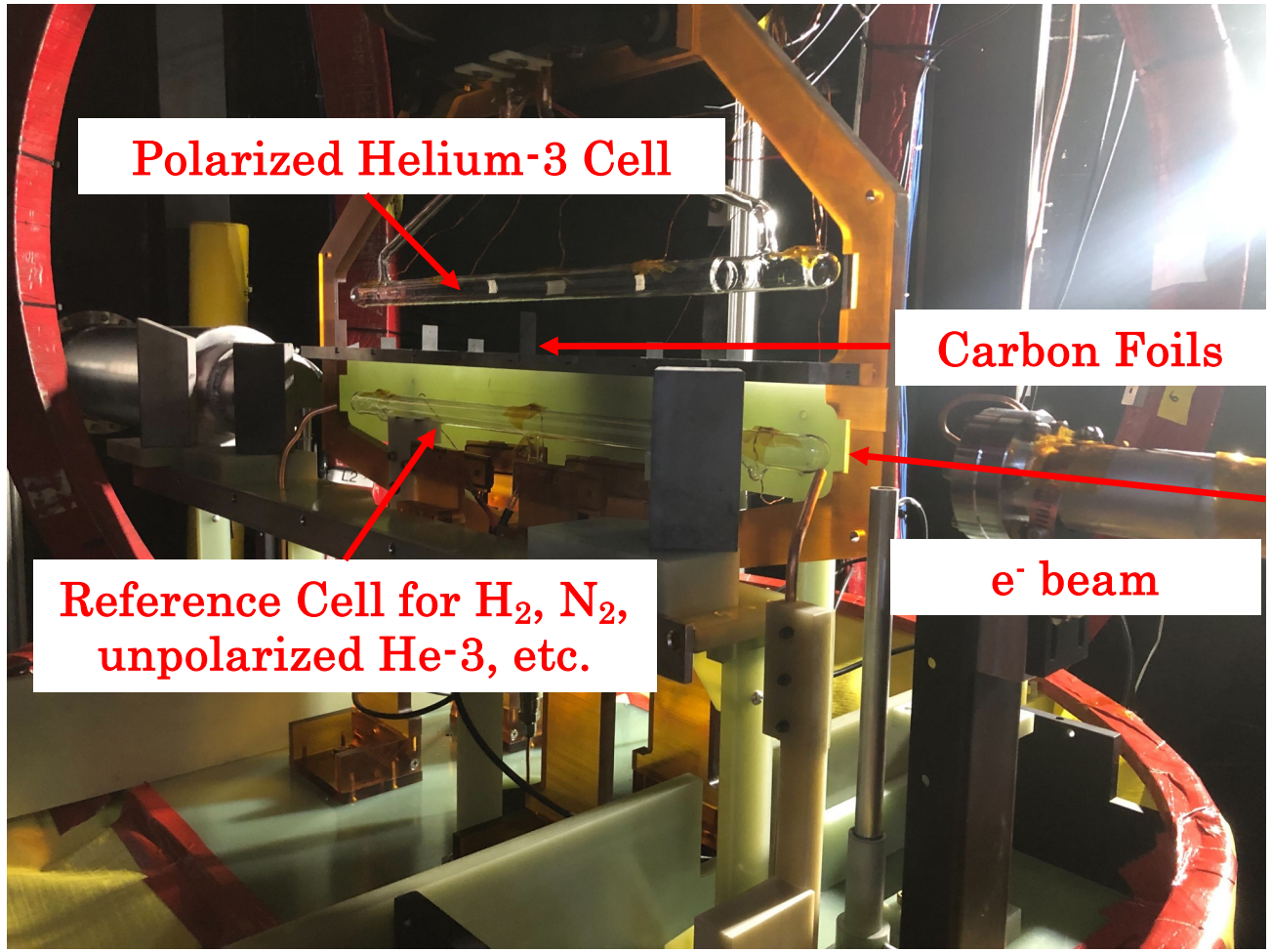

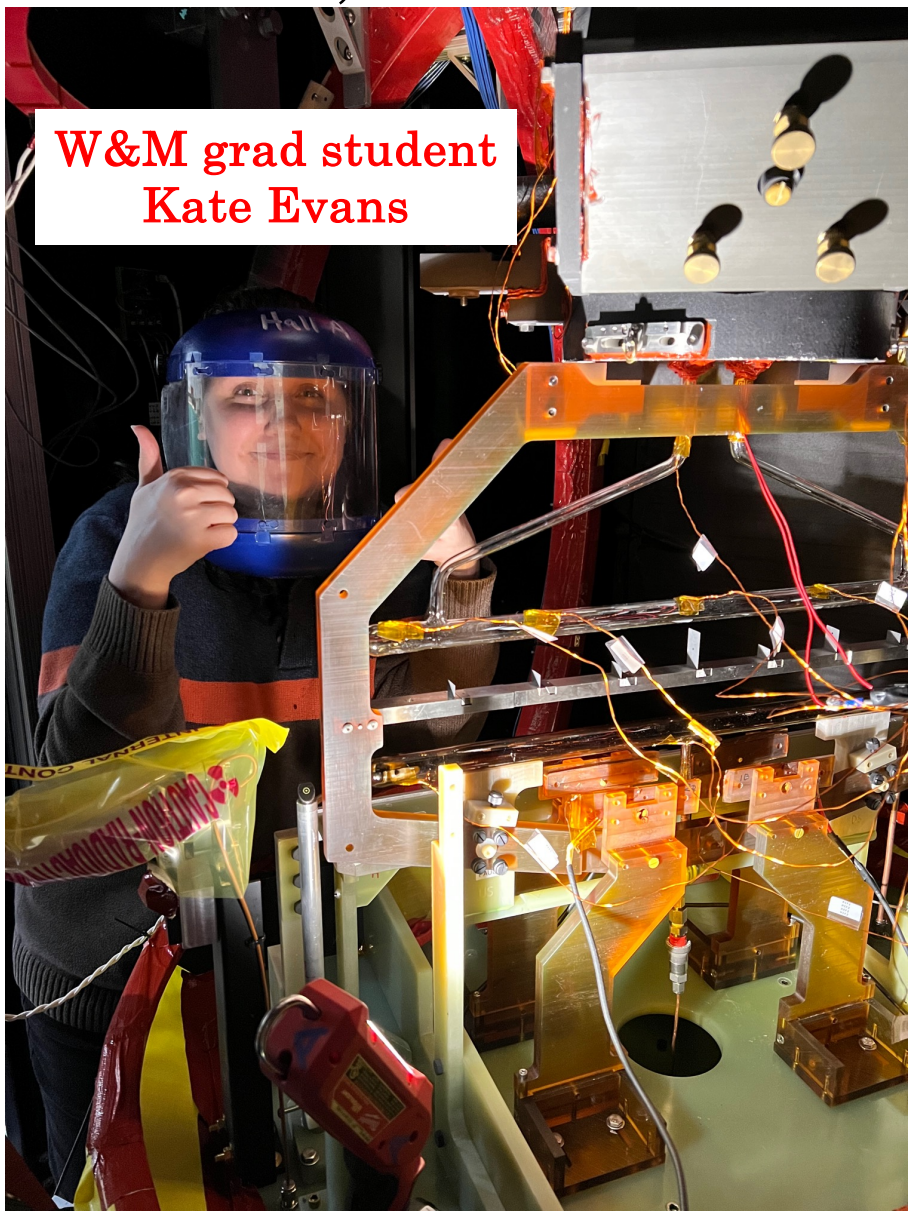

GEn-II polarized ^{3}He performance

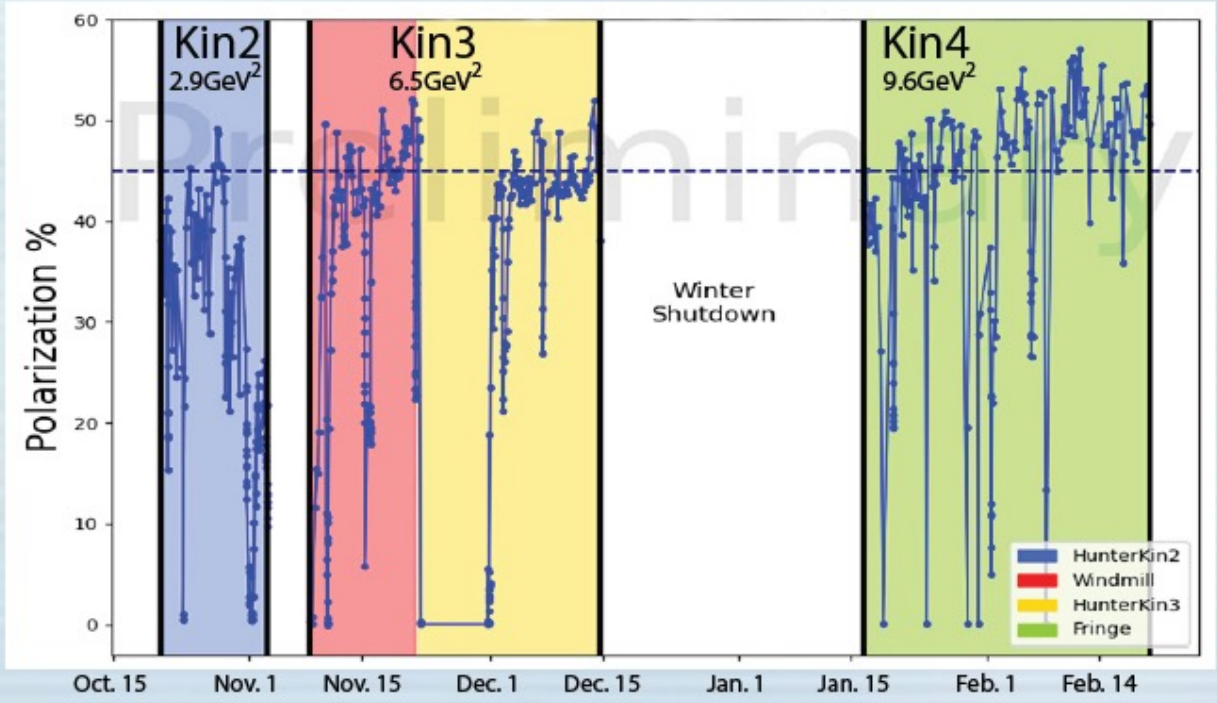

- At left is the polarization as a function of time for the three GEn-II kinematic settings.
- Note that we used Kin2 for commissioning which was possible because of the higher event rates at the lower value of Q^2 (2.9 GeV^2).
- Most data were taken with a beam current of 45μA (versus 30μA) previously
- With the 60 cm target chamber, the luminosity was a factor of 2.25 higher than all previous polarized 3He experiments at JLab.

- At right is shown the figure-of-merit (FoM) achieved for several JLab experiments including GEn-II.
- We define the FoM as luminosity times polarization squared, shown in units where the Hall C A1n experiment is set equal to unity.
- Typical performance of the GEn-II target was nearly x2 higher than A1n, with peak performance nearly x3 higher.
- It is notable that the integrated luminosity of GEn-II (thus far) is roughly equal to all previous 3He experiments at JLab.

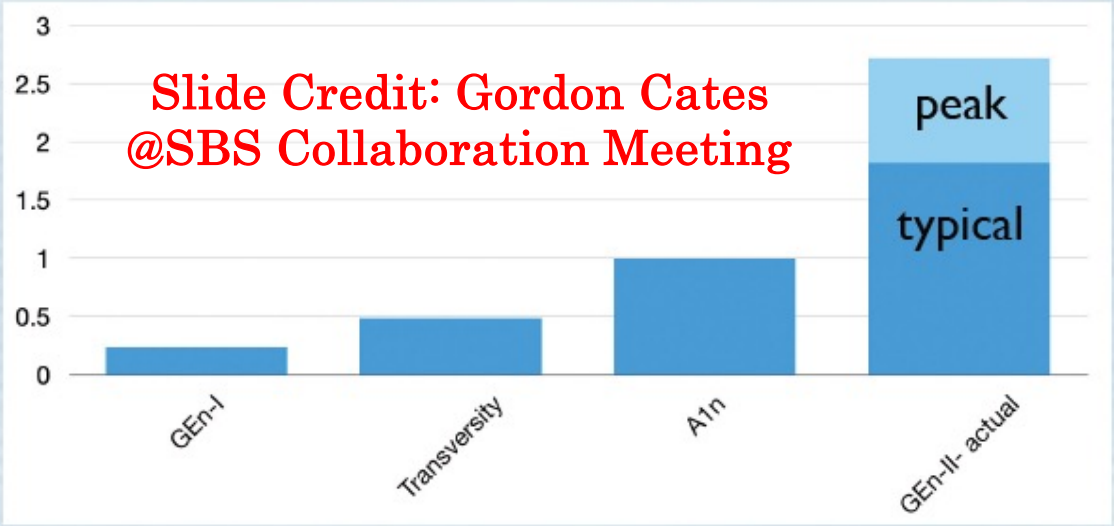

SBS-GEN: Quasi-elastic Event Selection ($Q^2 = 3\ GeV^2$)

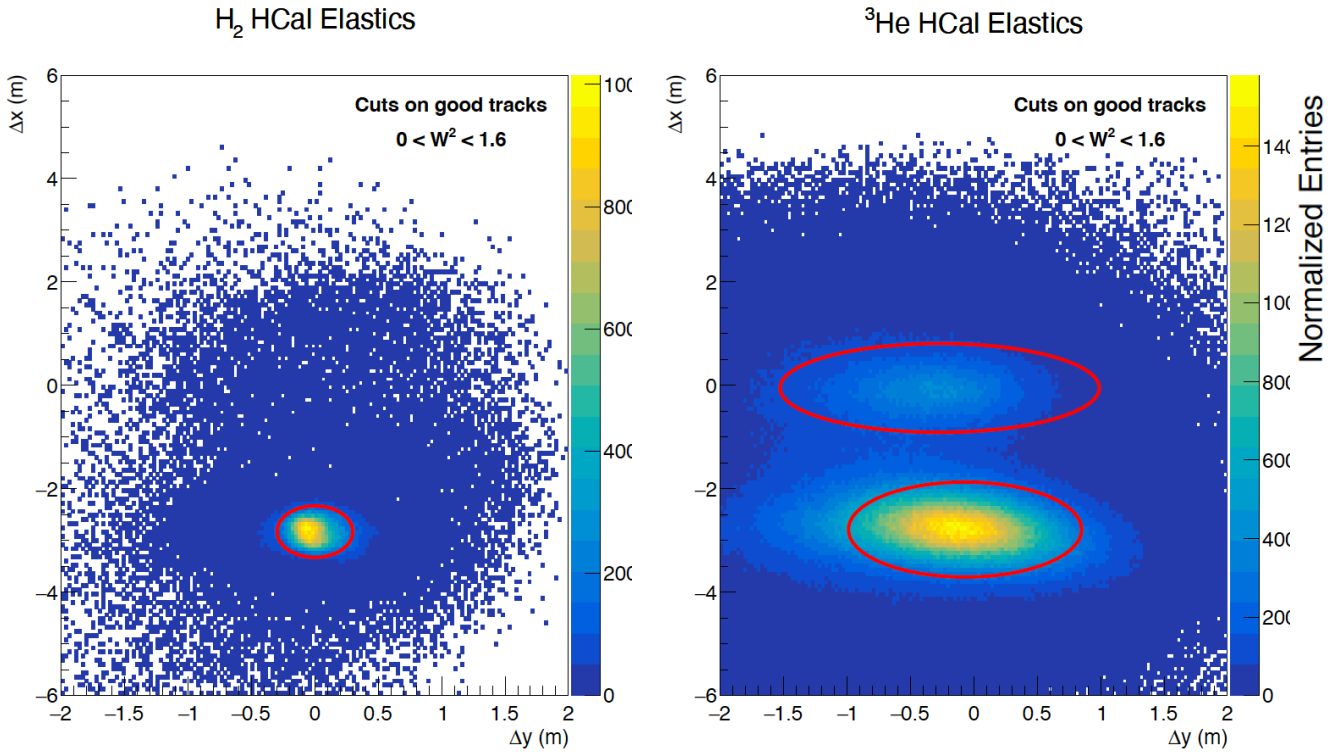

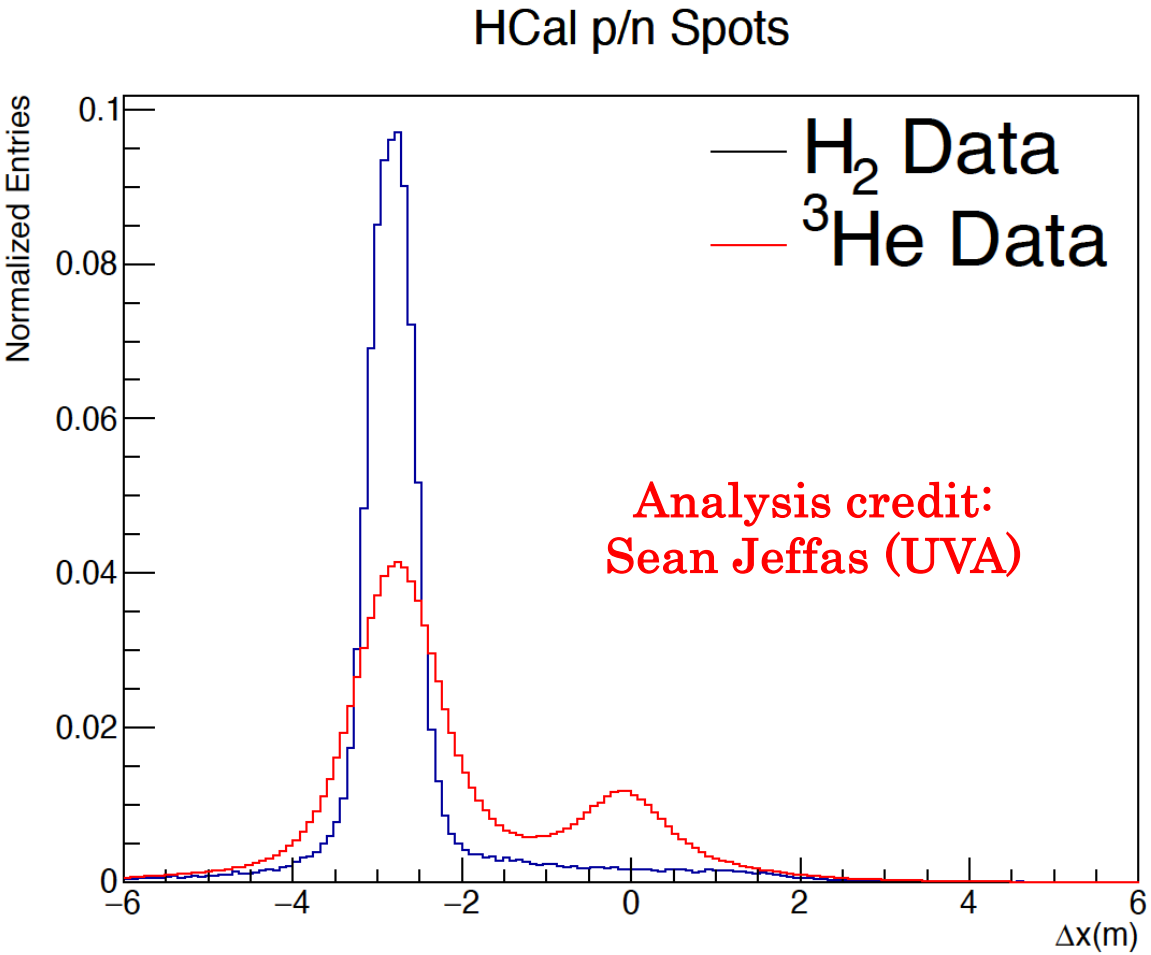

- Above, left (right): BigBite-HCAL angular correlation for hydrogen (Helium-3);
- Ellipses represent cuts for (e,e'p(n)) events
- Comparison between Helium-3 and hydrogen illustrates effects of Fermi motion.

- Projection along Δx (vertical) axis of the plots on the left

SBS GEN—Estimated ^{3}He(e,e'n)pp statistics, all Q^2 points

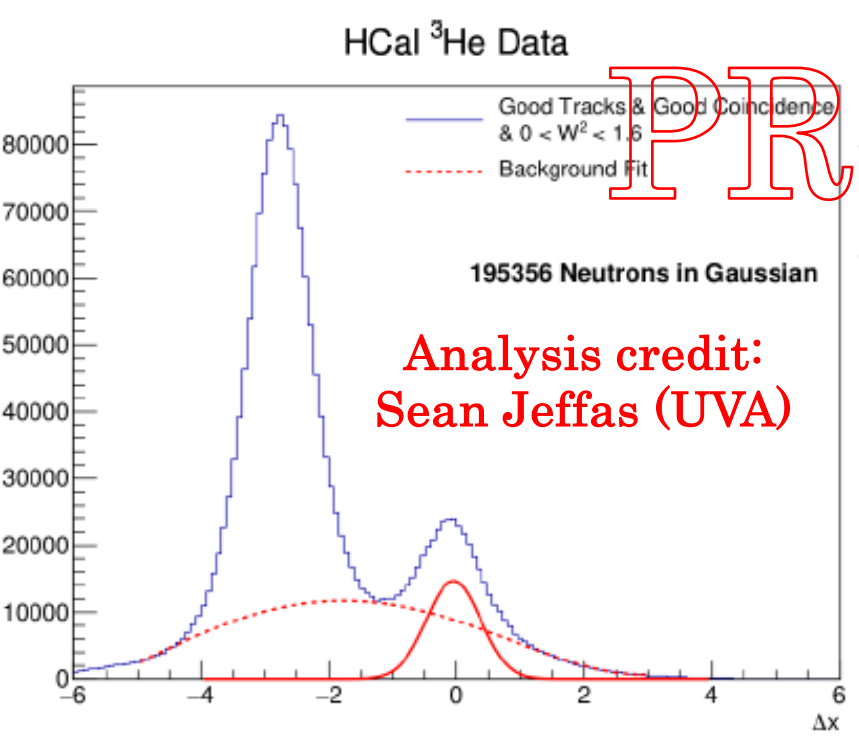

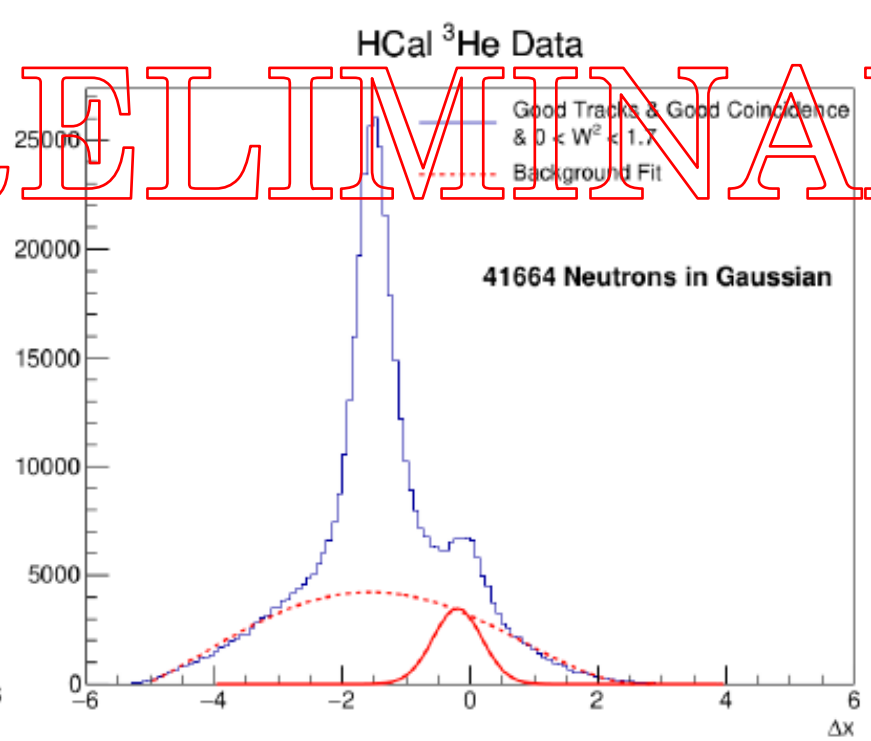

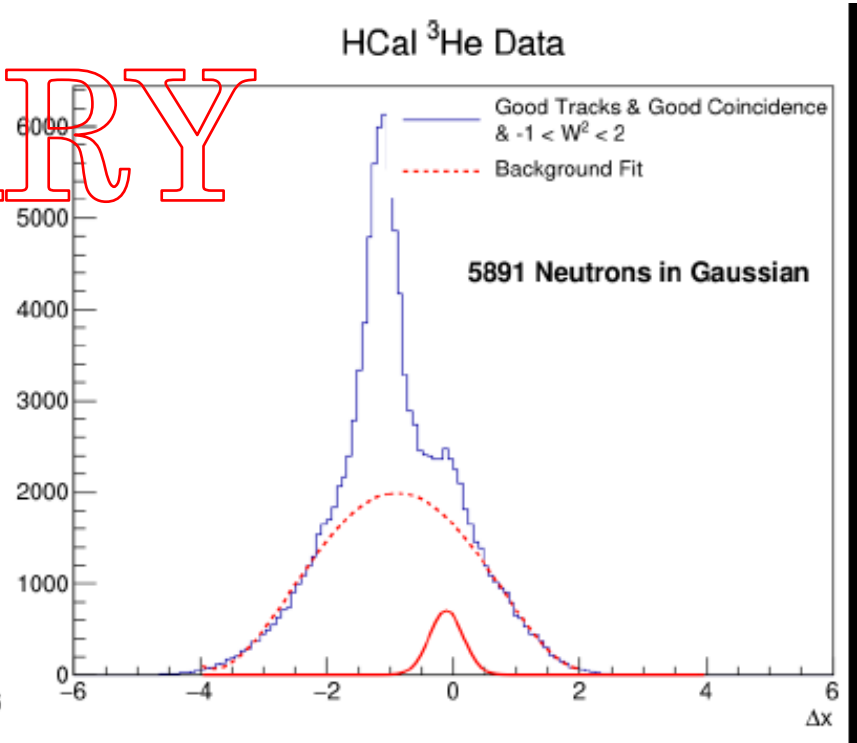

PRELIMINARY

Analysis credit: Sean Jeffas (UVA)

$Q^2 = 3.0$ GeV^2 $Q^2 = 6.8$ GeV^2 $Q^2 = 9.8$ GeV^2

- Estimated (e,e'n) coincidence yields with loose cuts on W^2 (and no other variables), from the first full reconstruction pass (statistics should increase in subsequent passes with improved calibrations and cuts)
- Signal/background will improve with more aggressive cuts (without meaningful reduction in (e,e'n) stats).
- These yields are in good agreement with expectations (for the present stage of analysis).
- **The data for $Q^2 = 9.8$ GeV^2 represent only half of the collected statistics (Fall 2023 data not yet "cooked")**

SBS GEN—"raw" asymmetries and projected physics results

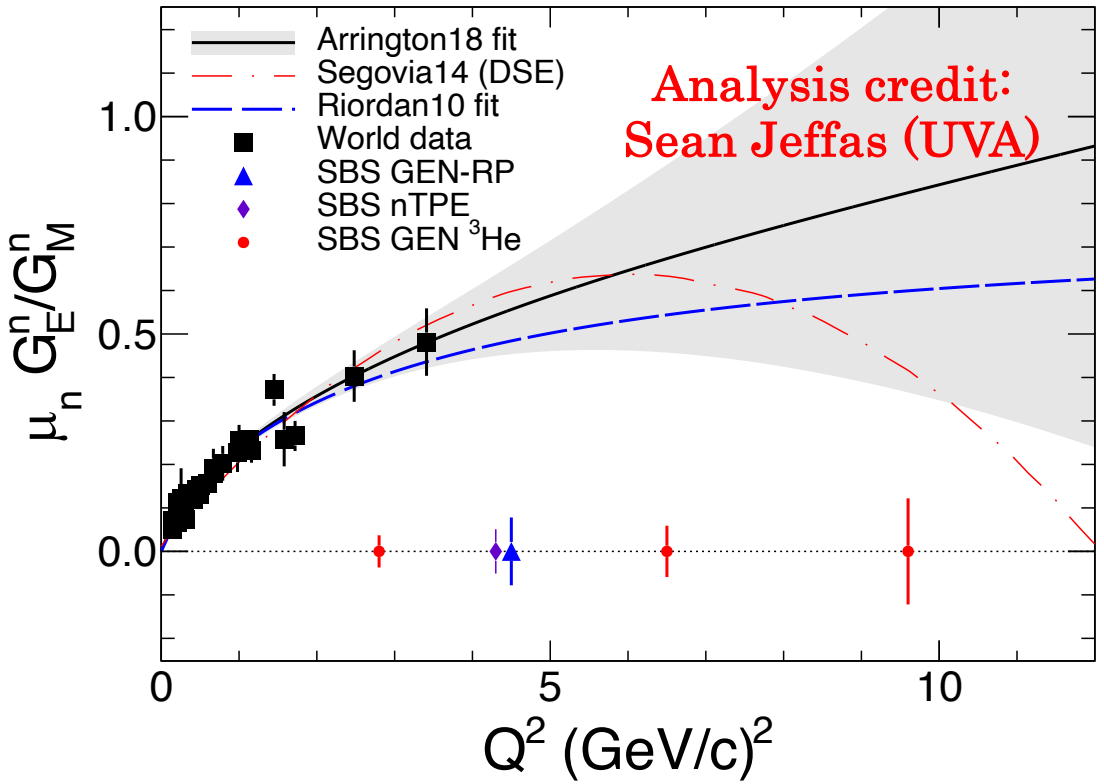

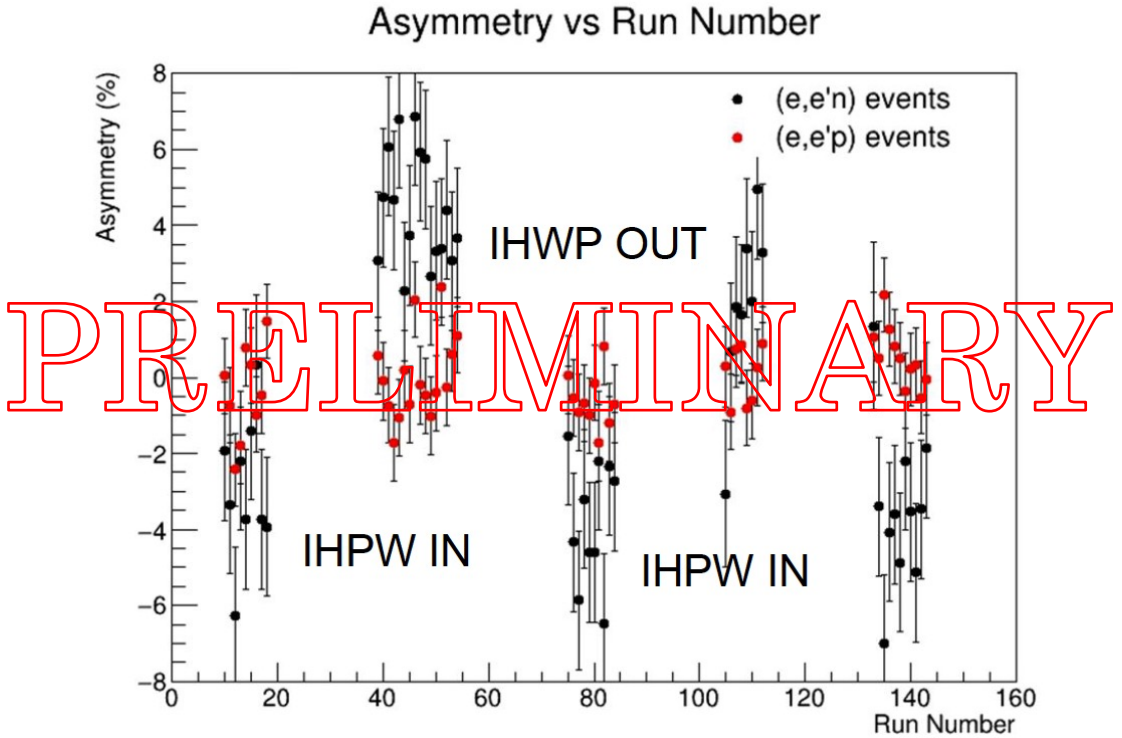

- Above, right: Projected statistical uncertainties in $\frac{\mu_n G_E^n}{G_M^n}$
- Above, left: Sanity-checking "raw" helicity asymmetries (neutron changes sign with IHWP reversal and proton asymmetries ~0)
- Below, right: Raw (e,e'n) yields (not background-subtracted) by helicity (IHWP corrected) and raw asymmetries

	GEN2		GEN3		GEN4	
	IHWP IN	IHWP OUT	IHWP IN	IHWP OUT	IHWP IN	IHWP OUT
Y+ Events	81981	52765	13341	10260	1893	2667
Y- Events	73381	47783	12502	9424	1857	2543
A	5.54% +/- 0.25%	4.95% +/- 0.31%	3.25% +/- 0.62%	4.25% +/- 0.71%	0.96% +/- 1.63%	2.38% +/- 1.39%
Total A	5.31% +/- 0.20%		3.25% +/- 0.62%		1.79% +/- 1.06%	

PRELIMINARY

E12-17-004 (GEN-RP): G_E^n/G_M^n to 4.5 GeV² via charge-exchange recoil polarimetry

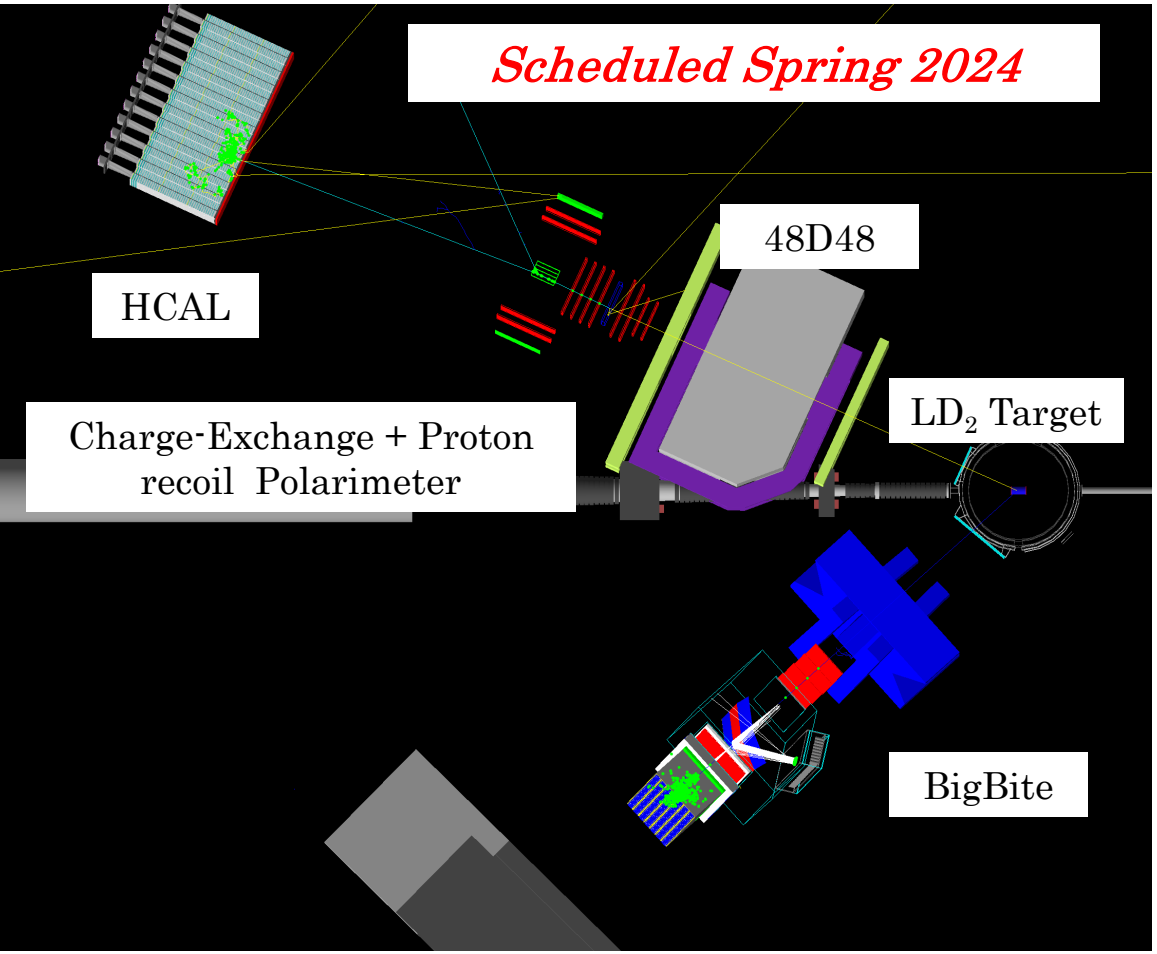

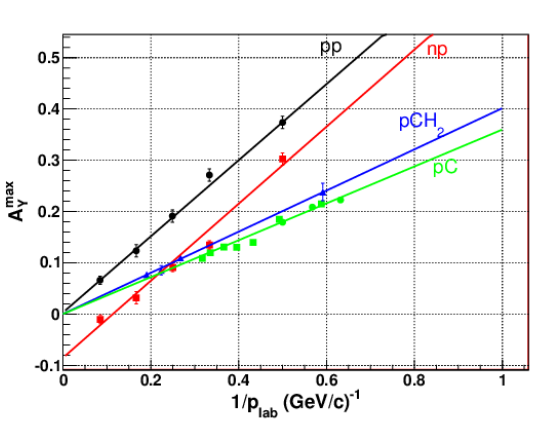

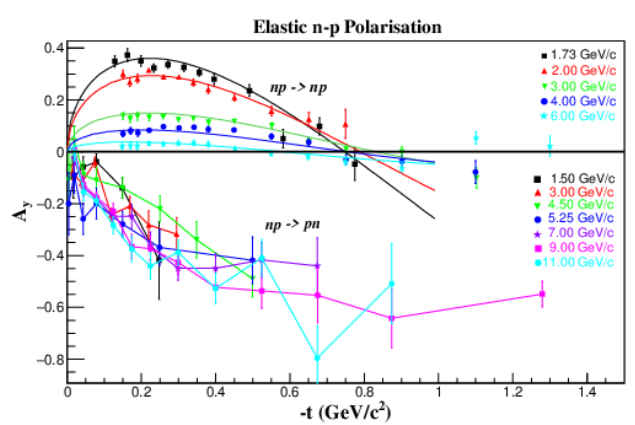

Analyzing powers for np, pp, pA scattering vs. initial momentum (left) and vs. transferred momentum (right)

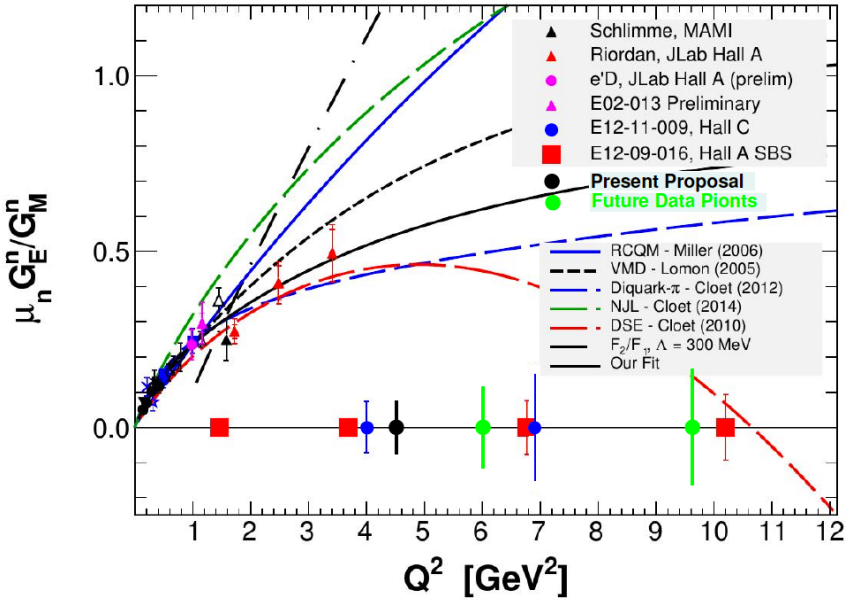

- E12-17-004 layout (above) and projected results (right):
  - First use of charge-exchange polarimetry in a FF experiment
- E12-20-008 approved as add-on to measure K_{LL} for $\gamma n \to \pi^- p$

The SBS G_E^p Experiment (E12-07-109): Scheduled 2024-2025

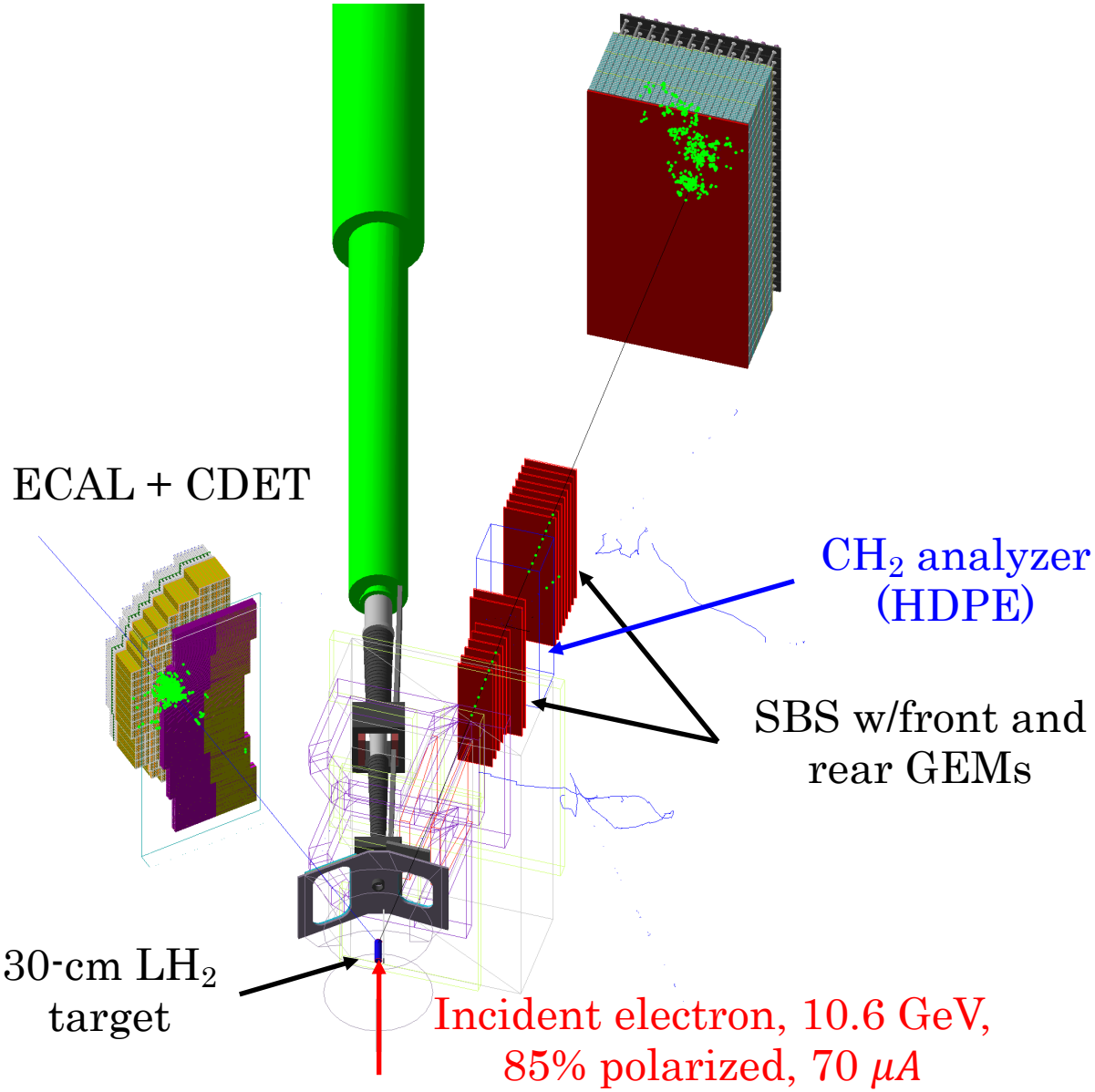

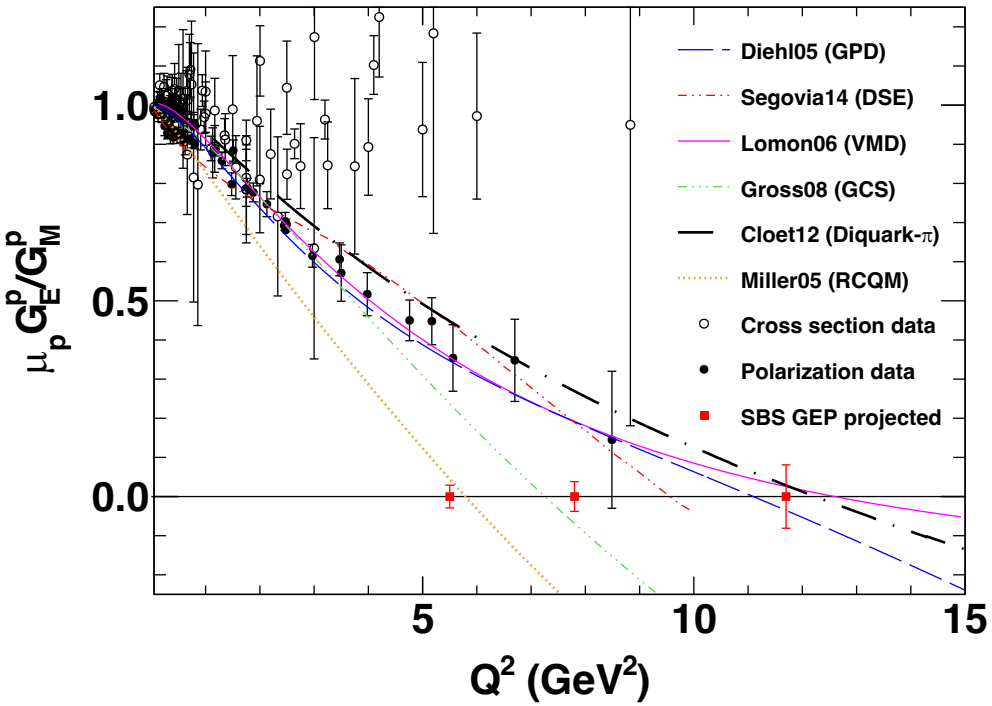

- Original motivation for SBS concept—first approved 2007
- **Designated "High Impact Experiment" by JLab PAC41**
- Jeopardy proposal reapproved by PAC47 in 2019
- **Currently scheduled to run 2024-2025**
- Novel high-temperature lead-glass calorimeter detects scattered electron with scintillator-based coordinate detector—trigger, aid tracking in front GEMs, and reject inelastics
- GEM-based trackers with CH_2 analyzer for proton polarimetry
- HCAL for trigger and preferential selection of nuclear scattering events with high analyzing power

SBS-GEP details; kinematics, event rates, uncertainties

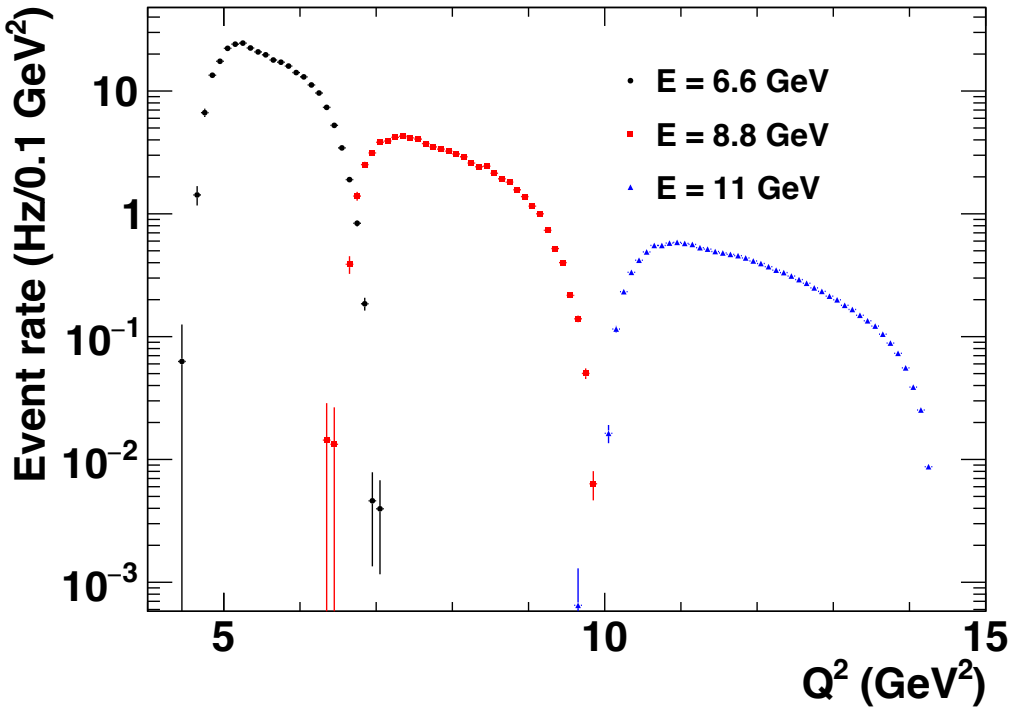

Above: Rate-weighted Q^2 acceptance of SBS GEP

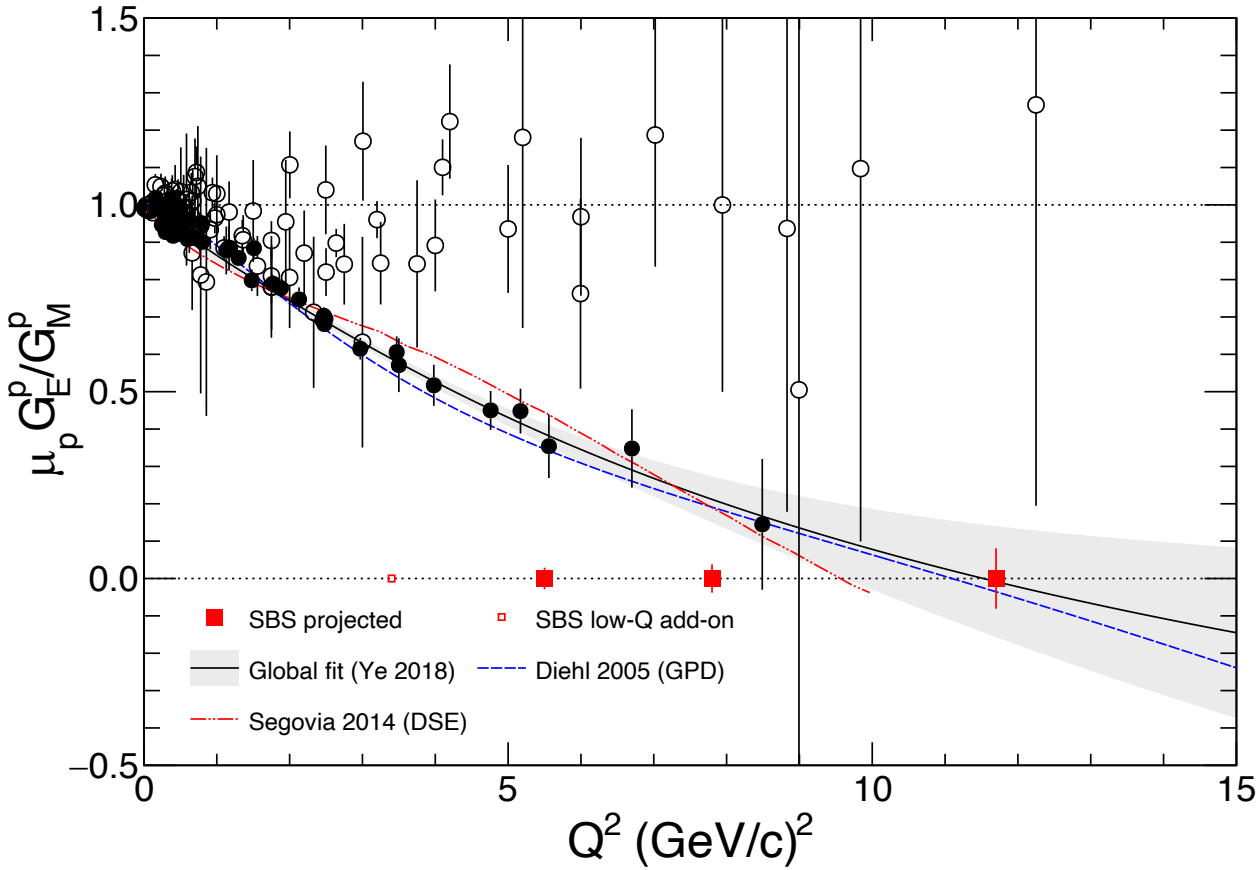

TABLE I. Kinematics, projected accuracy and beam time allocations. The projected statistical uncertainties in the form factor ratio include the assumption of 70% overall event reconstruction efficiency due to the combined efficiencies of the individual detectors, including DAQ dead-time.

E_{beam}, GeV	Q^2 range, GeV^2	$\langle Q^2 \rangle$ GeV^2	θ_{ECAL} degrees	$\langle E'_e \rangle$, GeV	θ_{SBS} degrees	$\langle P_p \rangle$ GeV	$\langle \sin\chi \rangle$ degrees	Event rate Hz	Days	$\Delta(\mu G_E/G_M)$
4.4[a]		3.4	32.5	2.54	31.1	2.56	0.44	1,050	1	0.01
6.6	4.5-7.0	5.5	29.0	3.66	25.7	3.77	0.72	291	2	0.029
8.8	6.5-10.0	7.8	26.7	4.64	22.1	5.01	0.84	72	11	0.038
11.0	10.0-14.5	11.7	29.0	4.79	16.9	7.08	0.99	13	32	0.081

[a] Add-on upcoming GEP run, to be proposed for comparison to future e^+p measurement

- SBS GEP status:
  - JLab Experiment Readiness Review completed April 2023
  - Scheduled Run in Hall A, Oct. 2024-March 2025

Future Directions in high-Q^2 EMFFs

Positrons @JLab

- https://inspirehep.net/literature/1809448

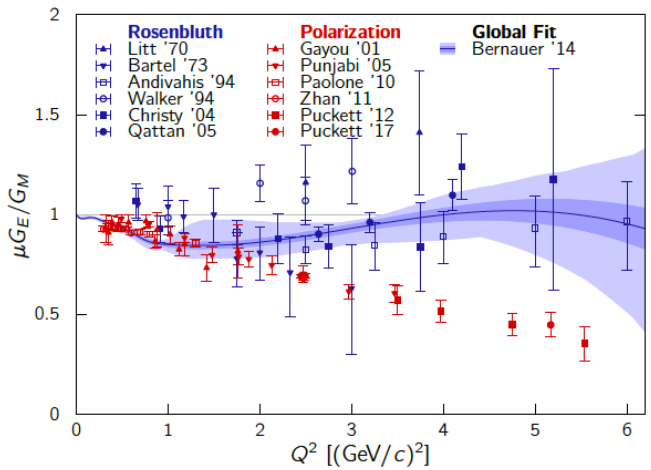

Fig. 1 A representative sample of the world data on the proton's form factor ratio, $\mu_p G_E/G_M$ shown as a function of squared four-momentum transfer, Q^2. Rosenbluth separations of unpolarized cross sections are shown in blue [48,49,50,51,52,53]. Polarized measurements are shown in red [35,36,37,38,39,40]. A global fit to unpolarized cross sections [59] is shown, along with statistical and systematic uncertainties, by a blue curve with light blue bands.

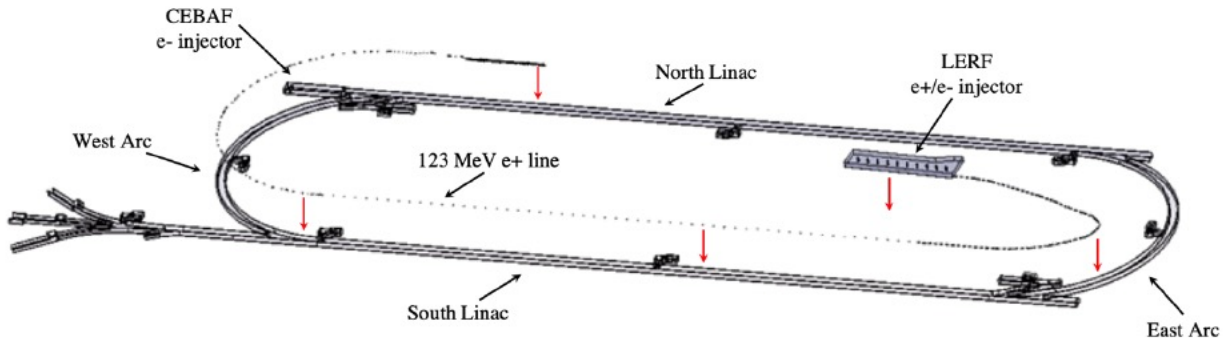

Figure 44: A new tunnel and beam line (shown raised) connects the LERF to CEBAF and transports the 123 MeV e^+ beam for injection and acceleration into CEBAF 12 GeV.

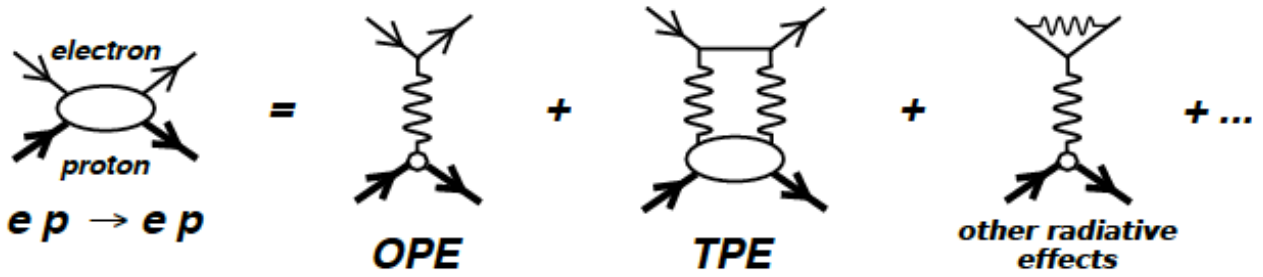

Fig. 2 Feynman diagram series for elastic electron-proton scattering. The two-photon exchange amplitude contributes at the same order as several other radiative processes.

Future of High-Q^2 EMFF measurements: EIC

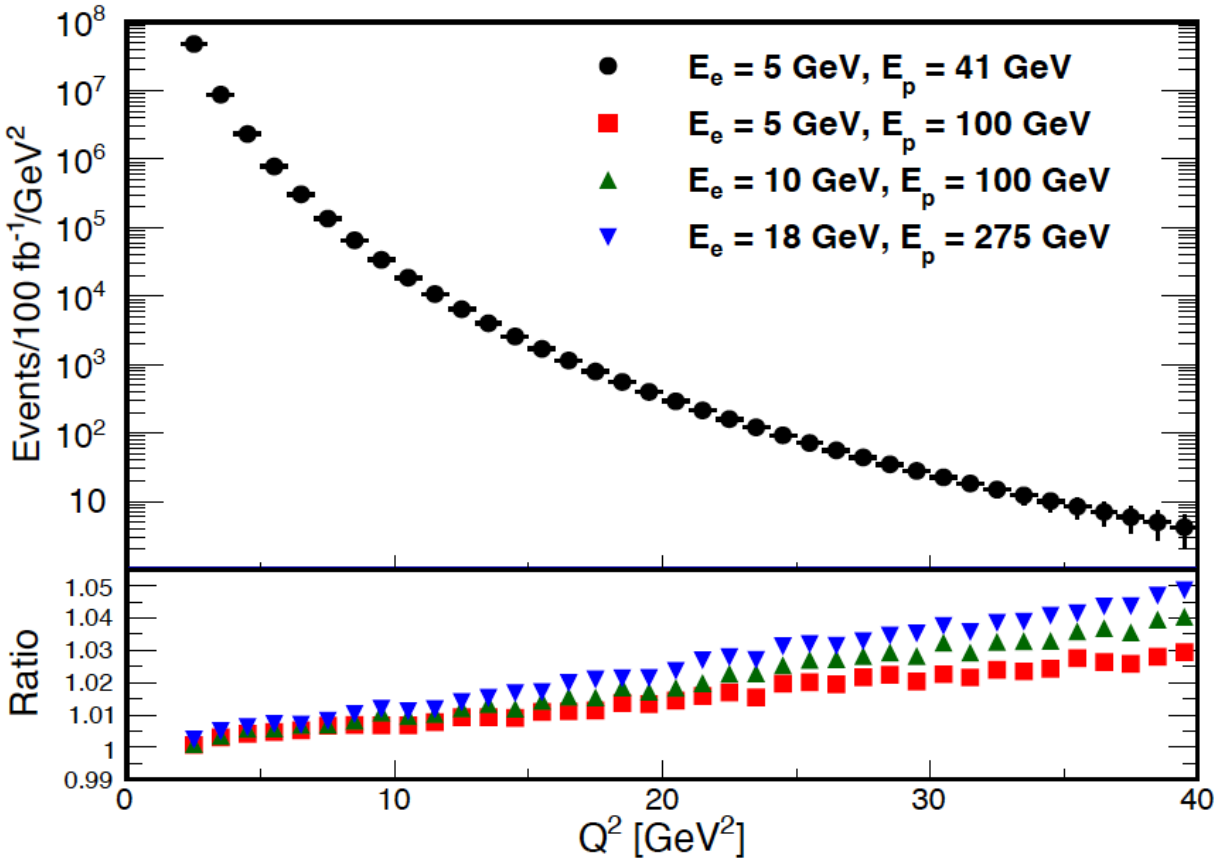

- Schmookler *et al.,* "High-Q^2 Electron-Proton Elastic Scattering at the Future Electron-Ion Collider": https://inspirehep.net/literature/2108947

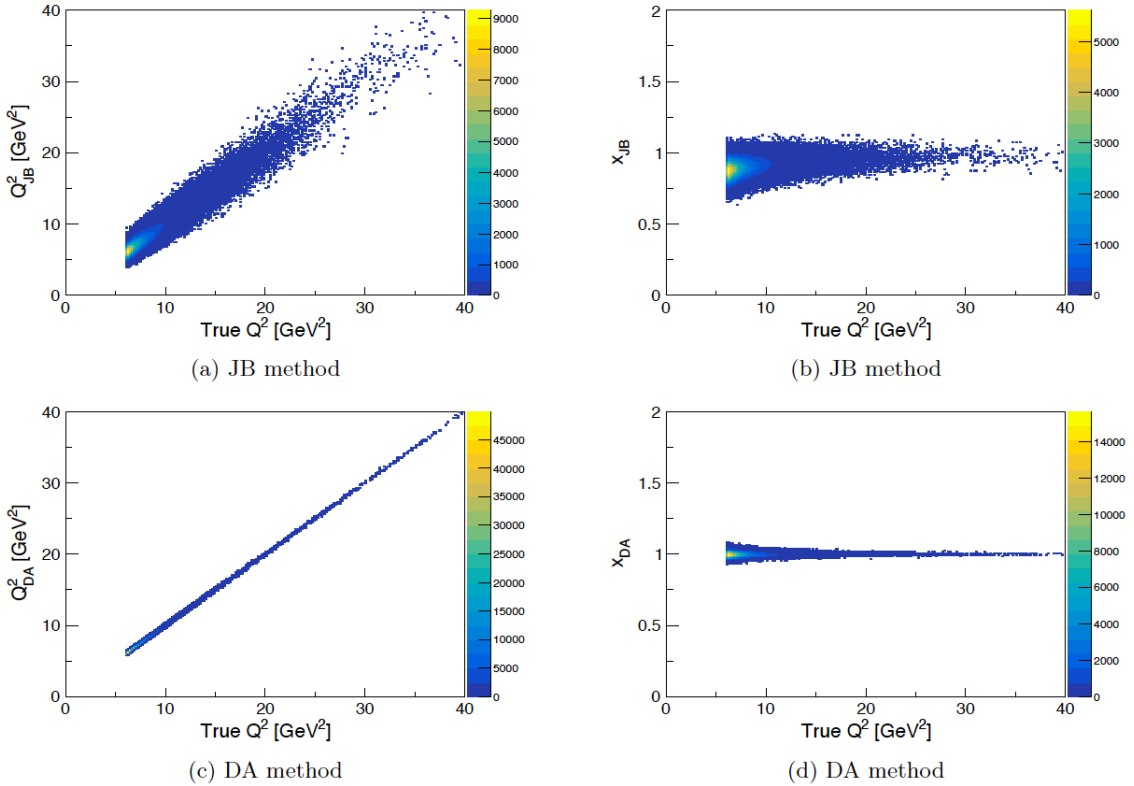

(a) JB method (b) JB method

(c) DA method (d) DA method

- At lowest CM energies that EIC will conceivably run, elastic $ep \rightarrow ep$ cross sections can conceivably be measured for $Q^2 \leq 40$ GeV^2 at $\epsilon \approx 1$.
- Requires detection of both proton and electron with good angular resolution/PID to cleanly tag elastic events

Future of high-Q^2 EMFFs: JLab22

$$\frac{d\sigma}{dQ^2} = \frac{4\pi\alpha^2}{Q^4}\frac{E'}{E}\cos^2\left(\frac{\theta}{2}\right)\frac{\epsilon G_E^2 + \tau G_M^2}{\epsilon(1+\tau)}$$

$$\frac{d\sigma}{d\Omega_e} = \frac{E'^2}{\pi}\frac{d\sigma}{dQ^2}$$

Experiment Design Considerations

- Precision ep cross sections determine G_M^p→High luminosity, precision spectrometers, e.g., Hall C HMS/sHMS. Detect scattered electron. Invariant mass resolution sufficient for clean selection of elastic.
- Medium-acceptance spectrometers (SBS+BigBite/ECAL): σ_n/σ_p for G_M^n, polarization transfer for G_E^p, G_E^n, high-luminosity polarized ^{3}He for G_E^n.
- Large-acceptance spectrometers (CLAS12 or SOLID): polarized proton targets (e.g., NH_3)

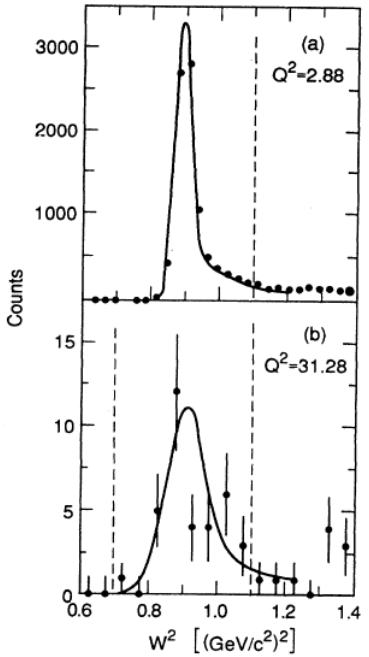

FIG. 19. Histograms of raw counts vs the missing mass squared at the highest and lowest values of Q^2 in this experiment. (a) $Q^2=2.883$ (GeV/c)^2. (b) $Q^2=31.28$ (GeV/c)^2. The curves show the expected resolution of the apparatus for each case, as determined from a Monte Carlo simulation of the experiment, including acceptance and radiative effects, but neglecting inelastic reactions. The data in each case show a clear peak with no significant background in the kinematically forbidden region of W^2 below the peak. The elastic radiative tail is visible above the peak. The data depart from the Monte Carlo curve near the threshold for pion production [$W^2=1.17$ (GeV/c)^2], as expected. The counts between the dashed vertical lines were summed to obtain the cross sections.

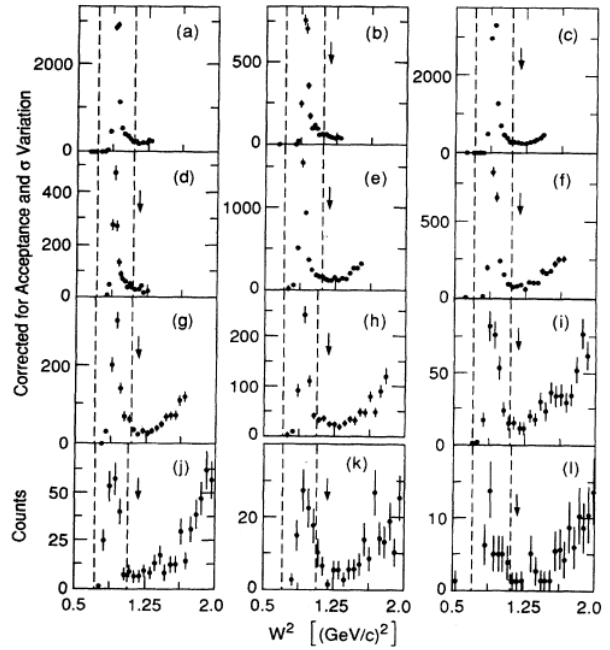

FIG. 20. Histograms of counts vs the missing mass squared corrected for the acceptance and summed over $\Delta\theta_{tot}$ as in Eq. (15). (a) $Q^2=2.9$ (GeV/c)^2, $\theta=21°$; (b) $Q^2=3.6$ (GeV/c)^2, $\theta=25°$; (c) $Q^2=5.0$ (GeV/c)^2, $\theta=21°$; (d) $Q^2=5.0$ (GeV/c)^2, $\theta=33°$; (e) $Q^2=7.3$ (GeV/c)^2, $\theta=21°$; (f) $Q^2=9.7$ (GeV/c)^2, $\theta=21°$; (g) $Q^2=11.9$ (GeV/c)^2, $\theta=21°$; (h) $Q^2=15.7$ (GeV/c)^2, $\theta=21°$; (i) $Q^2=19.4$ (GeV/c)^2, $\theta=21°$; (j) $Q^2=23.2$ (GeV/c)^2, $\theta=21°$; (k) $Q^2=27.0$ (GeV/c)^2, $\theta=25°$; (l) $Q^2=31.2$ (GeV/c)^2, $\theta=33°$. The threshold for pion production is marked by an arrow on these plots. Data points between the dashed lines were summed to yield the total counts N_{peak}. Counting rates in the kinematically forbidden region of W^2 below the lower cut value of 0.7 (GeV/c)^2 were negligible.

Sill, PRD, 48, 29 (1993): Note: highest SLAC beam energy was 21 GeV for these data

Future of high-Q^2 EMFFs: JLab22: https://arxiv.org/abs/2306.09360

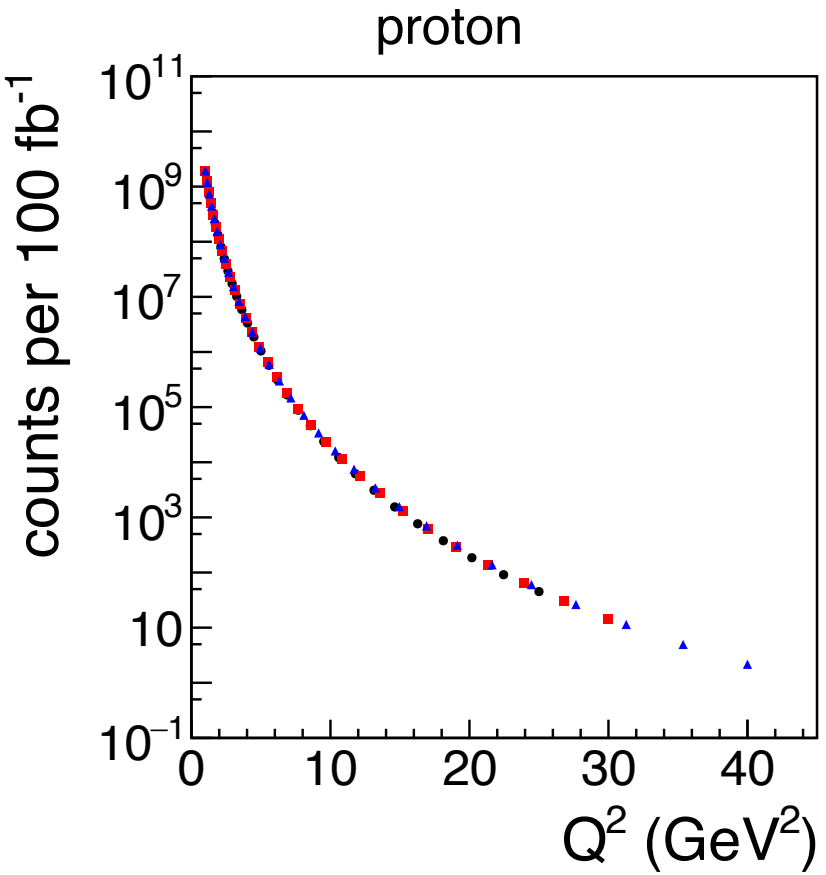

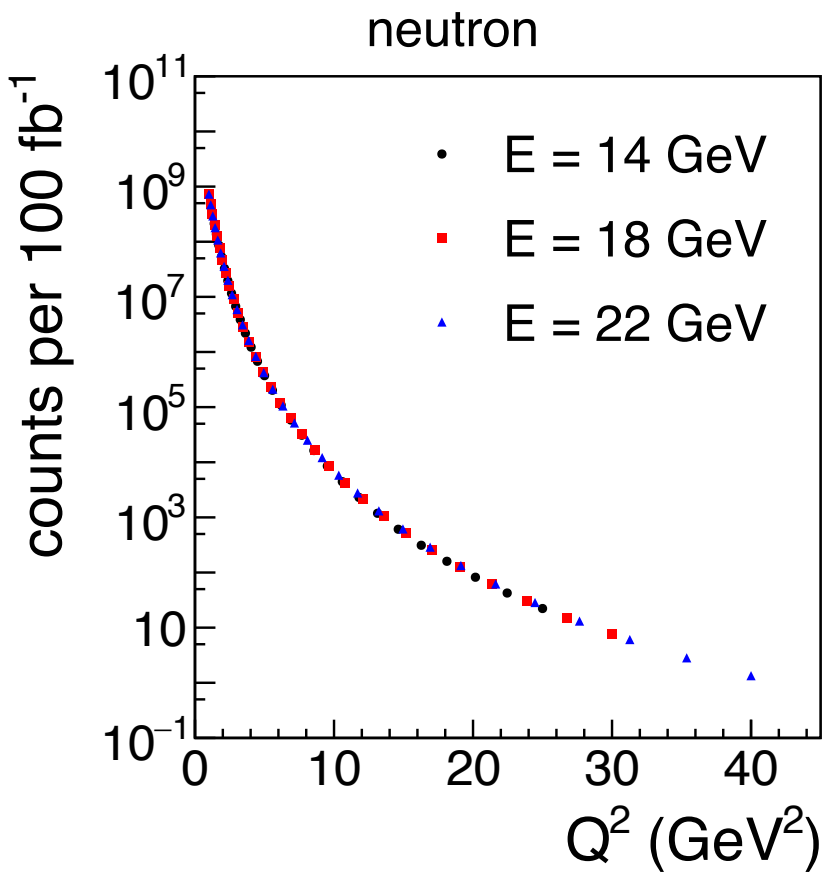

Luminosity (cm^{-2} s^{-1}, electron-nucleon)	fb^{-1}/day
10^{35} (NH_3/ND_3), polarized p/n	8.64
10^{37} (Helium-3 SEOP), polarized n	864
10^{38}-10^{39} (liquid hydrogen, deuterium)	8,640-86,400

- JLab high luminosity provides plenty of count rate up to max. accessible Q^2
- EIC ~100 fb^{-1} per YEAR (best-case)

- High-Q^2 measurements of G_E^p, G_E^n , require polarization observables; transverse asymmetry/recoil polarization maximum at $\epsilon = 0.5$.
- Need high luminosity and relatively large *lab-frame* electron scattering angle; only fixed-target experiments at higher energy can go significantly beyond JLab12/SBS for Sachs electric (G_E)/Pauli (F_2) form factors.

Summary and Conclusions

- High-Q^2 nucleon form factor measurements remain a highly active area.
- The SBS program (in Hall A), designed to facilitate these measurements, is roughly 2/3 complete as of today
- Neutron form factor measurements (nearly) completed; Q^2 coverage and precision goals largely achieved
- Proton FF ratio to 12 GeV^2 coming 2024-2025
- Future positron program at CEBAF to address TPE in elastic scattering
- EIC and (especially) JLab 22-GeV upgrade holds promise to enable the next major push beyond JLab12/SBS
- Expect a dramatic leap forward in understanding over the next few years as the SBS results come out!

Backups

Elastic *eN* Scattering Kinematics for JLab 22

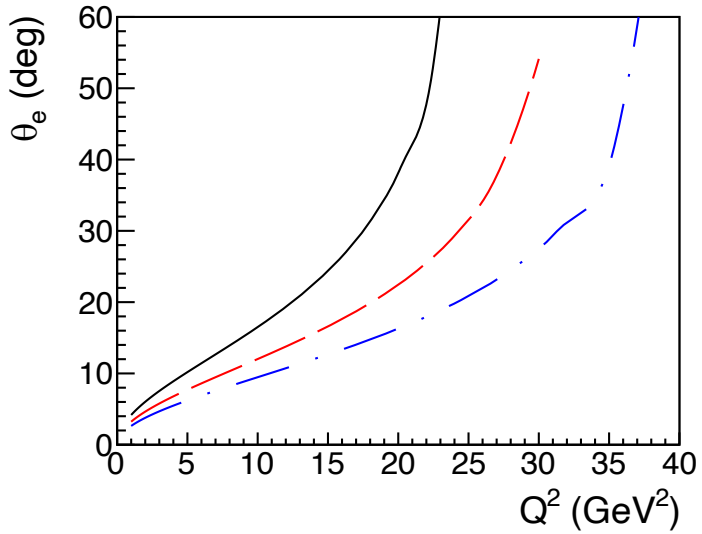

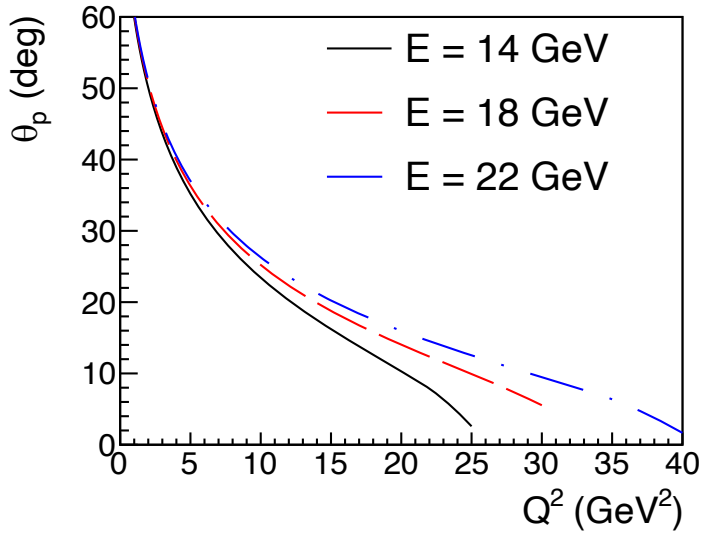

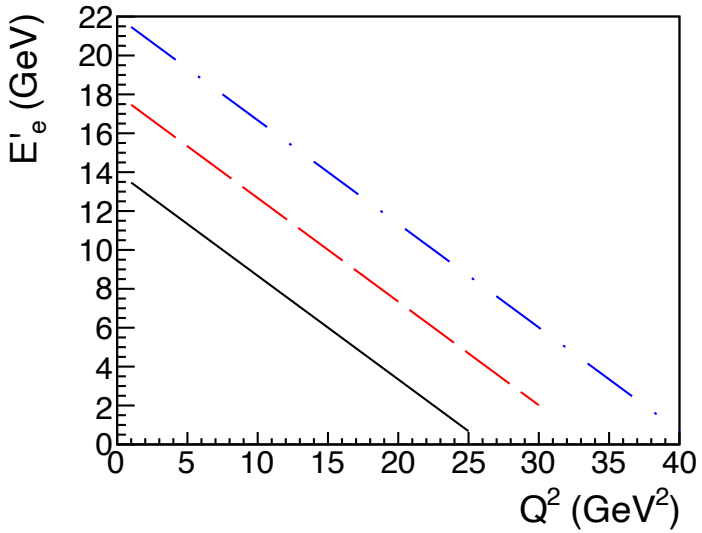

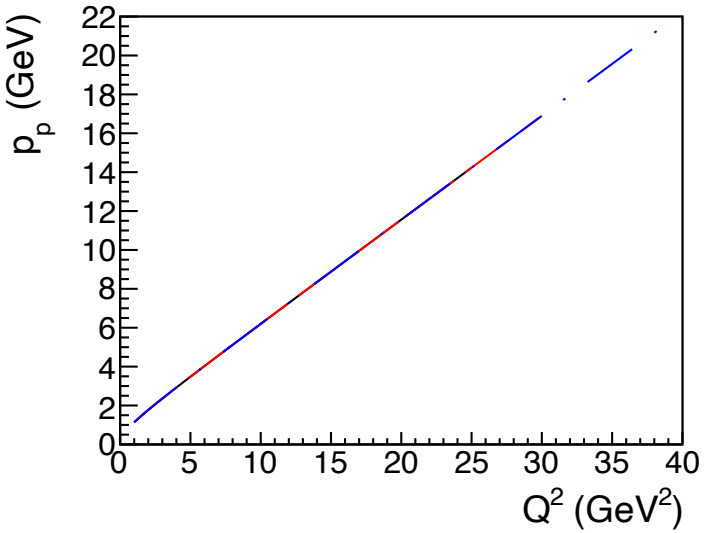

- Scattering angles are well matched to the acceptances of both small-acceptance and large-acceptance devices (CLAS12, SOLID, SBS+BigBite, HMS/SHMS)
- Particle momenta are rather high →
  - Challenge for Hall C spectrometers in some kinematic regions
  - Challenging in terms of resolution for large-acceptance spectrometers in some kinematic regions
- Nonetheless, even existing spectrometers should be able to cover a lot of new phase space

Virtual photon polarizations

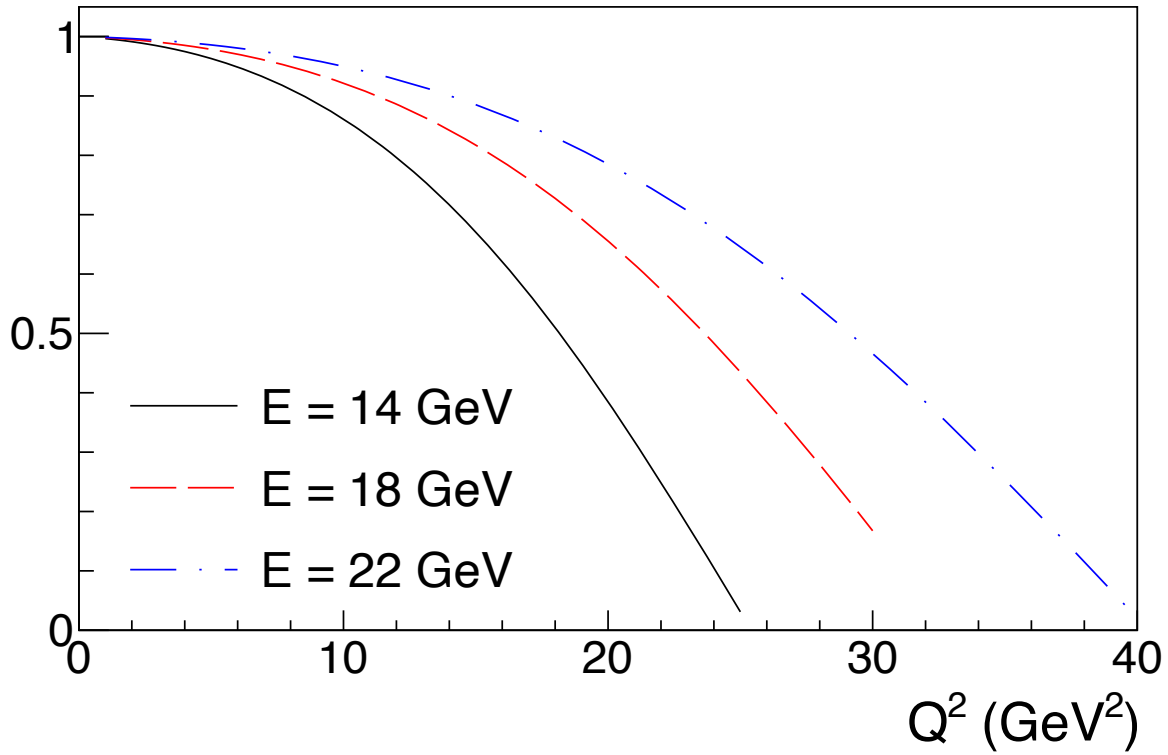

$$A_{eN} \equiv \frac{\sigma_+ - \sigma_-}{\sigma_+ + \sigma_-} = P_{\text{beam}} P_{\text{targ}} \left[A_t \sin\theta^* \cos\phi^* + A_\ell \cos\theta^* \right]$$

$$A_t = -\sqrt{\frac{2\epsilon(1-\epsilon)}{\tau}} \frac{r}{1 + \frac{\epsilon}{\tau} r^2}$$

$$A_\ell = -\frac{\sqrt{1-\epsilon^2}}{1 + \frac{\epsilon}{\tau} r^2}$$

$$r \equiv \frac{G_E}{G_M}$$

- Higher passes provide good lever arm in ϵ, for polarization observables and Rosenbluth separations in the range $10 \leq Q^2 \leq 30$ GeV^2
- Optimal beam energy at a given Q^2 for polarization observables is $\epsilon \approx 0.5$
- **Unique to JLab; EIC always has $\epsilon \approx 1$**

Asymmetries/Polarizations: Proton

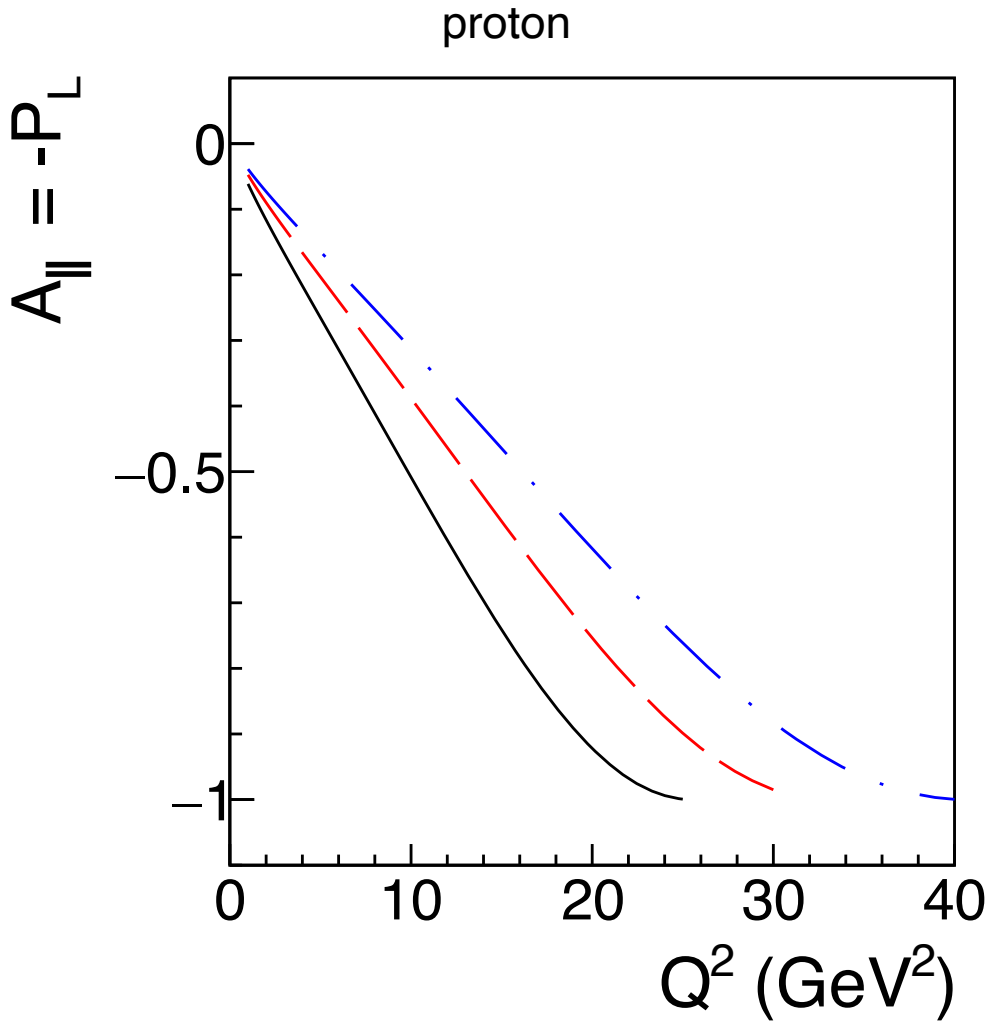

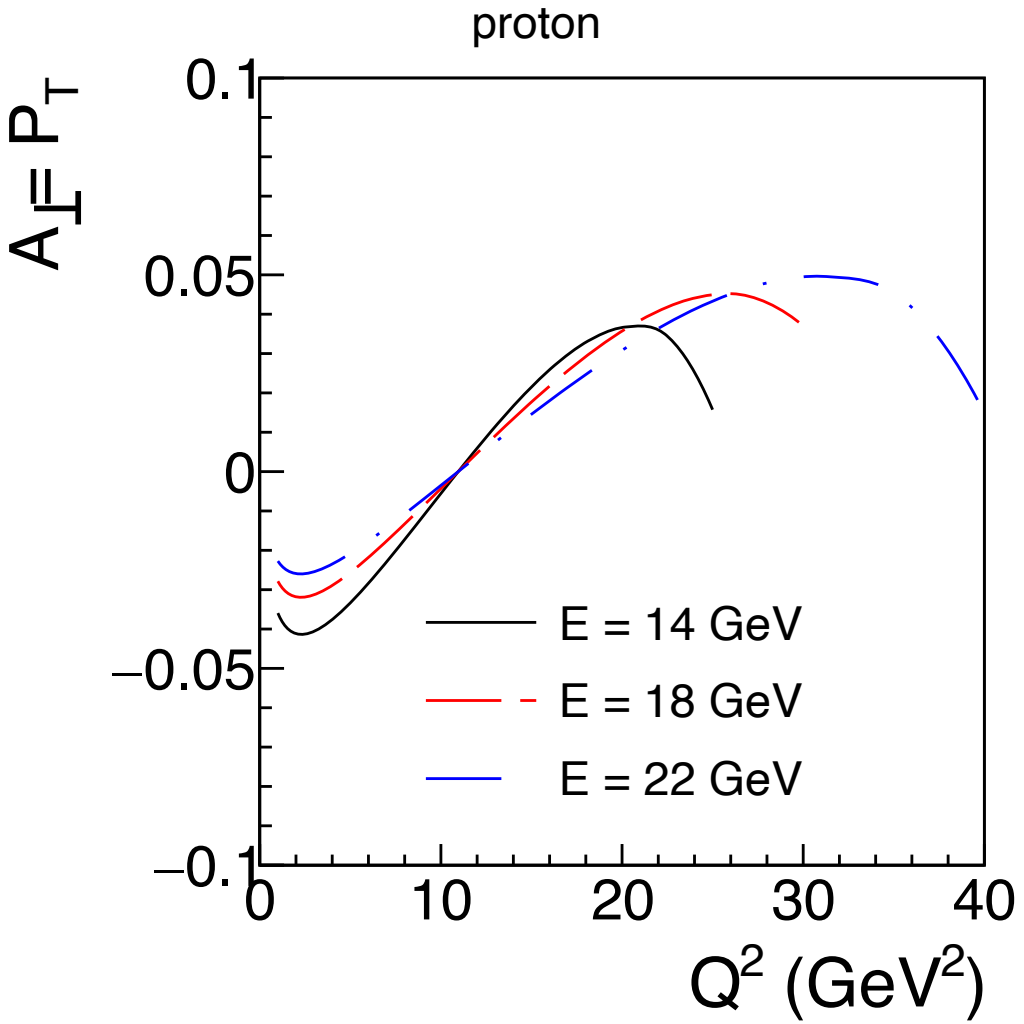

Different passes give optimal FOM for different Q^2's

Asymmetries/Polarizations: Neutron

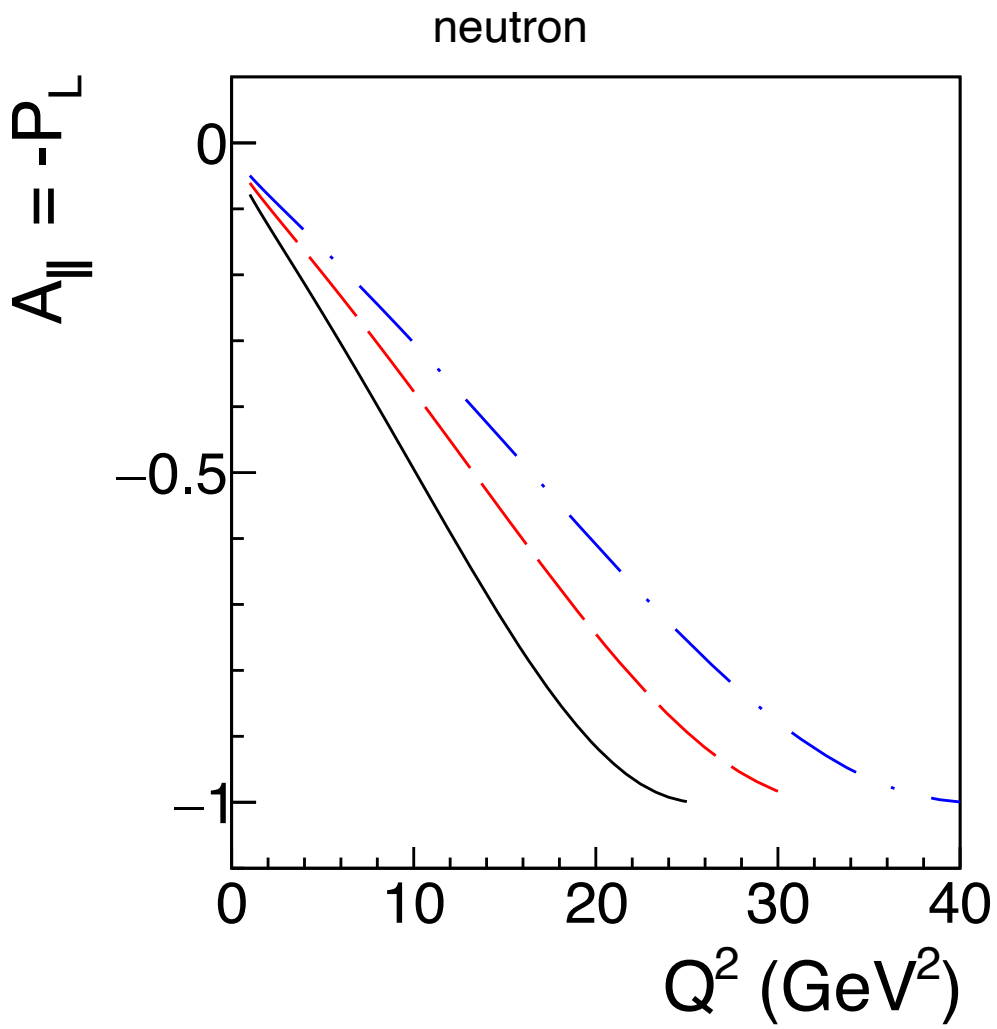

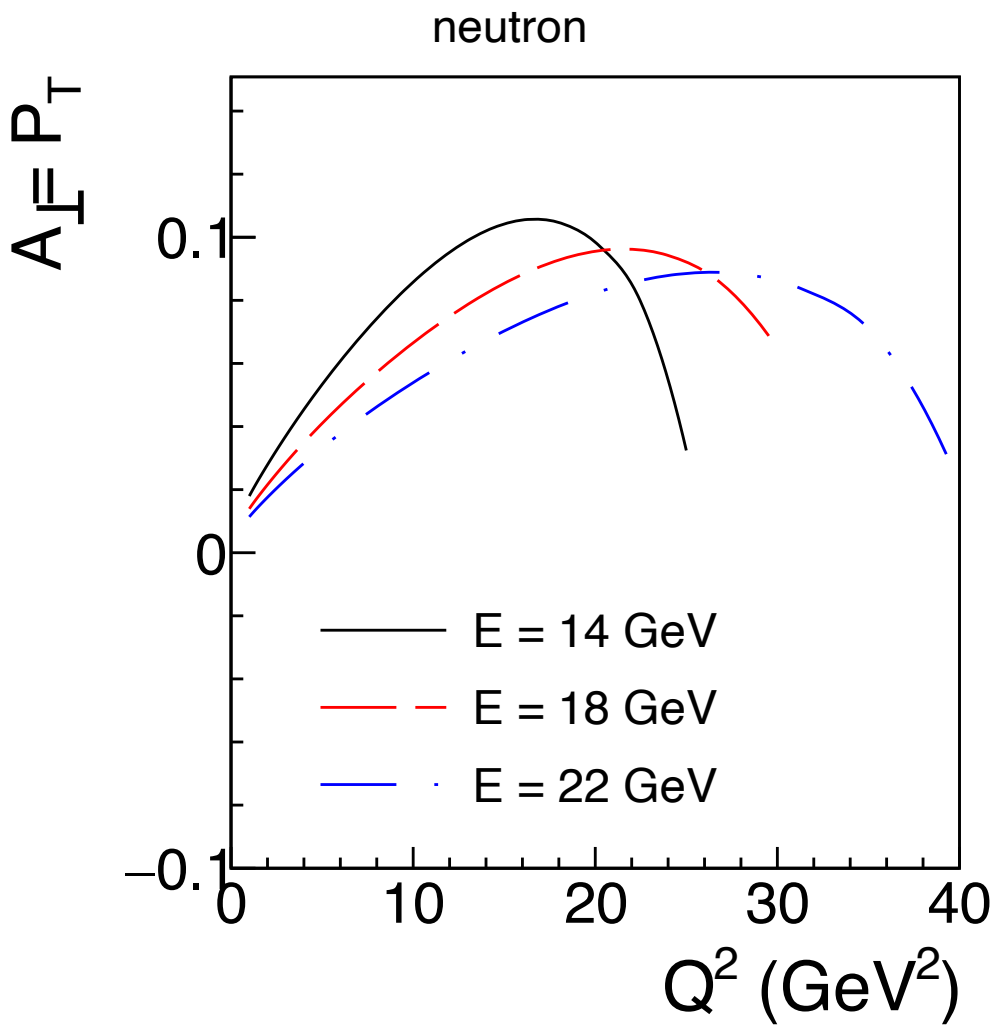

Different passes give optimal FOM for different Q^2's

Neutron Form Factors

- More difficult to measure than the proton due to lack of free neutron targets
- Far less accurately known than the proton FFs over a far more limited Q^2 range
- Cross section dominated by G_M^n over most of measured Q^2 range
- Most reliable G_E^n data come from polarization observables
- Most reliable G_M^n data come from "ratio" method on deuterium: first proposed by Durand, Phys. Rev. 115, 1020 (1959)
  - Some extractions also exist from absolute cross section and polarization measurements

"Ratio" method for G_M^n

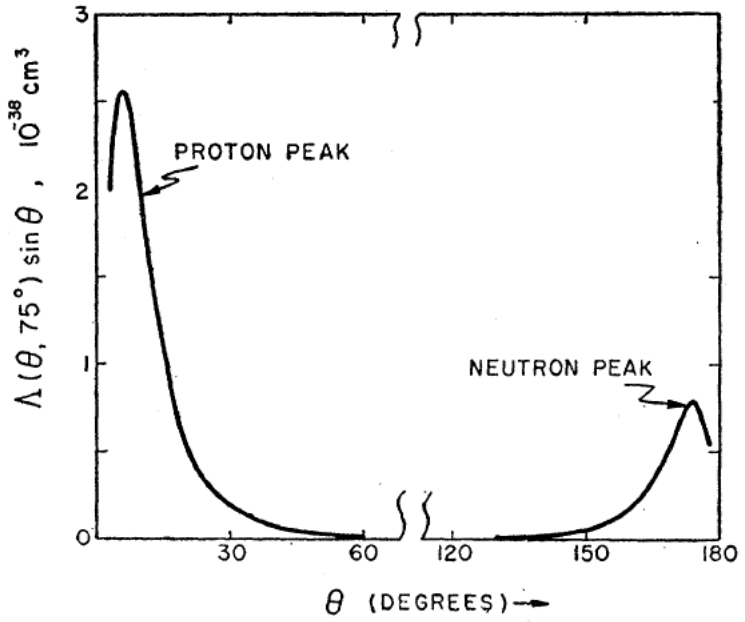

FIG. 1. The angular distribution function $\Lambda(\theta,\vartheta)\sin\theta$ in the absence of final-state interactions is plotted as a function of the proton scattering angle in the nucleon center-of-mass system $[\cos\theta=\hat{p}\cdot\hat{q}]$ for the scattering of 500-Mev electrons through an angle $\vartheta=75°$ with a momentum transfer giving $p=\frac{1}{2}q=1.3\times10^{13}$ cm^{-1}. $\Lambda(\theta,\vartheta)$ is defined in Eq. (11.2); the function $F(\theta)$ entering the definition was evaluated using a Hulthén wave function for the deuteron. The cross section $d^3\sigma/(d\theta d\Omega_e dE_e')$ is given by $(4.71\times10^5$ cm^{-1} rad^{-1} sterad^{-1} Mev$^{-1})$ $\Lambda(\theta,\vartheta)\sin\theta$. No nucleon form factors have been introduced into the results.

Figure from Durand, 1959 (see previous slide for reference)

- Idea: simultaneous measurement of $d(e,e'n)p$ and $d(e,e'p)n$ in quasi-elastic kinematics
- Simultaneous measurement cancels many sources of experimental systematic uncertainty (electron acceptance/detection efficiency, luminosity, detector and DAQ livetime, etc).
- Small nuclear model dependence—nuclear effects similar/nearly identical for (e,e'n) and (e,e'p) cross sections
- Combine with existing knowledge of free proton cross section to extract free neutron cross section
- **Major remaining source of systematic uncertainty is the relative acceptance/efficiency between protons and neutrons! → SBS-HCAL was designed to minimize this**

High-Q^2 G_M^n and quark flavor FFs

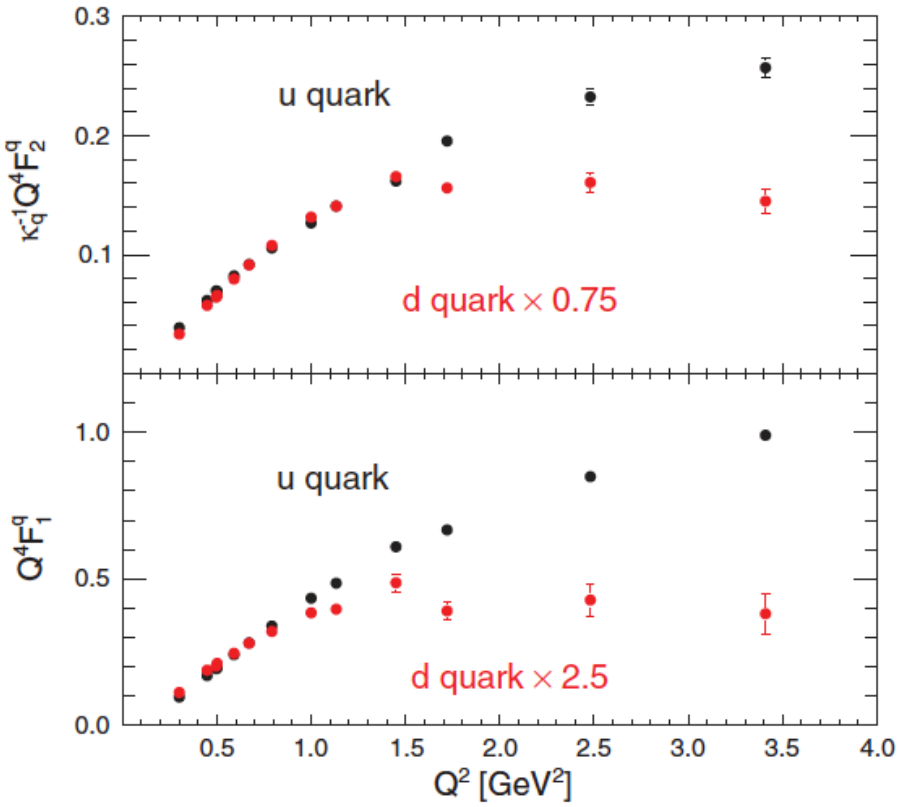

FIG. 3 (color). The Q^2 dependence for the u and d contributions to the proton form factors (multiplied by Q^4). The data points are explained in the text.

Cates *et al.*, PRL 106, 252003 (2011)

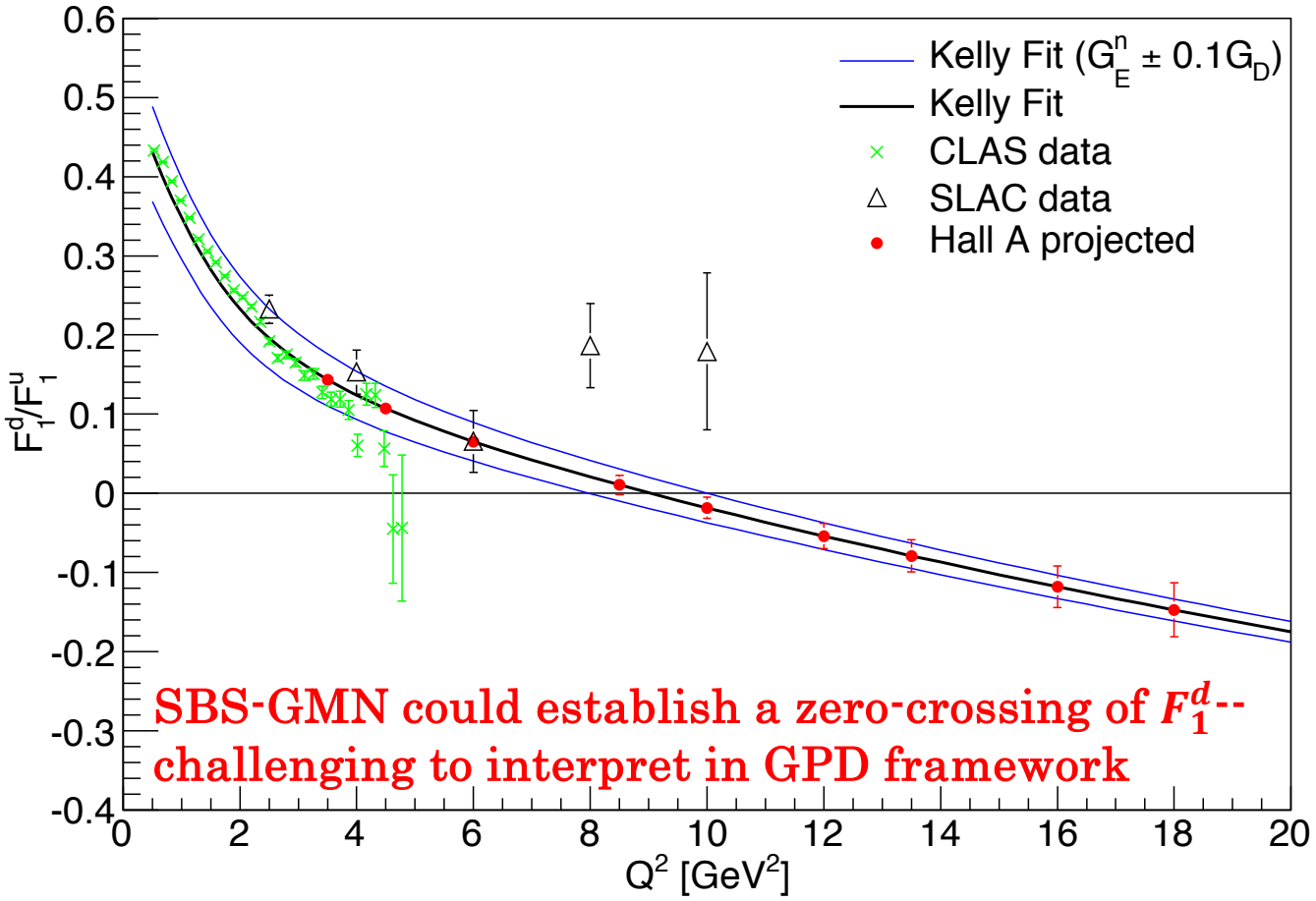

- Notable behaviors: d and u quark FFs show dramatically different Q^2 dependence.
- Flavor FF ratios F_2^q/F_1^q almost constant for both u and d above 1 GeV^2

Nuclear corrections—Mainly FSI

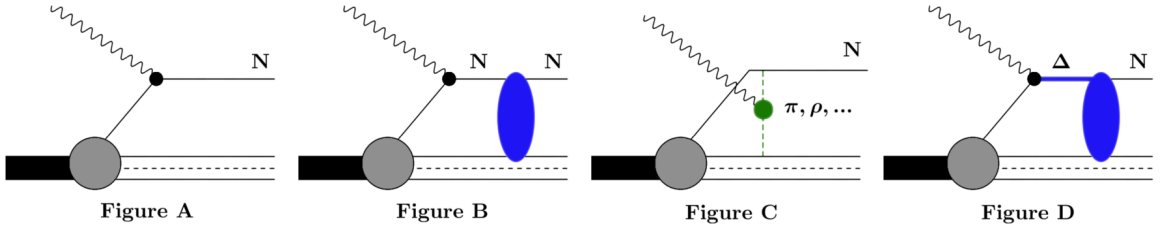

Figure A Figure B Figure C Figure D

- Nuclear corrections calculated within Generalized Eikonal Approximation framework
  - Cross section/asymmetry calculation code provided by Misak Sargsian (FIU)
  - Event-by-event MC simulation folded with experimental acceptance—lots of numerical integration, computationally expensive! (Much easier to do with 2019 JLab scientific computing facilities than 2009)
- A: PWIA
- B: FSI/charge-exchange
- C: Meson Exchange Currents
- D: Isobar Configurations
- Diagrams "A" and "B" dominant in E02-013 kinematics
- Exclusivity selection increases effective neutron polarization from the canonical 86% (of P_{He}) in the inclusive case to 96% in the coincidence—quasi-elastic case.

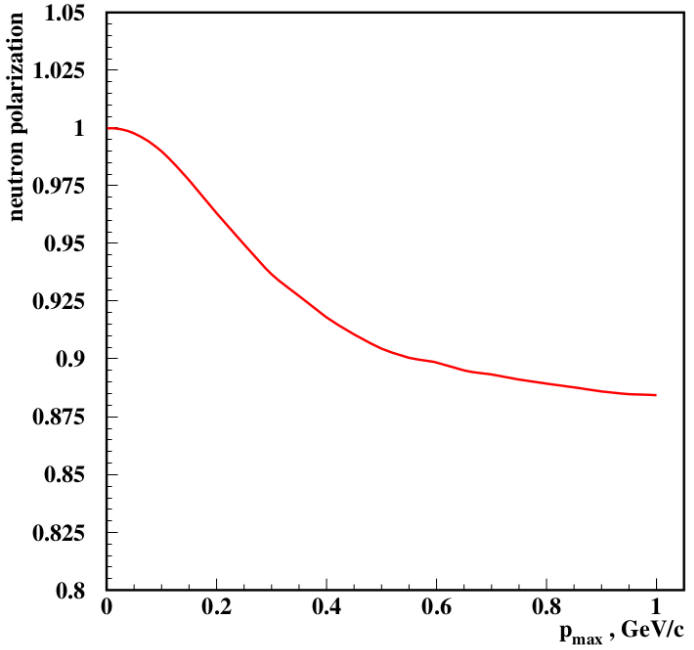

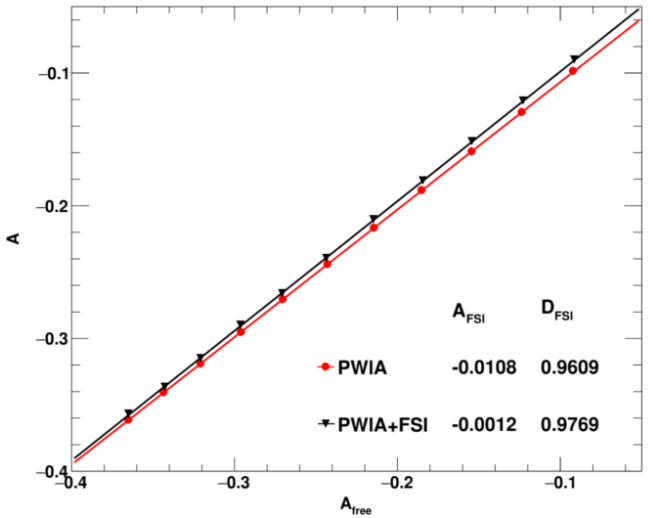

GEN in *g4sbs*: Overview

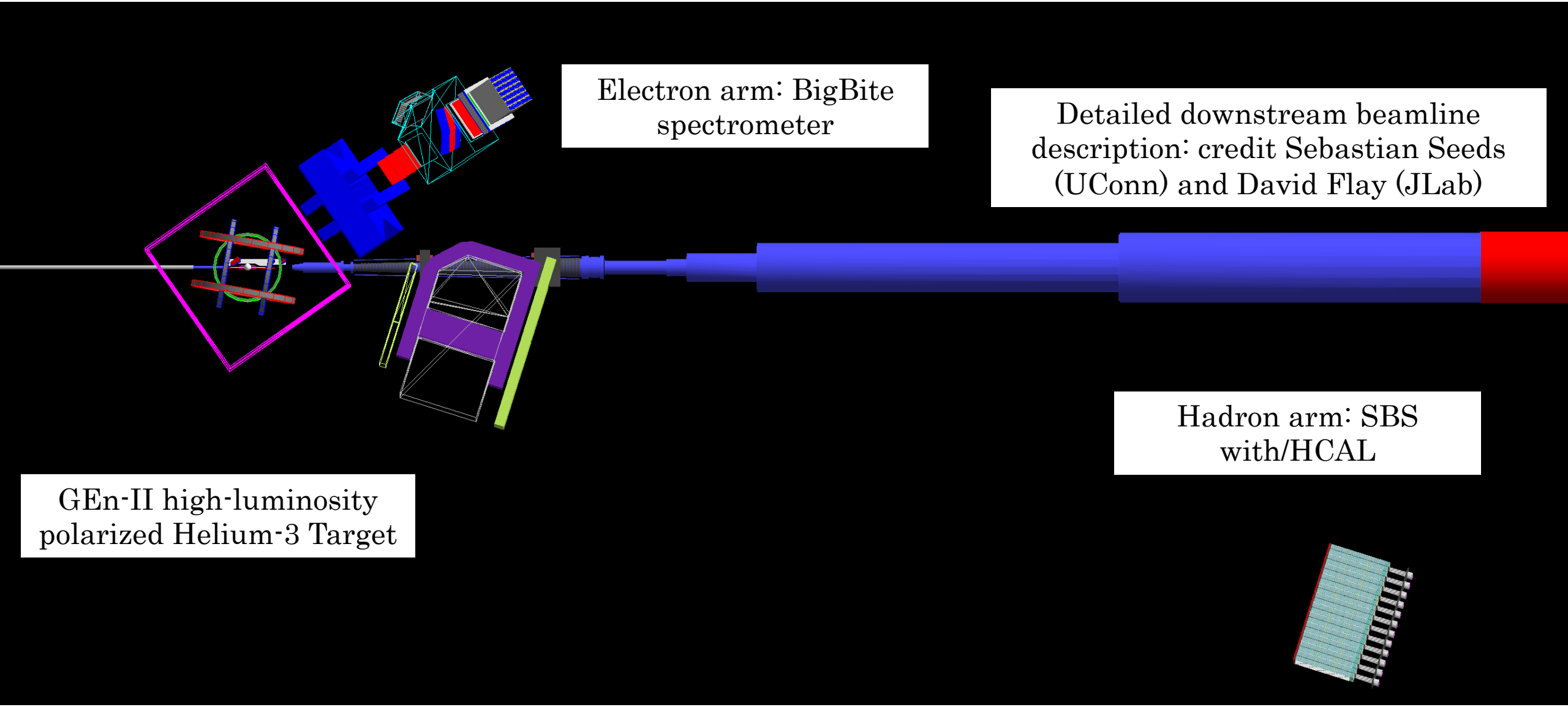

GEN simulations: nucleon charge ID

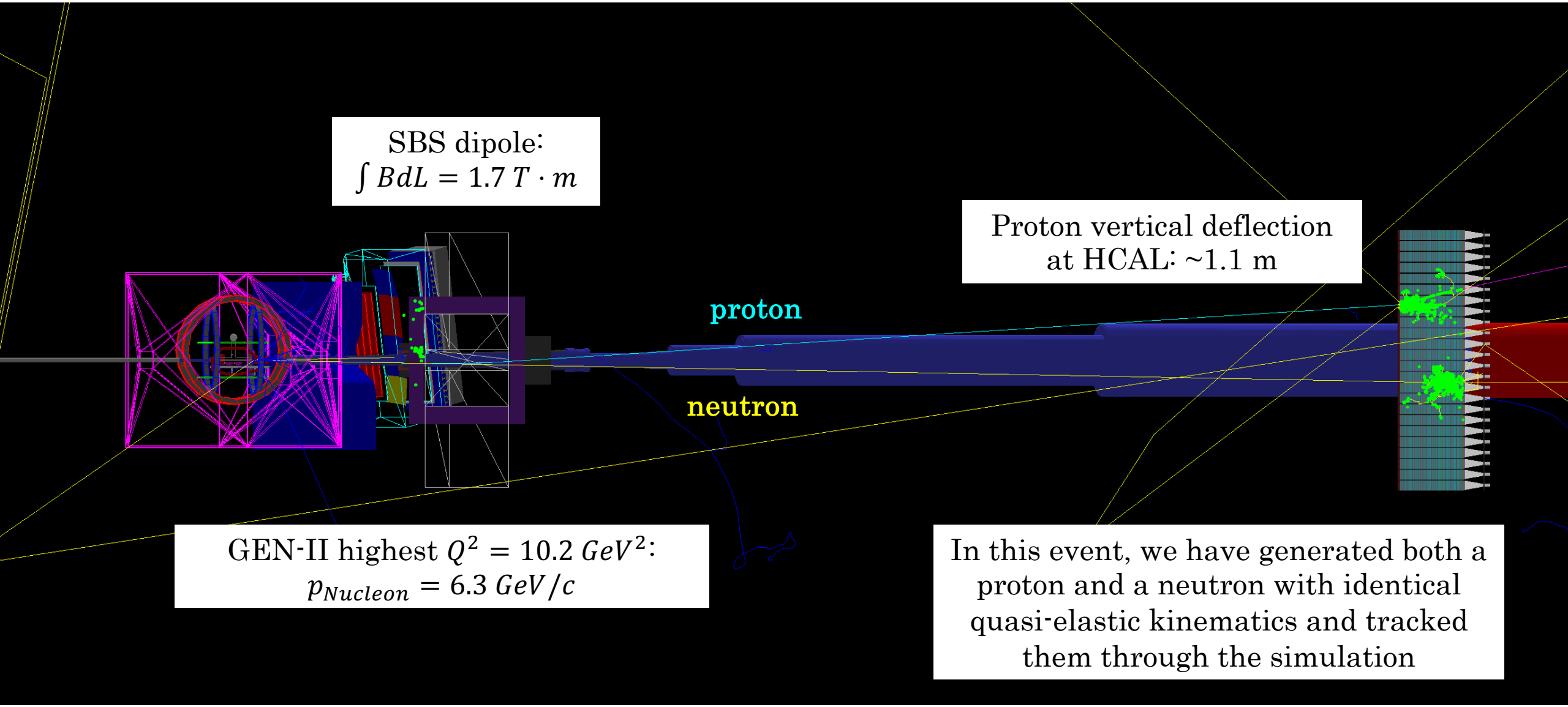

Overview of SBS Program—Actual and Potential

Fully Approved:

- E12-07-109 (GEP): 45 PAC days, A- rate, "High Impact"
- E12-09-019 (GMN): 25 PAC days, B+ rate
- E12-09-016 (GEN): 50 PAC days, A- rate
- E12-09-018 (SIDIS): 64 PAC days, A- rate
- E12-17-004 (GEN-RP): 5 PAC days, A- rate
- E12-20-010 (nTPE): 2 PAC days, A- rate
- E12-20-008 (K_{LL} in $\vec{\gamma}n \to \pi^- \vec{p}$): 2 PAC days, B+ rate

Conditionally Approved:

- C12-15-006 (TDIS): 27 PAC days, A- rate; "C1" approval status
  - "Run-group" add-on of kaon structure measurement also C1 approved

Potential future physics using SBS:

- A_1^n: formerly an approved BigBite experiment (2006), withdrawn at jeopardy (2019) due to imminent Hall C run, new proposal with BB+SBS likely (pending Hall C results)
- J/ψ photoproduction polarization observables/LHCb pentaquark physics: LOI submitted 2017… need observation of pentaquark in photoproduction at JLab energy…
- e^+p elastic scattering polarization transfer—part of science program for positron beam at CEBAF in LOI, now published in special issue of EPJ A 57, 188 (2021): https://doi.org/10.1140/epja/s10050-021-00509-5
- More DIS/SIDIS/TMD physics:
  - Longitudinally polarized SIDIS on ^{3}He and spin-flavor decomposition (deferred PR12-14-008)
  - Transversely polarized DIS/SIDIS on proton: g_2^p, Collins, Sivers, etc.
- Polarization observables and xsec in exclusive ϕ production
- Strange FFs at high Q^2 (not really an "SBS" proposal *per se*, but re-using some SBS components)
- Higher-Q^2 EMFFs/higher-x physics w/future CEBAF energy upgrade?

ECT* diquarks workshop, Trento, Sept. 23-27, 2019

Progress in Particle and Nuclear Physics 116 (2021) 103835

Contents lists available at ScienceDirect

Progress in Particle and Nuclear Physics

journal homepage: www.elsevier.com/locate/ppnp

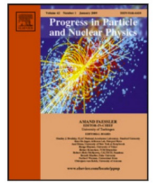

Review

Diquark correlations in hadron physics: Origin, impact and evidence

M.Yu. Barabanov [1], M.A. Bedolla [2], W.K. Brooks [3], G.D. Cates [4], C. Chen [5], Y. Chen [6,7], E. Cisbani [8], M. Ding [9], G. Eichmann [10,11], R. Ent [12], J. Ferretti [13], R.W. Gothe [14], T. Horn [15,12], S. Liuti [4], C. Mezrag [16], A. Pilloni [9], A.J.R. Puckett [17], C.D. Roberts [18,19,*], P. Rossi [12,20], G. Salmé [21], E. Santopinto [22], J. Segovia [23,19], S.N. Syritsyn [24,25], M. Takizawa [26,27,28], E. Tomasi-Gustafsson [16], P. Wein [29], B.B. Wojtsekhowski [12]

[1] *Joint Institute for Nuclear Research, Dubna, 141980, Russia*

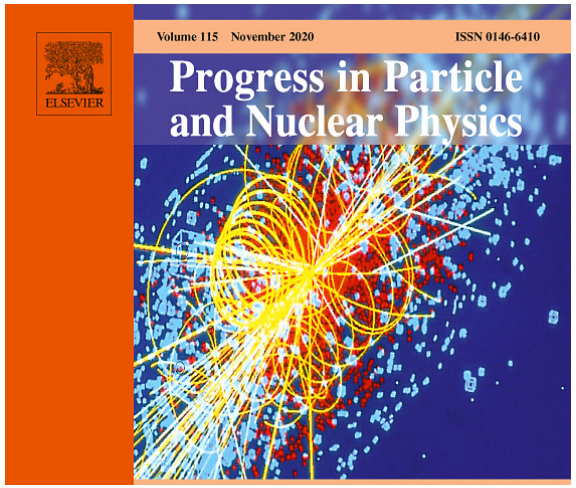

- High-Q^2 form factors are among the most sensitive experimental signatures of diquark correlations, now thought to play an important role in hadron structure; 2019 workshop brought together theorists and experimentalists at ECT* in Trento, Italy
- PPNP article now published as PPNP 116, 103835 (2021): https://doi.org/10.1016/j.ppnp.2020.103835

The Problem with Rosenbluth Separations

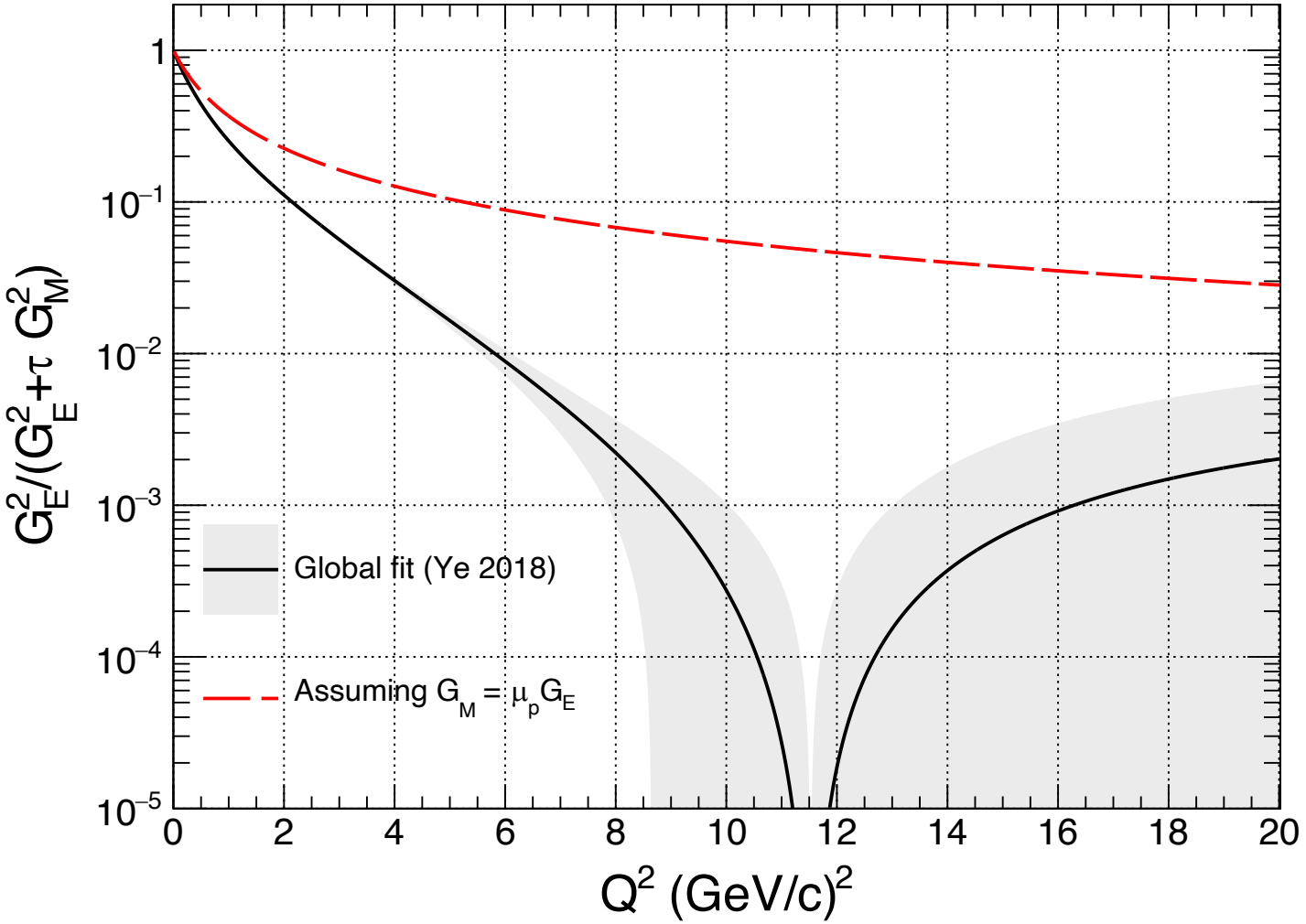

Maximum Fraction of the Reduced Cross Section Carried by the electric term versus Q^2

Density interpretations of Form Factors: 3D (Kelly 2002)

Nonrelativistic interpretation:

$$\rho_{ch}^{NR}(r) = \frac{2}{\pi}\int_0^\infty dQ\, Q^2 j_0(Qr) G_E(Q^2),$$

$$\mu\rho_m^{NR}(r) = \frac{2}{\pi}\int_0^\infty dQ\, Q^2 j_0(Qr) G_M(Q^2),$$

Rest-frame density is Fourier Transform of "intrinsic FF" in wavenumber space:

$$\rho(r) = \frac{2}{\pi}\int_0^\infty dk\, k^2 j_0(kr)\tilde{\rho}(k).$$

(Model-dependent) Relativistic prescription to relate Sachs FF to intrinsic FF:

$$\tilde{\rho}_{ch}(k) = G_E(Q^2)(1+\tau)^{\lambda_E}, \qquad \lambda_E = \lambda_M = 2$$

$$\mu\tilde{\rho}_m(k) = G_M(Q^2)(1+\tau)^{\lambda_M},$$

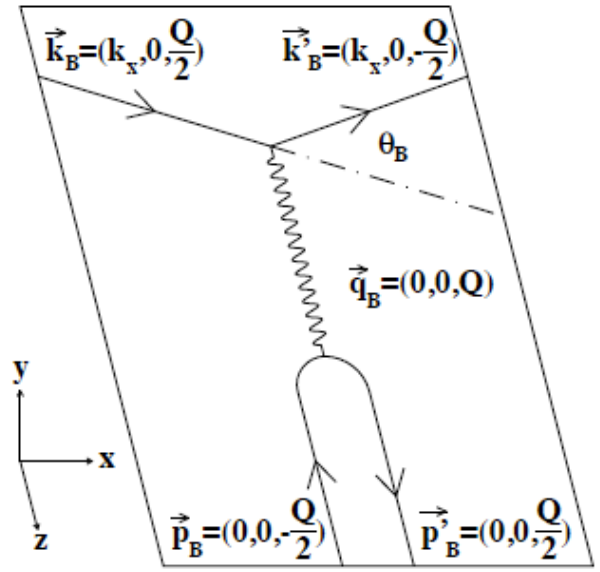

Figure 1-2: Elastic scattering in the Breit frame

Interpret Sachs FF as FT of Breit-frame density. Rest frame wavenumber related to Q^2 by boost along momentum transfer:

$$k^2 = \frac{Q^2}{1+\tau} \qquad \tau = \frac{Q^2}{4M^2}$$

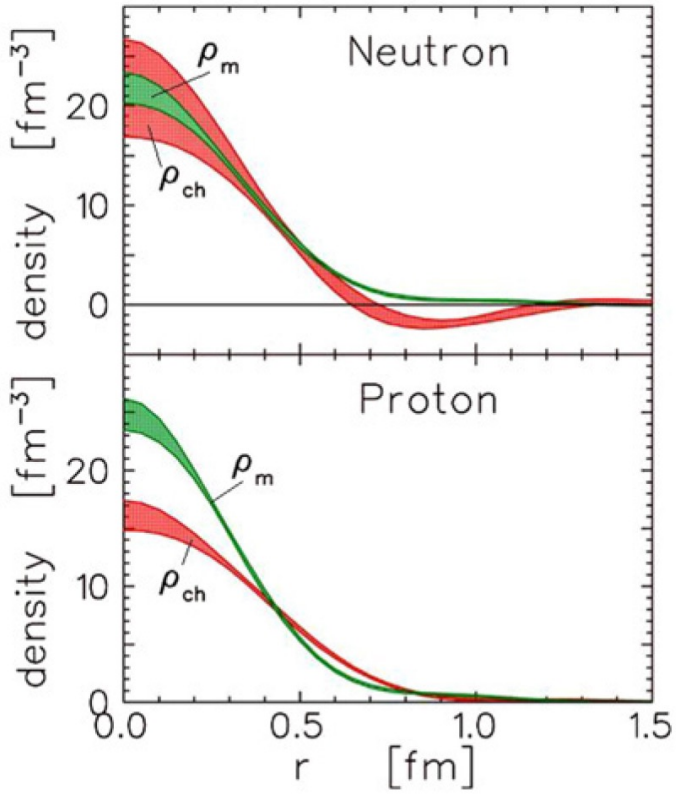

J. J. Kelly: PRC 66, 065203 (2002)

GPDs and transverse densities:

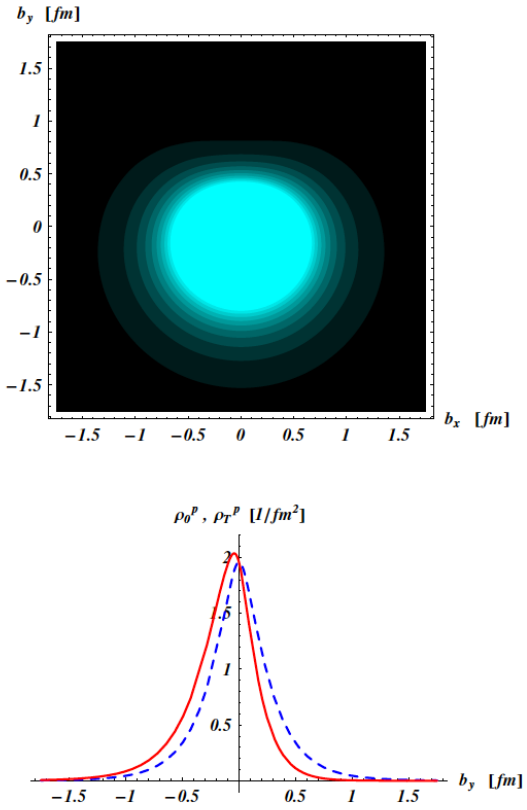

FIG. 1: Quark transverse charge densities in the *proton*. The upper panel shows the density in the transverse plane for a proton polarized along the x-axis. The light (dark) regions correspond with largest (smallest) values of the density. The lower panel compares the density along the y-axis for an unpolarized proton (dashed curve), and for a proton polarized along the x-axis (solid curve). For the proton e.m. FFs, we use the empirical parameterization of Arrington *et al.* [14].

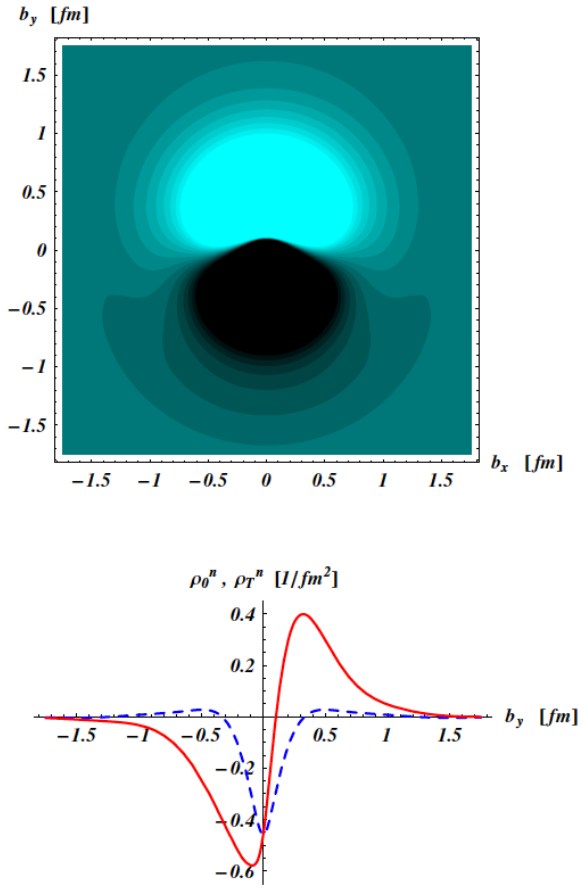

FIG. 2: Same as Fig. 1 for the quark transverse charge densities in the *neutron*. For the neutron e.m. FFs, we use the empirical parameterization of Bradford *et al.* [15].

Proton (left) and neutron (right) 2D transverse charge densities from Carlson and Vanderhaeghen: Phys. Rev. Lett. 100, 032004 (2008)

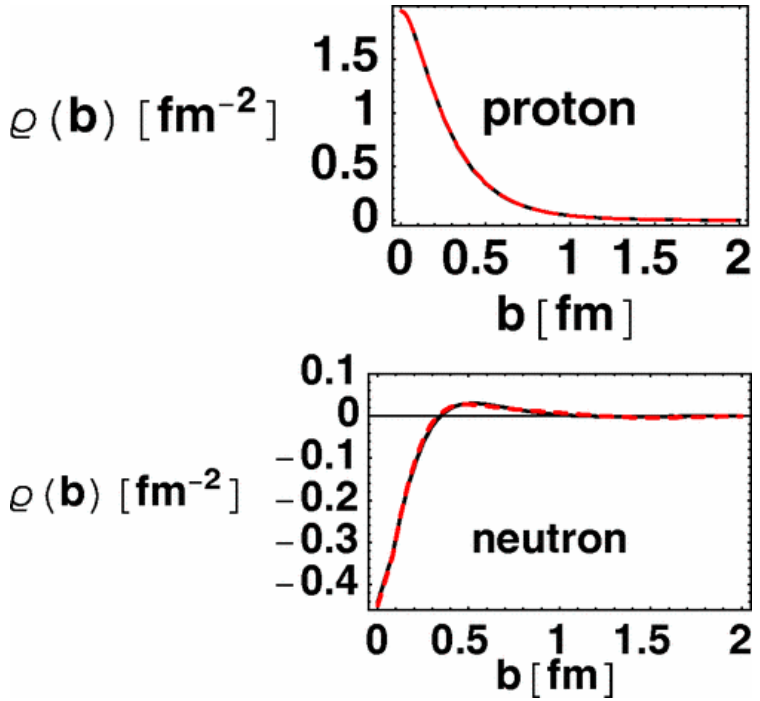

- G. Miller, *Phys.Rev.Lett.* 99 (2007) 112001
- G. Miller, *Ann. Rev. Nucl. Part. Sci.* 60 (2010) 1-25
- Model-independent sum rules relating FF to GPD moments lead to model-independent impact-parameter-space densities as 2D FT of FF in the infinite momentum frame

The Super BigBite Spectrometer in Hall A

Proton form factors ratio, GEp(5) (E12-07-109)

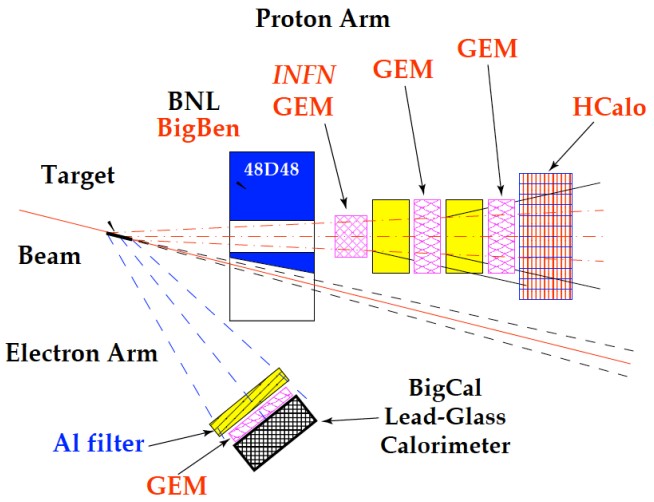

Neutron form factors, E12–09–016 and E12–09–019

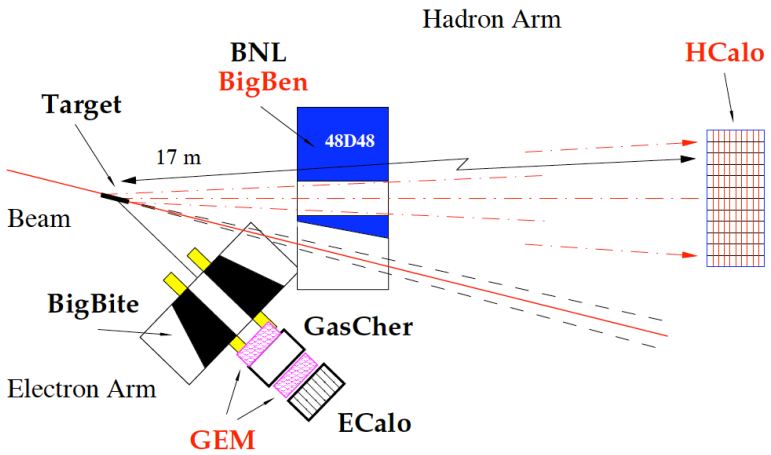

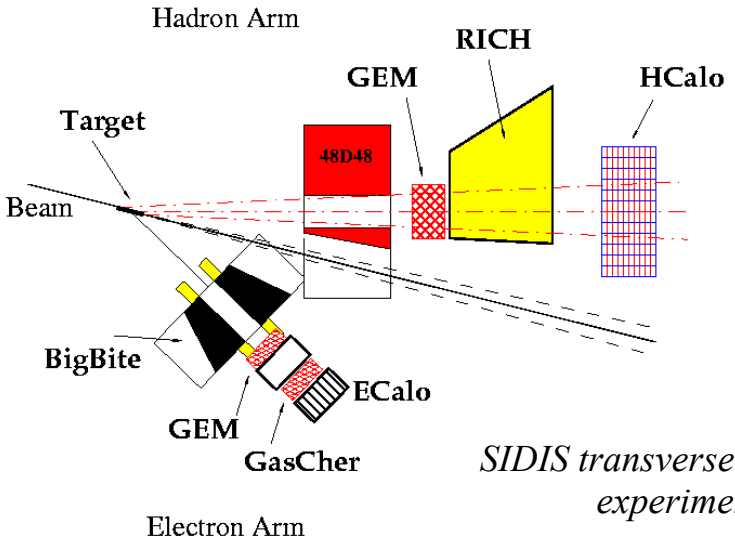

SIDIS transverse single-spin asymmetry experiment: E12-09-018

- What is SBS? → A 2.5 T*m dipole magnet with vertical bend, a cut in the yoke for passage of the beam pipe to reach forward scattering angles, and a flexible/modular configuration of detectors.
- Designed to operate at luminosities up to 10^{39} cm^{-2} s^{-1} with large momentum bite, moderate solid angle
- Time-tested "Detectors behind a dipole magnet", two-arm coincidence approach—historically most productive in fixed-target expts.
- Study large-momentum transfer exclusive and semi-inclusive reactions in electron-nucleus scattering
- ***Large solid-angle + high luminosity @ forward angles = most interesting physics!***

Polarization Transfer Concept

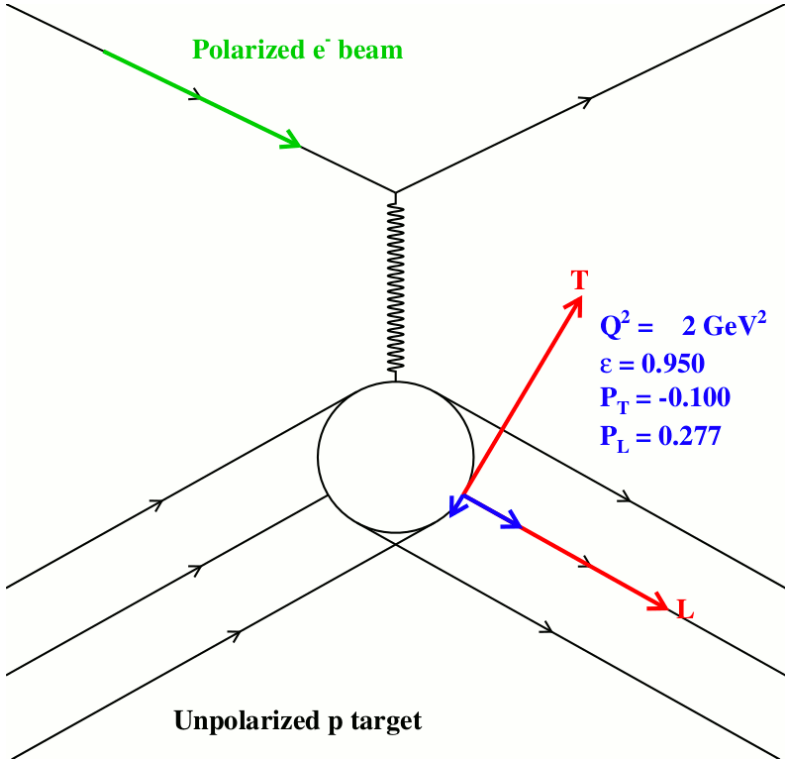

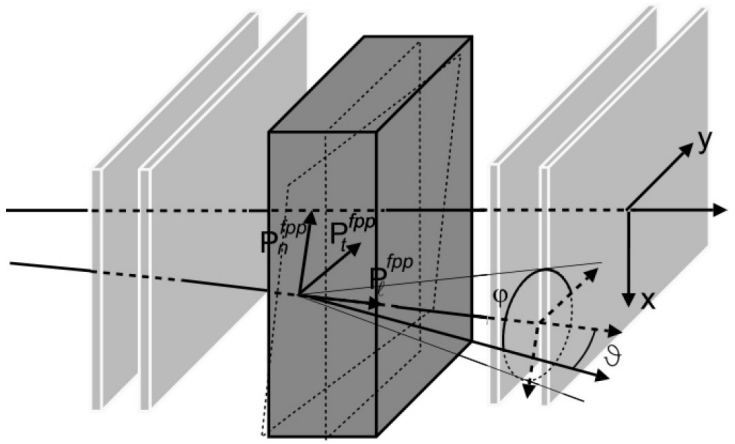

FIG. 9. Principle of the polarimeter, showing a noncentral trajectory through the front chambers, scattering in the analyzer, and a track through the back chambers; ϑ is the polar angle, and φ is the azimuthal angle from the y direction counterclockwise.

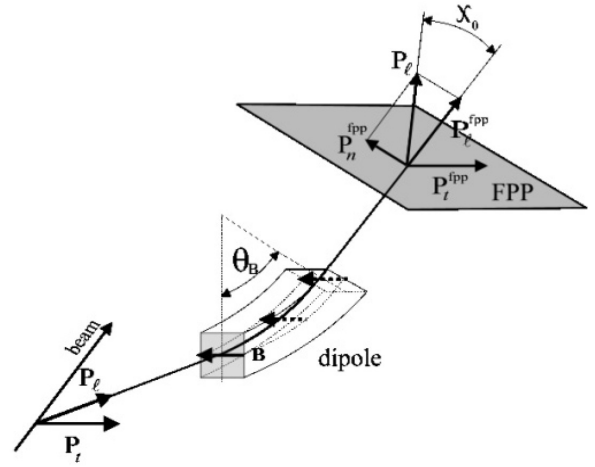

FIG. 15. Precession of the polarization component P_ℓ in the dipole of the HRS by an angle χ_θ.

- Based on spin-orbit coupling in proton-nucleus scattering

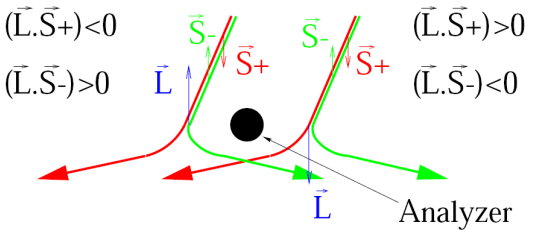

If more S+ than S- ($+P_x^{fpp}$) ...

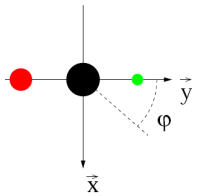

... more events left than right

- A spin-1/2 particle, such as a proton, is preferentially deflected by the nuclear spin-obrit force along the direction of $\vec{p}\times\vec{S}$, where $\vec{p}$ is the incident proton momentum, and $\vec{S}$ is the proton spin.
  - A spin-orbit force is insensitive to longitudinal polarization!
  - Precession in a magnetic field rotates P_L into a transverse component that can be measured
- Azimuthal asymmetry in the angular distribution of secondary scatterings measures $\vec{S}$

SBS/BigBite with GEMs—Hall A enters the "Big Data" era

SBS G_M^n Data Acquisition (DAQ) Facts

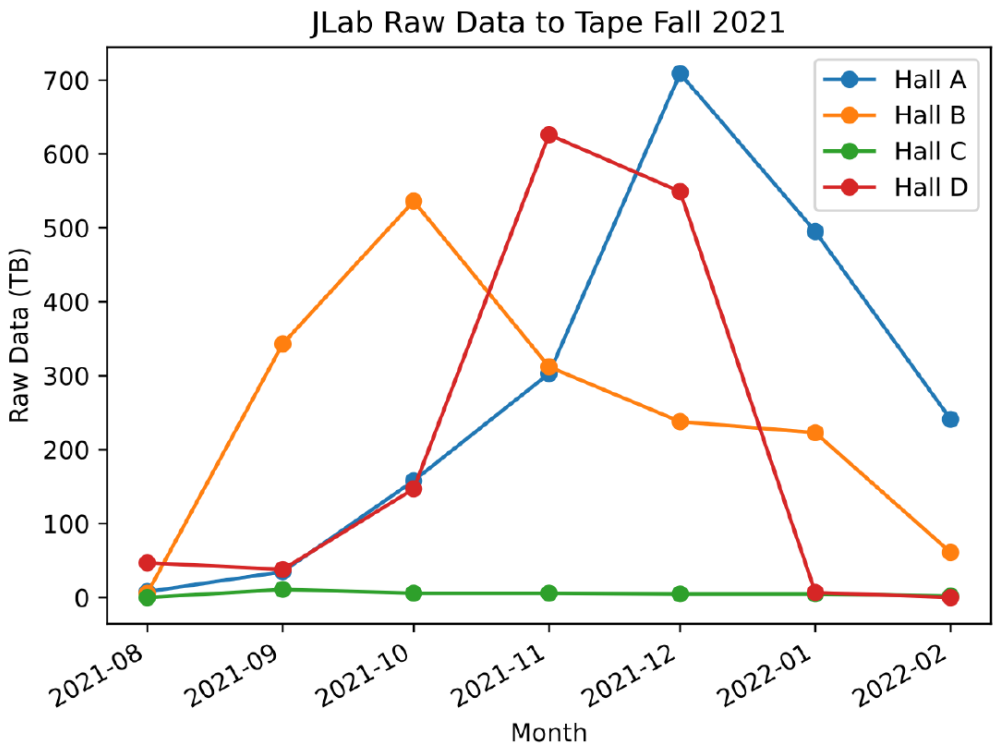

- Data Acquisition challenges:
  - 43,000+ detector readout channels!
  - Very high luminosity, $\sim 10^{38}\ cm^{-2}s^{-1}$
- During 5 months (Oct 2021 - Feb 2022) of SBS G_M^n running, Hall A has recorded ~2 PB worth of raw data!
  - This is more than any other Hall.
  - Also, 5 times more data than all prior Hall A experiments combined in 25 years!

[*] Graphic from Ole Hansen (JLab), Jan 2022

GEM-based tracking in BigBite: what we're up against (run 13727, 12 uA LD2, $Q^2 = 4.5\ GeV^2, E = 4\ GeV$)

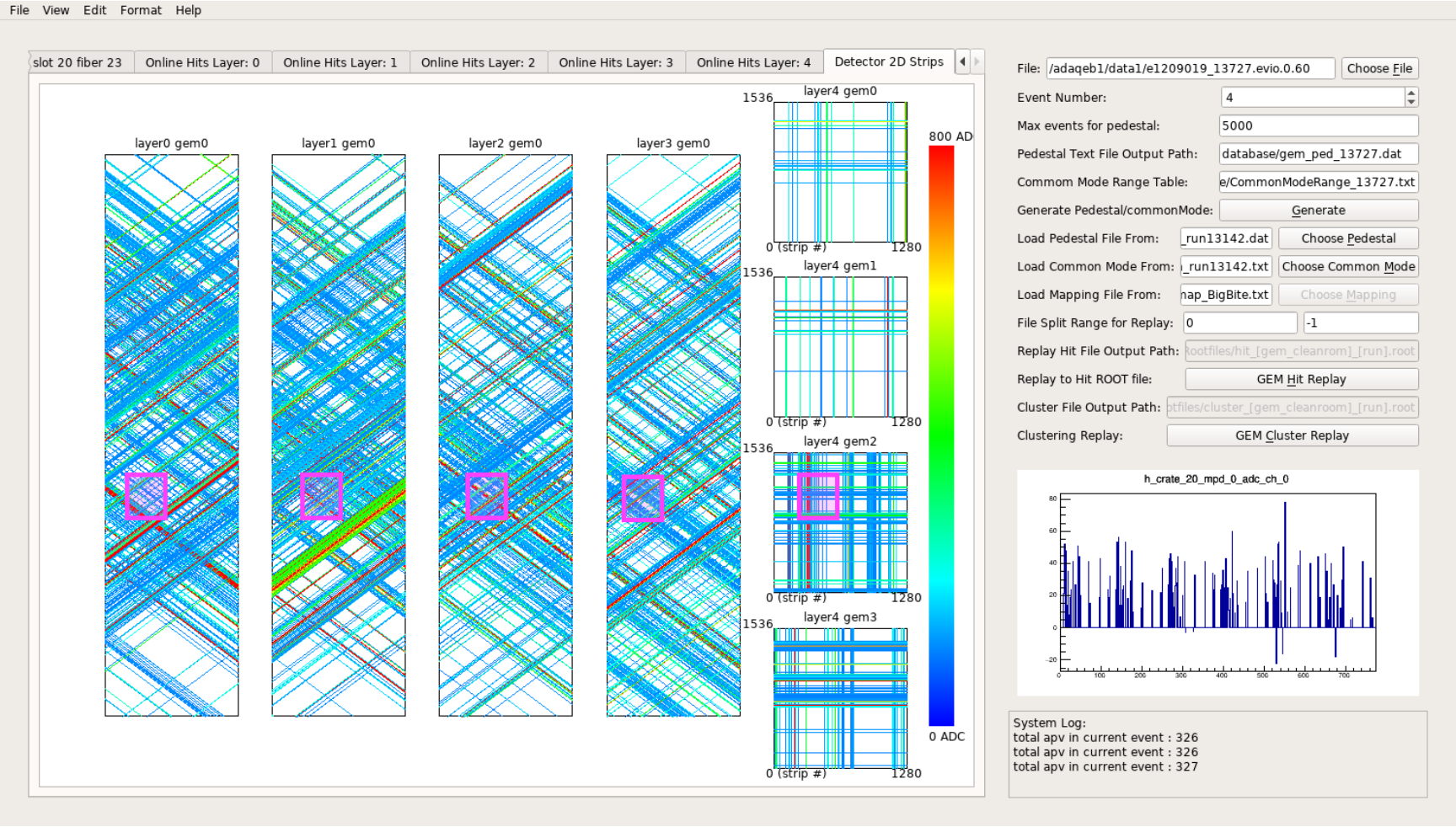

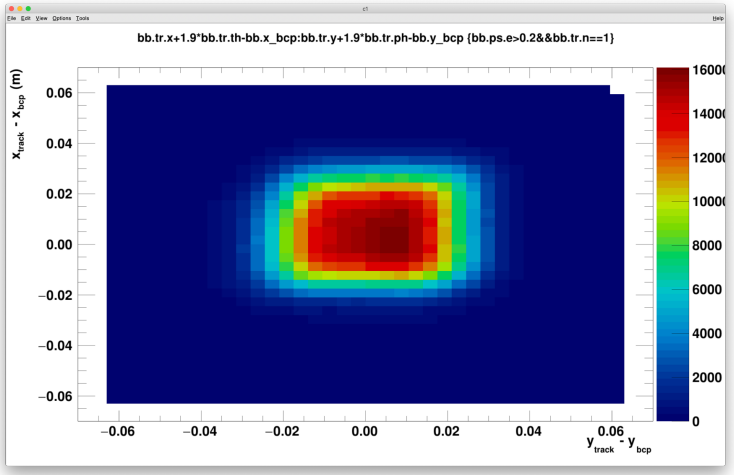

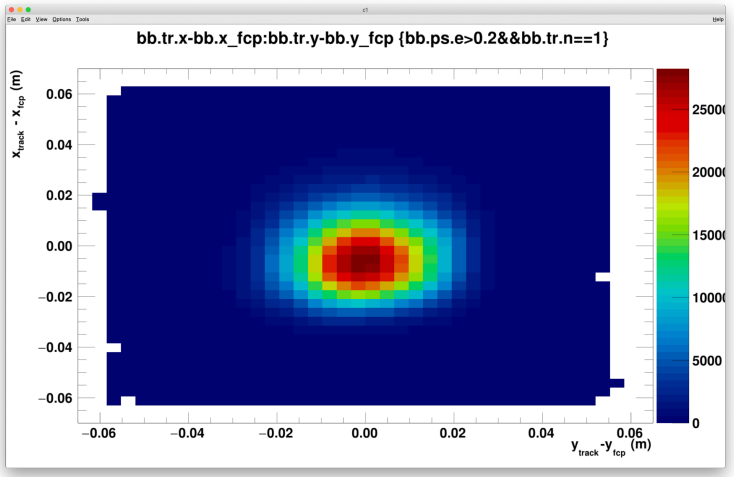

- Single-event display from BigBite GEM trackers during typical SBS GMN production run

BigBite calorimeter narrows search region for tracking

= approximate size of calorimeter-constrained track search region at each layer

W^2 versus θ_{pq}

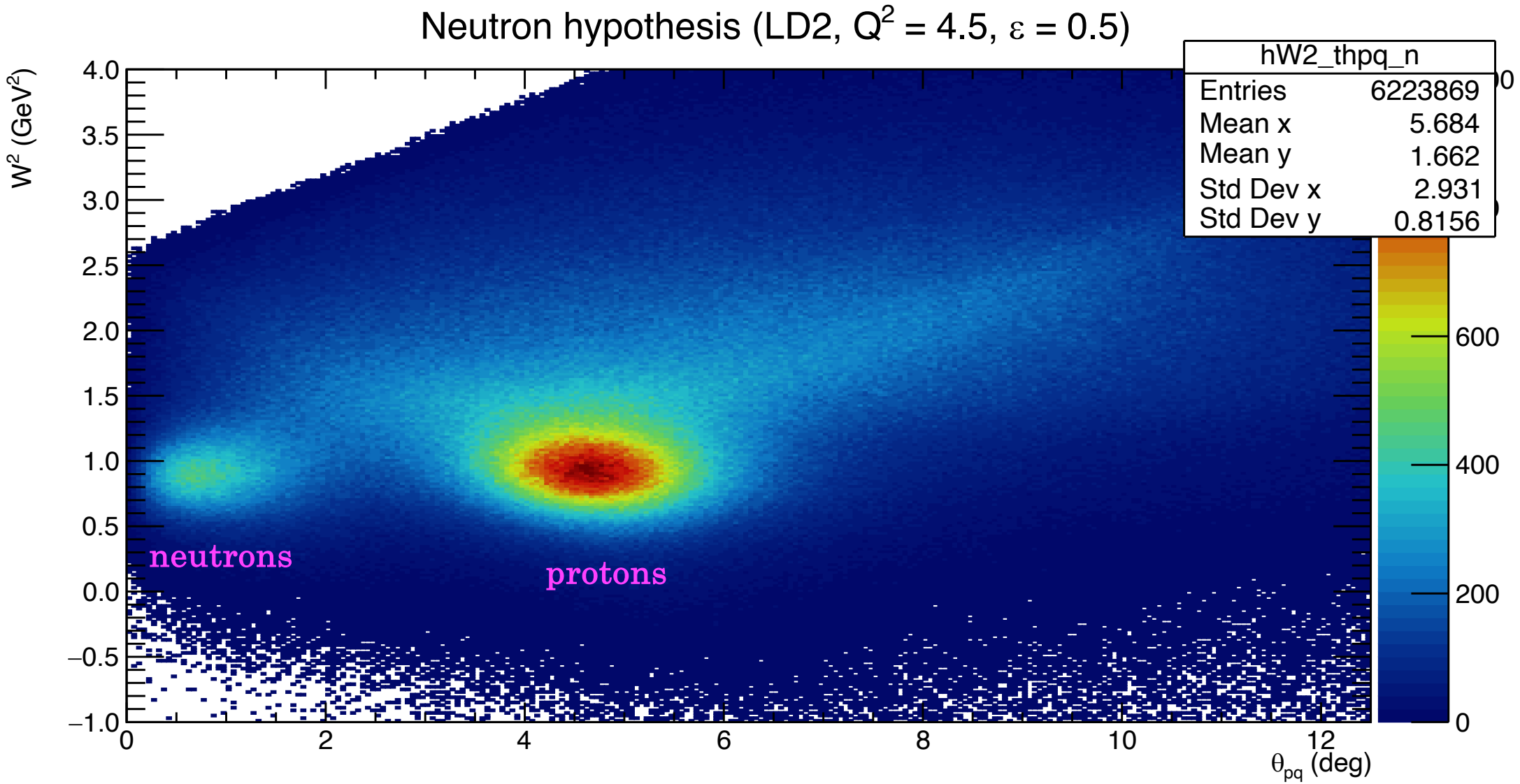

Rough n and p estimates from Δx projection, effect of fiducial cuts

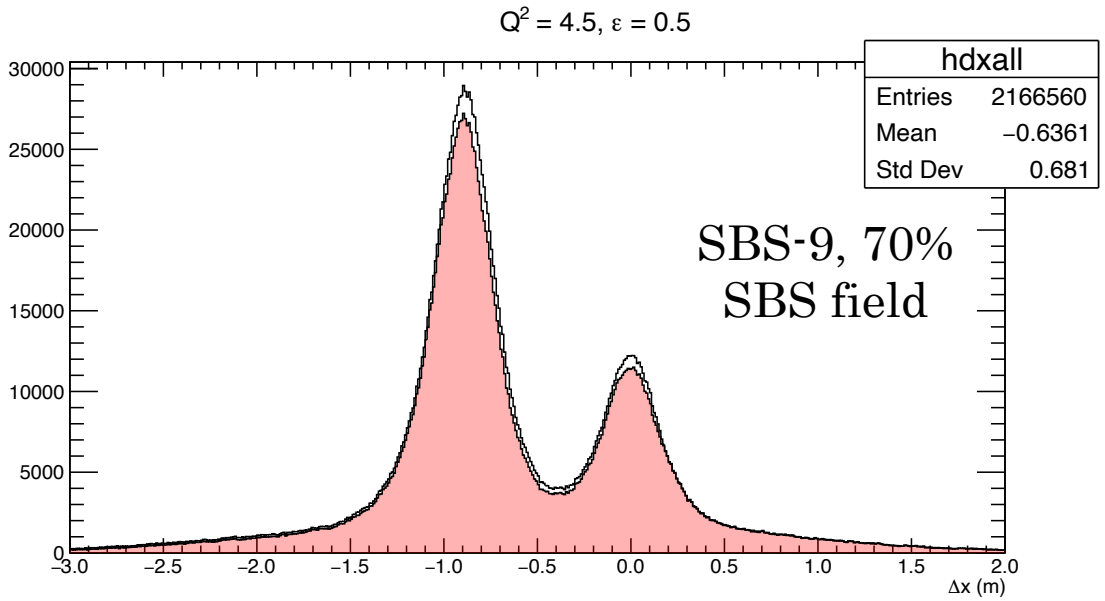

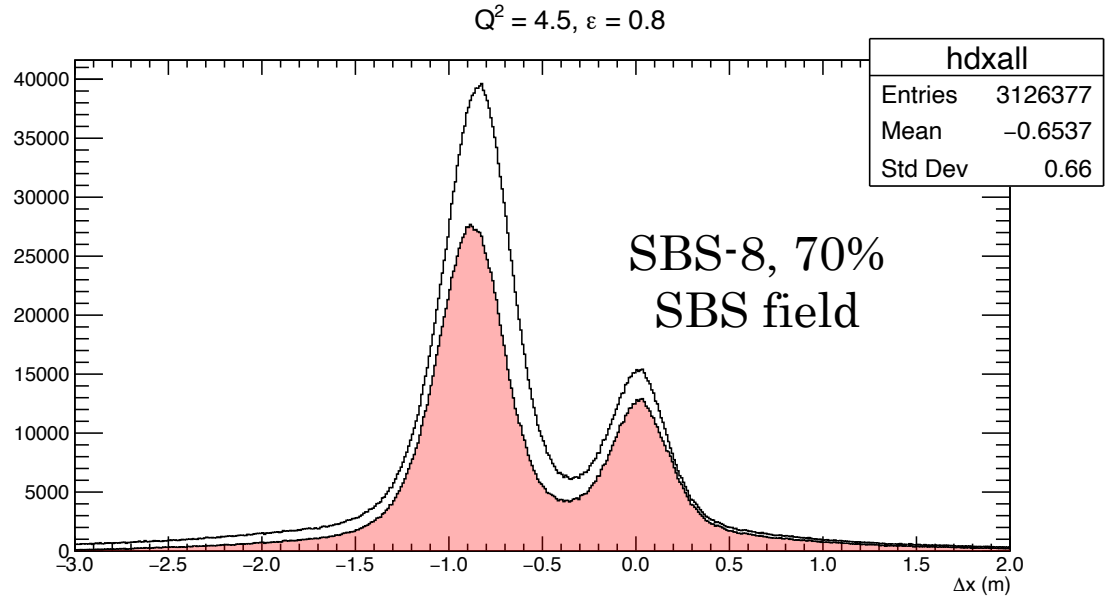

- Δx projection **with** (**without**) fiducial cut shows effect of this cut for the two different ϵ points at 4.5 GeV^2
- Envelope of elastic events on HCAL is much smaller for low ϵ, effect of fiducial cut is much greater for high ϵ
- *Raw* n/p ratios from crude fit method are in good qualitative agreement across field settings AFTER applying fiducial cut
- Interpretation of ϵ dependence requires more precise analysis, inclusion of electric form factors, bin centering, etc

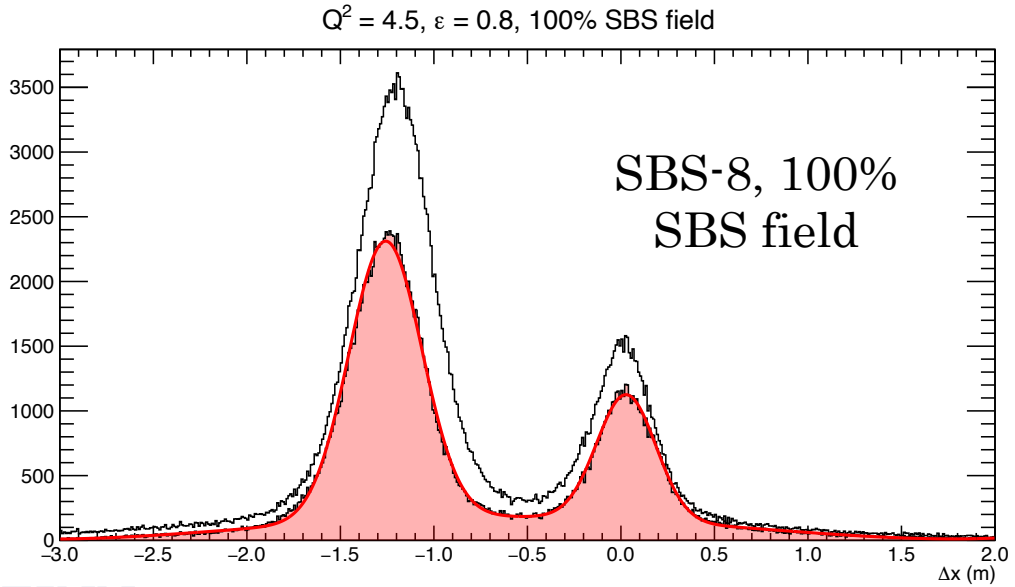

Helium-3 as an Effective Polarized Neutron Target

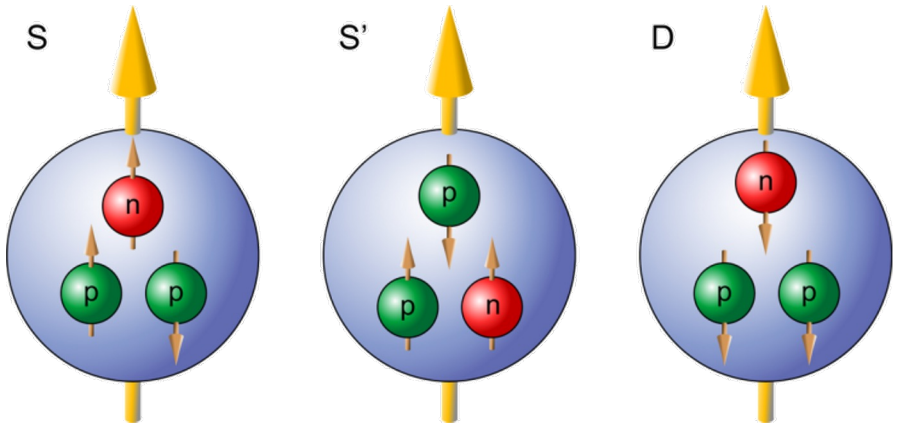

~87% ~8% ~1.5%

$$A_{^3\mathrm{He}} = P_n(1-f_p)A_n + P_p f_p A_p$$
$$P_n = 0.86^{+0.036}_{-0.02}$$
$$P_p = -0.028^{+0.009}_{-0.004}$$
$$f_p = \frac{2\sigma_p}{\sigma_{^3\mathrm{He}}}$$

Effective nucleon polarization approximation for DIS on Helium-3:
Scopetta, Phys. Rev. D 75, 054005 (2007)

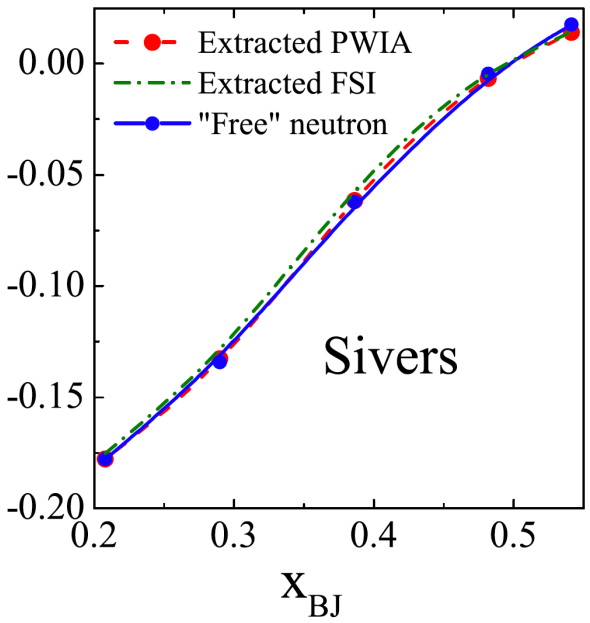

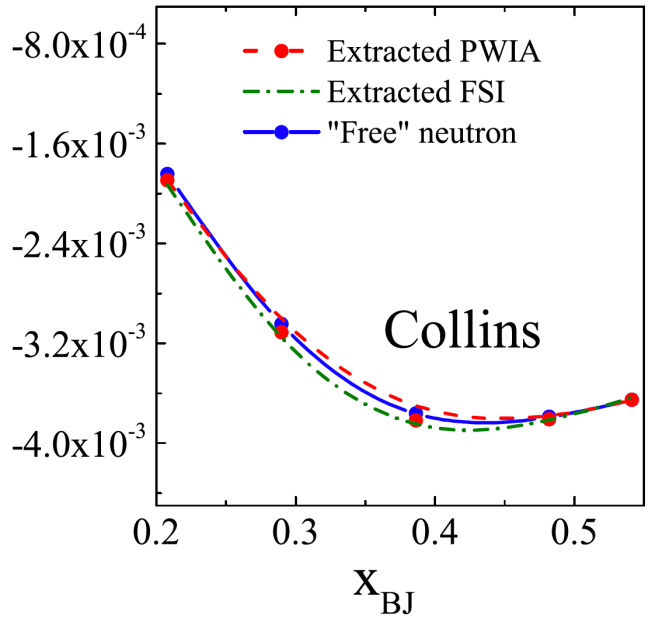

Del Dotto *et al.*, Phys. Rev. C 96, 065203 (2017)

- Effect of nuclear FSI on extraction of neutron Collins and Sivers effects from SIDIS on ^{3}He under good theoretical control
- Advantages of Helium-3 for study of polarized neutron:
  - Protons almost unpolarized
  - High luminosity capability (up to several 10^{37} cm^{-2} s^{-1})
  - Small holding field → small systematics of target spin flips

The discrepancy at large Q^2 and hard TPE

A. Afanasev et al. / Progress in Particle and Nuclear Physics 95 (2017) 245–278

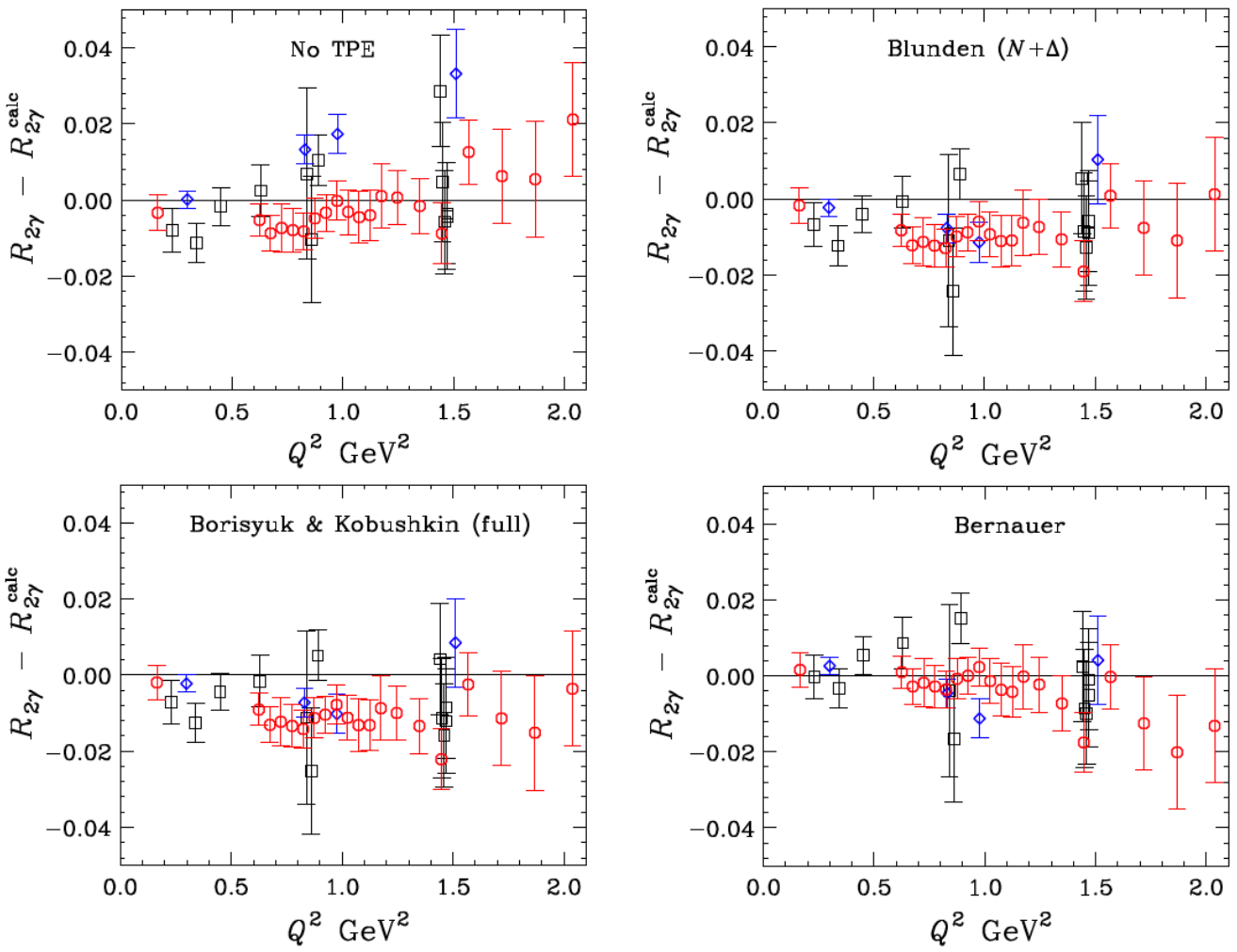

Fig. 3.16. Difference between $R_{2\gamma}$ and model predictions as a function of Q^2. Data symbols are the same as in Fig. 3.15.

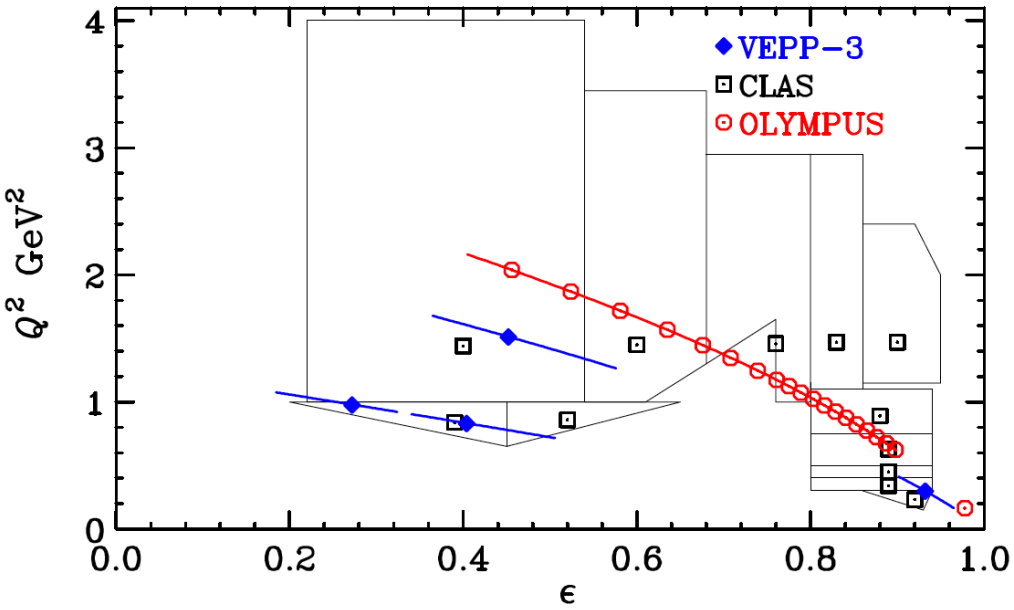

- Three dedicated experiments looked at e^+p/e^-p cross section ratio as a direct measurement of the TPE contribution to the scattering.
- Did not reach high enough Q^2 and/or low-enough ϵ to conclusively answer whether hard TPE resolves the discrepancy.
- Major motivation for developing a (polarized) positron source at CEBAF

New precision high-Q cross sections and TPE

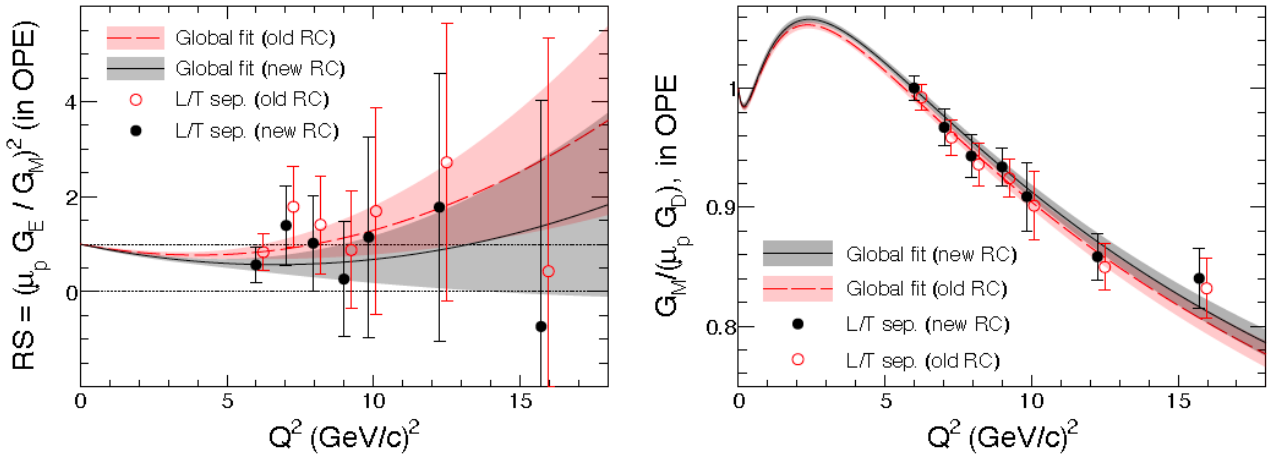

FIG. 5. Impact of applying the radiative corrections of Ref. [1] on the Rosenbluth slope (left) and $G_M/(\mu_p G_D)$ (right). In both panels, the black solid (red dashed) curve shows the global fit result using the cross sections with modified (originally published) radiative corrections. The black filled circles (red empty circles) show the L/T separation results obtained using the modified (originally published) radiative corrections. In both plots, the results obtained using the originally published radiative corrections have been offset by +0.25 $(GeV/c)^2$ in Q^2 for clarity.

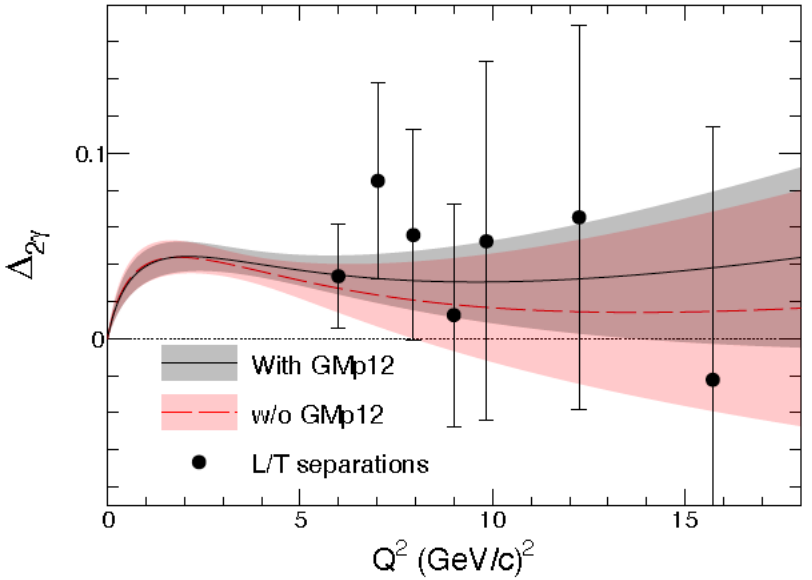

- From supplemental material to Christy *et al.,* PRL 128, 102002 (2022) https://journals.aps.org/prl/supplemental/10.1103/PhysRevLett.128.102002
- See Bogdan's talk (next) for more details.
- New L/T separations in the 6-16 GeV^2 region.
- Updated radiative corrections for JLab and SLAC high-Q data
- TPE contribution of ~4% required to account for the discrepancy in Rosenbluth Slope
- Impact of updating RCs for older experiments to more accurate Maximon-Tjon prescription is to reduce the significance of the discrepancy in the high-Q region from ~3σ to ~2σ.

The Nobel Prize in Physics, 1961 (R. Hofstadter)

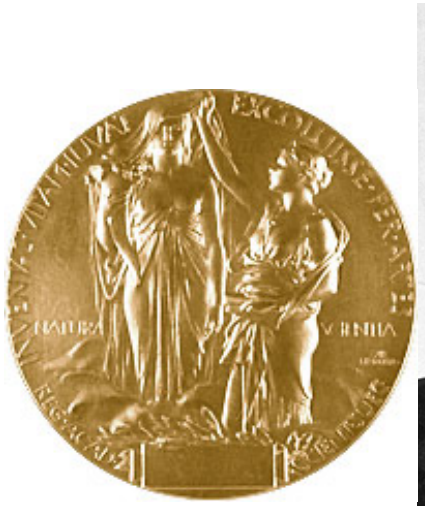

"for his pioneering studies of electron scattering in atomic nuclei and for his thereby achieved discoveries concerning the structure of the nucleons"

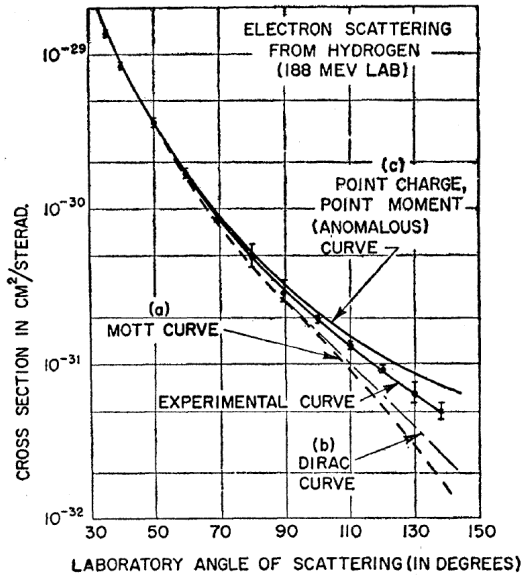

FIG. 24. Electron scattering from the proton at an incident energy of 188 Mev. The experimental points lie below the point-charge point-moment curve of Rosenbluth, indicating finite size effects.

Figures from [Rev. Mod. Phys, 28, 214 (1956)]

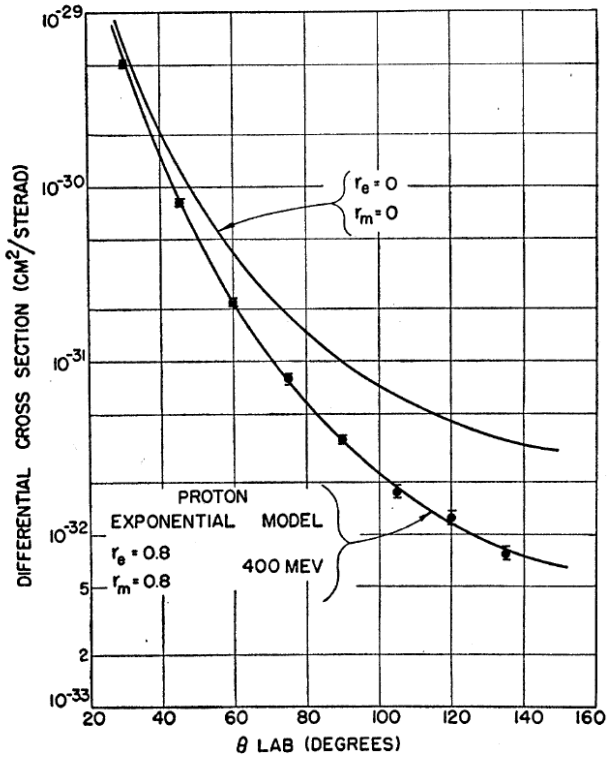

FIG. 26. Typical angular distribution for elastic scattering of 400-Mev electrons against protons. The solid line is a theoretical curve for a proton of finite extent. The model providing the theoretical curve is an exponential with rms radii $=0.80\times10^{-13}$ cm.

GMN measurement basics—ratio method

- Goal is to extract σ_n/σ_p in quasi-elastic kinematics with small uncertainties.
- Nuclear and radiative effects are expected to (mostly) cancel in the ratio, especially at high Q^2
- Electron acceptance, efficiency, luminosity/deadtime/etc also cancel
- Most important known sources of systematic uncertainty:
  - Relative acceptance/efficiency between neutrons and protons (if any)
  - Inelastic (and other) background contamination
- SBS HCAL was designed to minimize n/p acceptance/efficiency difference!
  - Large acceptance
  - High (and very similar) efficiencies for p, n (by design)

$$R_{np} \equiv \frac{\sigma_{d(e,e'n)p}}{\sigma_{d(e,e'p)n}} \approx \frac{\sigma_{en\to en}}{\sigma_{ep\to ep}} \approx \frac{\epsilon G_E^{n\,2} + \tau G_M^{n\,2}}{\epsilon G_E^{p\,2} + \tau G_M^{p\,2}}$$

$$\Longrightarrow G_M^n \approx \sqrt{\frac{R_{np}\sigma_R^p - \epsilon G_E^{n\,2}}{\tau}}$$

- BigBite gives $\vec{q}$ vector and interaction vertex
- Project to the surface of HCAL and compare to detected nucleon position/energy/time.

Polarization transfer and the ratio $\mu_p G_E^p / G_M^p$: early Hall A results

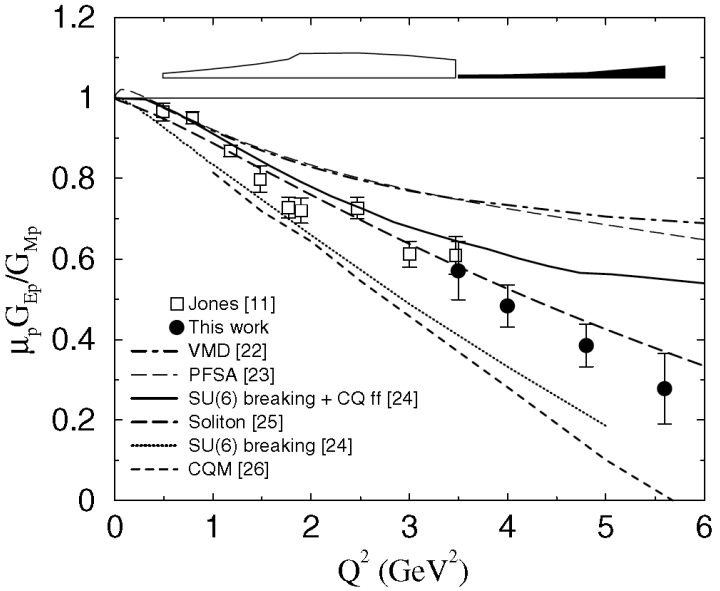

FIG. 2. The ratio $\mu_p G_{E_p}/G_{M_p}$ from this experiment and Jones *et al.* (Ref. [11]), compared with theoretical calculations. Systematic errors for both experiments are shown as a band at the top of the figure.

Gayou *et al.*, PRL 88, 092301 (2002) ("GEp-II")

- Figures at right are from Punjabi *et al.*, PRC 71, 055202 (2005)

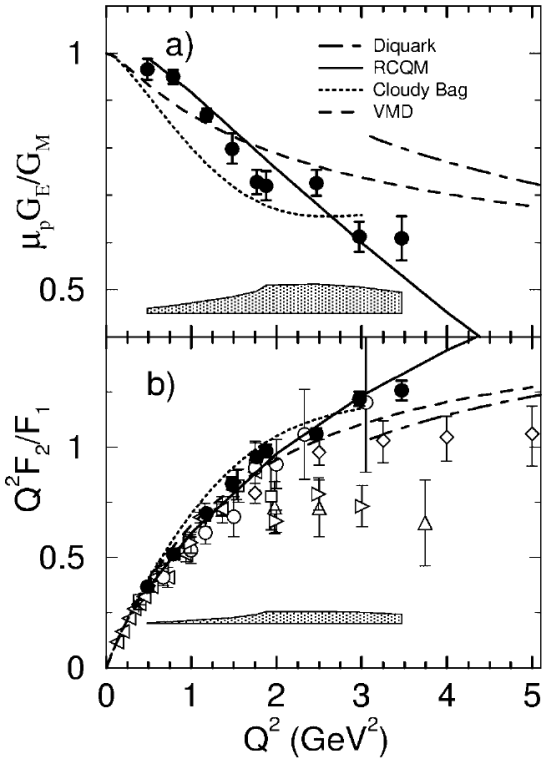

FIG. 2. (a) The ratio $\mu_p G_{E_p}/G_{M_p}$ from this experiment, compared with theoretical calculations. (b) The ratio $Q^2 F_{2_p}/F_{1_p}$ for the same data, compared to the same theoretical models as in (a) and world data; symbols as in Fig. 1. In both (a) and (b) the absolute value of systematic error from this experiment is shown by the shaded area.

Jones *et al.*, PRL 84, 1398 (2000) ("GEp-I")

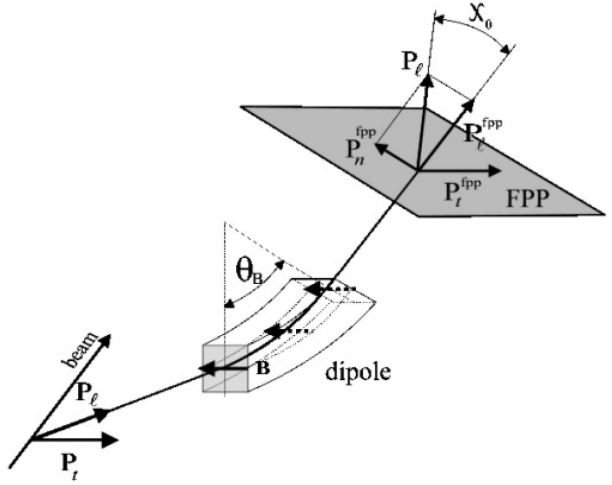

FIG. 15. Precession of the polarization component P_ℓ in the dipole of the HRS by an angle χ_θ.

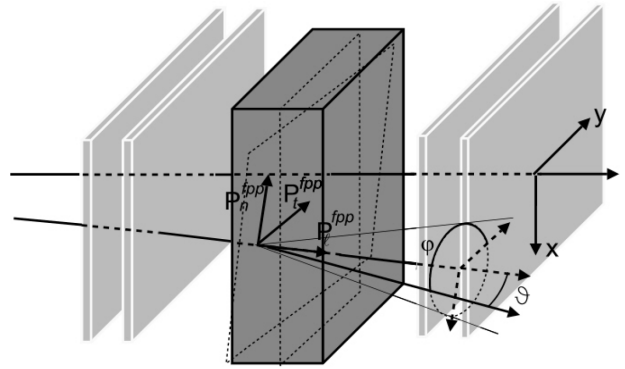

FIG. 9. Principle of the polarimeter, showing a noncentral trajectory through the front chambers, scattering in the analyzer, and a track through the back chambers; ϑ is the polar angle, and φ is the azimuthal angle from the y direction counterclockwise.

W^2 distributions with HCAL correlation cuts

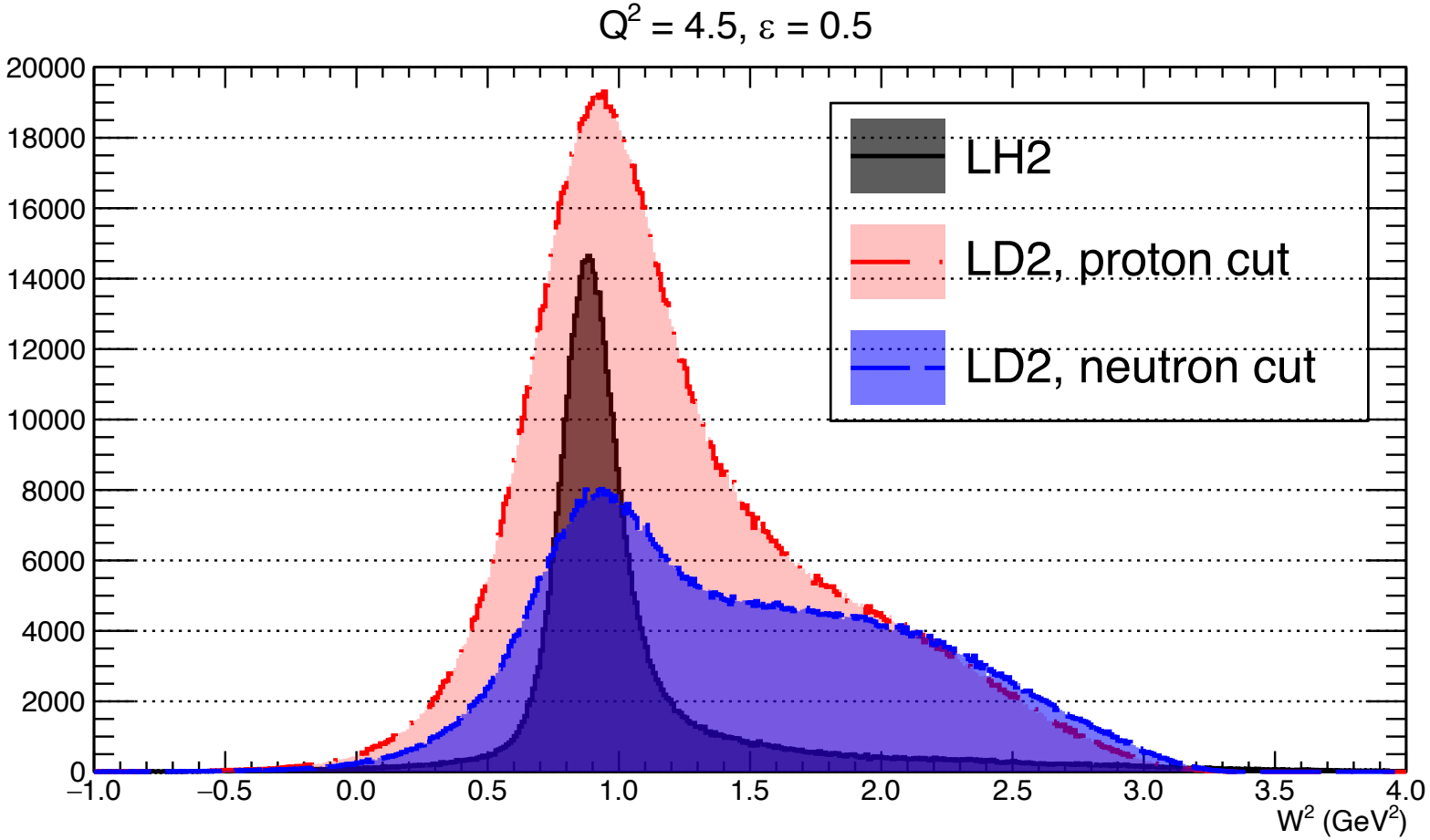

Invariant mass squared distributions obtained with 3σ elliptical cut around *p, n* peaks in previous slide (also loose coincidence time cut and HCAL energy cut)

Theoretical Interpretation of Nucleon Elastic Form Factors

- Density interpretations:
  - Low Q^2only: G_E, G_M are 3D Fourier transforms of nucleon's charge (magnetic moment) densities
  - At any Q, a model-independent density interpretation exists in which F_1 and F_2 are 2D Fourier-Bessel transforms of impact parameter-space densities in the infinite momentum frame (IMF)
- Perturbative QCD: for asymptotically large Q^2, form factor behavior is predicted by simple constituent counting rules; $F_1 \propto Q^{-4}, F_2 \propto \frac{F_1}{Q^2}$, assuming dominance of multiple hard-gluon exchange mechanism
- Constituent Quark Models—define quarks as effective degrees of freedom, solve bound-state Hamiltonian with confining quark-quark interaction, use wavefunction to predict FFs.
- Lattice QCD—Experiment far ahead of theory in precision, but data help to benchmark/improve the calculations
- Basis Light-Front Quantization
- Dyson-Schwinger Equations: approximate solutions of continuum non-perturbative QCD
- Connection to Generalized Parton Distributions from sum rules; relevant to Ji sum rule for proton spin decomposition.

NMR polarization measurements on SBS polarized ^3He target

SBS-GEN: Quasi-elastic Event Selection ($Q^2 = 3\ GeV^2$)

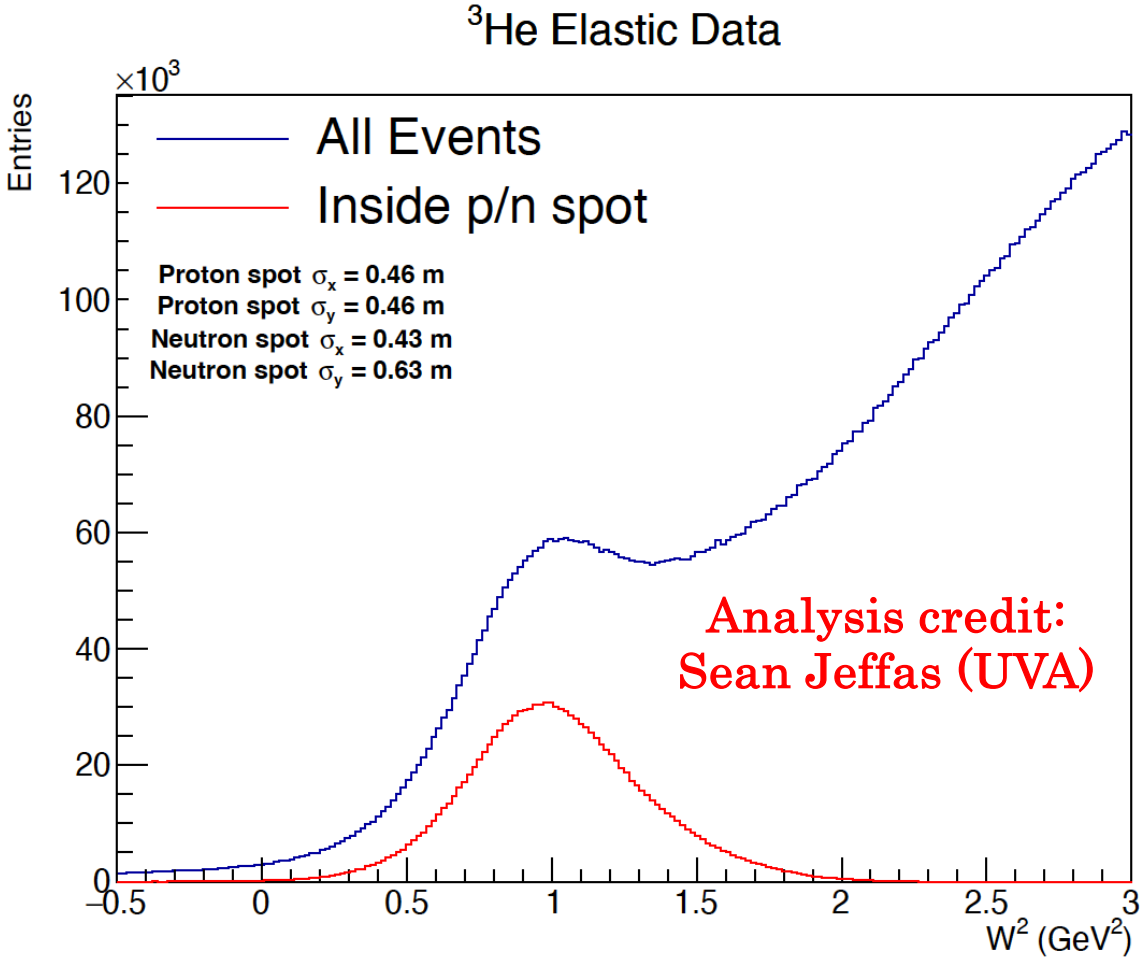

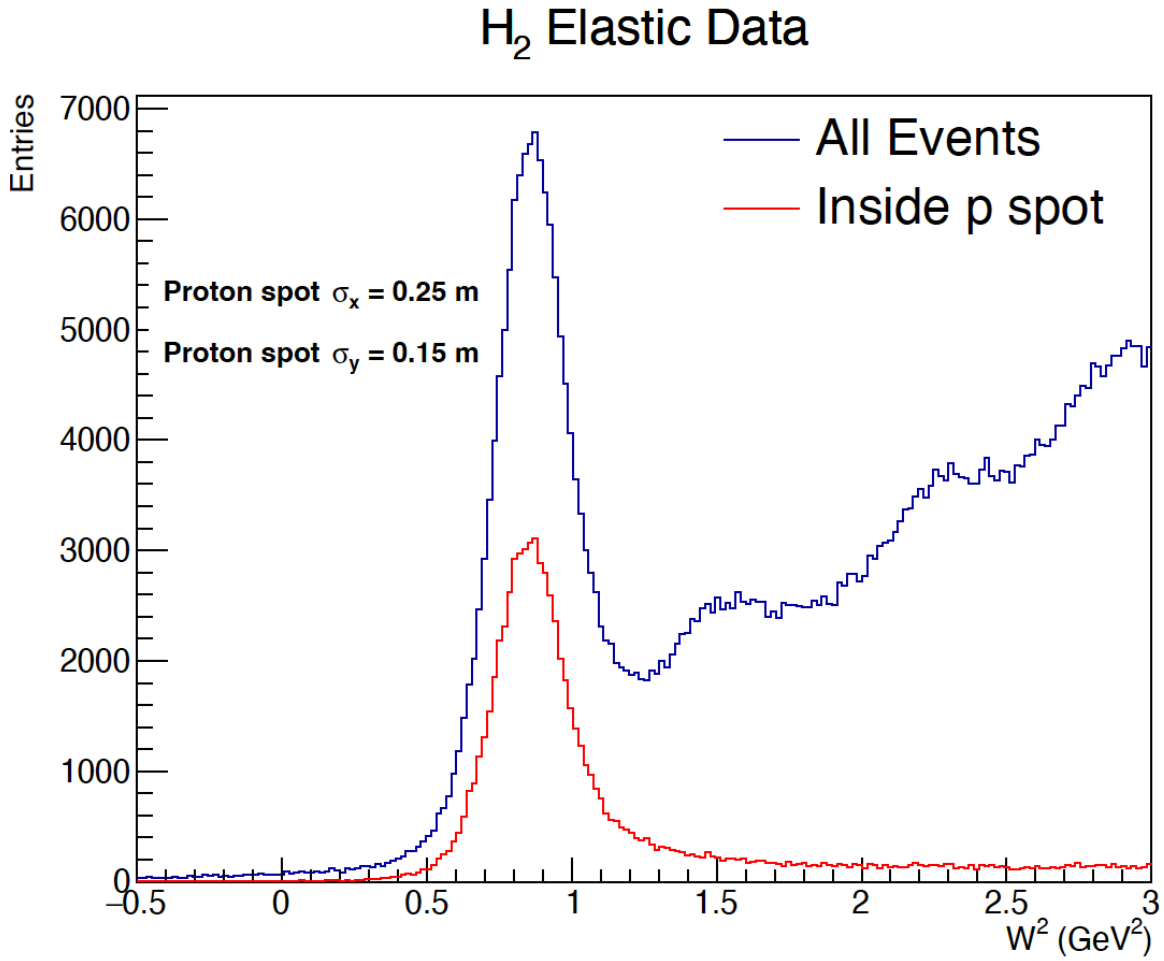

- Left (right): W^2 distribution for Helium-3 (H_2), with and without cuts on HCAL angular correlation

The high-temperature ECAL: motivation

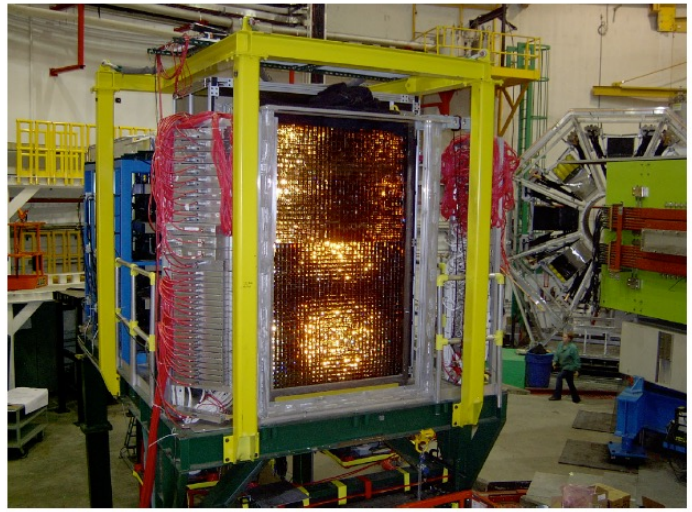

Figure G.1: BigCal in Hall C with the front opened, February 2008.

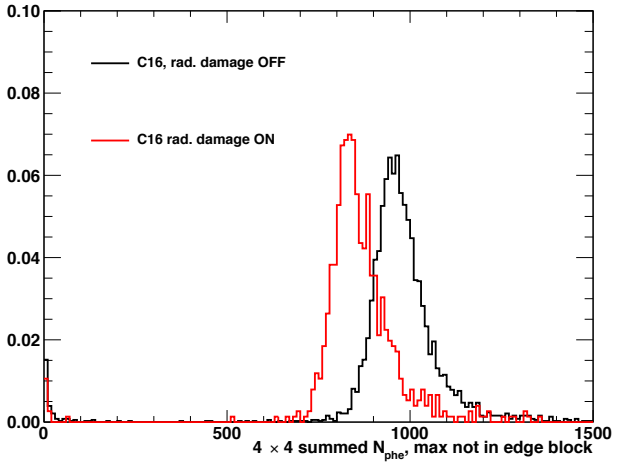

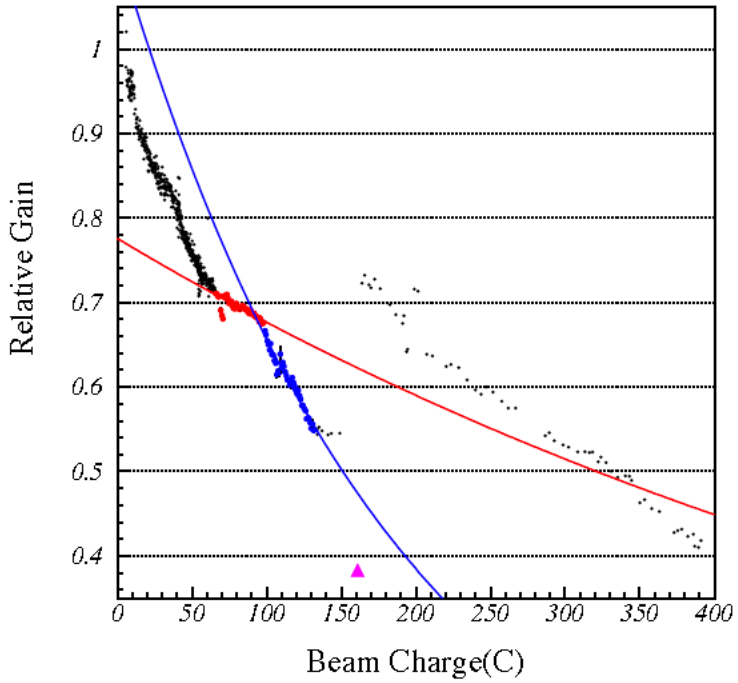

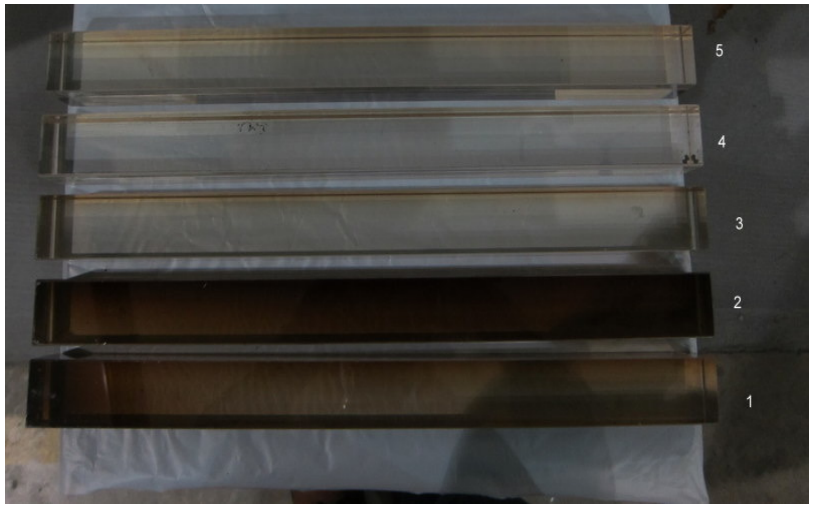

Figure 6 The lead glass blocks used to monitor the radiation dose after the C16 was placed at 10° and there was 20uA beam on the 15cm LH2 target. Block 1 was placed parallel to the C16 along the beamline side of the C16. Block 1 has damage at the front (left side of photo) and along the side. Block 2 was placed in front of the C16 and perpendicular to the front face. Blocks 3,4 and 5 were located at different locations on the spectrometer platform that was near 30°. These blocks show only moderate damage.

- Above, left: GEp-III BigCal, radiation-induced darkening of lead-glass, 2008
- Below, left: Benchmarking continuous thermal annealing prototype in simulation
- Above, center: Signal reduction due to radiation damage during GEp-III
- Above, right: Comparison of lead-glass blocks irradiated in Hall A, inside and outside the 250 deg. C oven

E12-17-004: G_E^n/G_M^n to 4.5 GeV² via charge-exchange recoil polarimetry

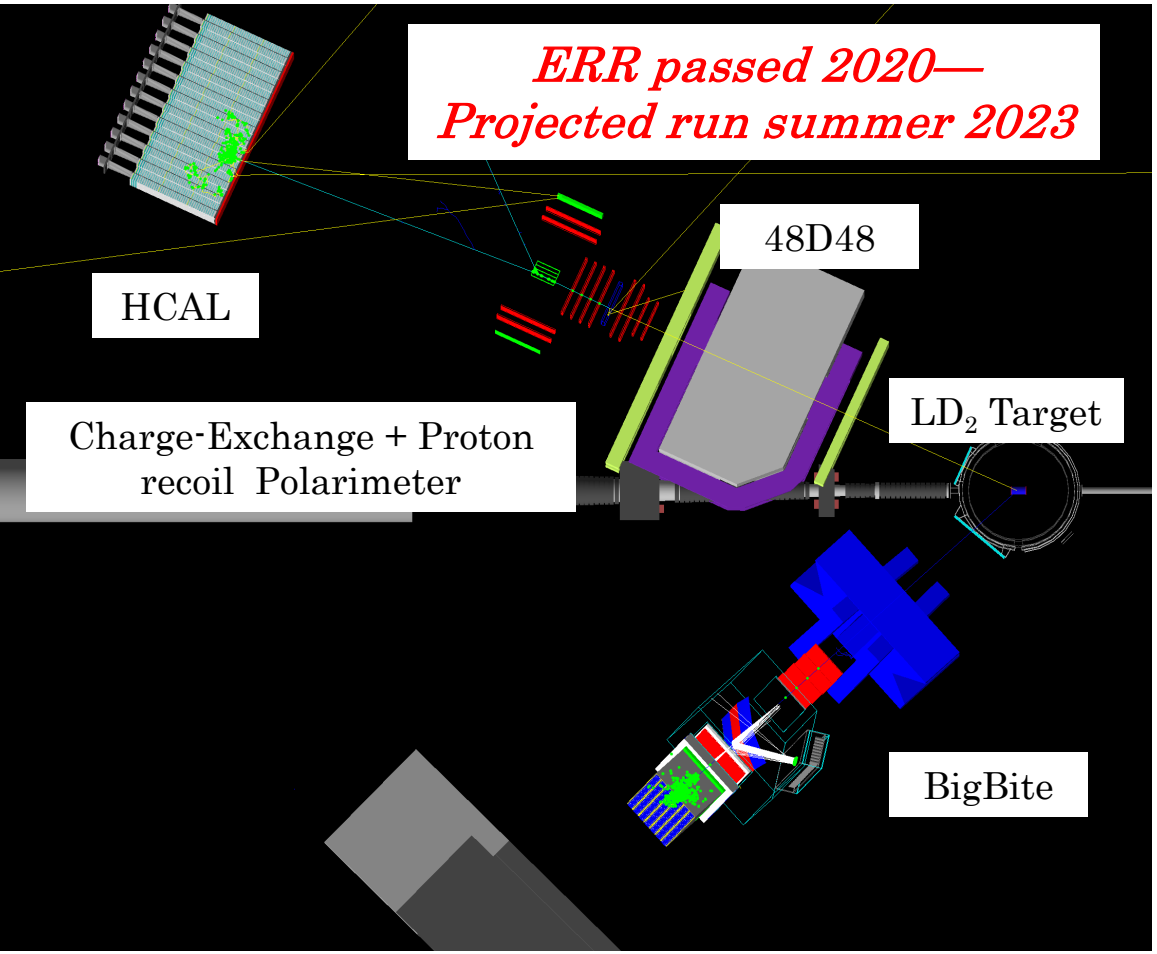

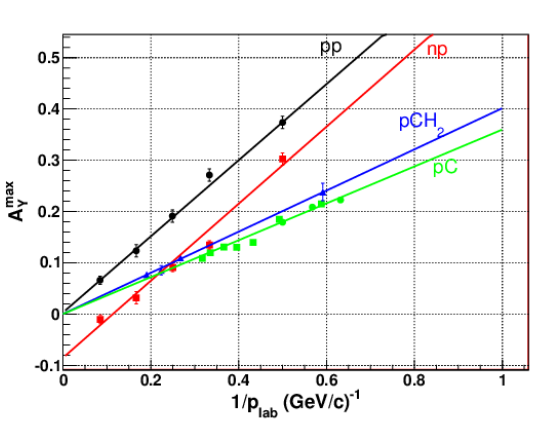

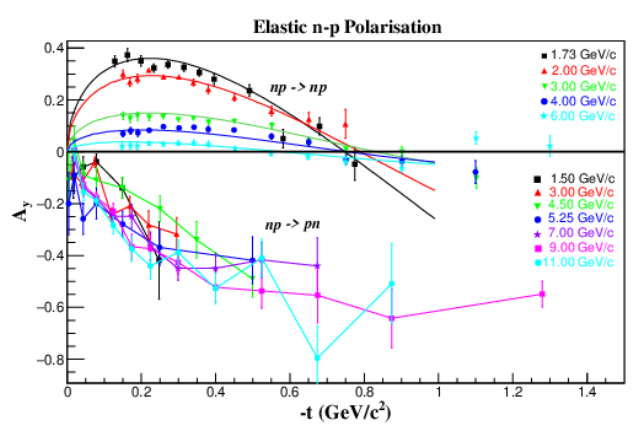

Analyzing powers for np, pp, pA scattering vs. initial momentum (left) and vs. transferred momentum (right)

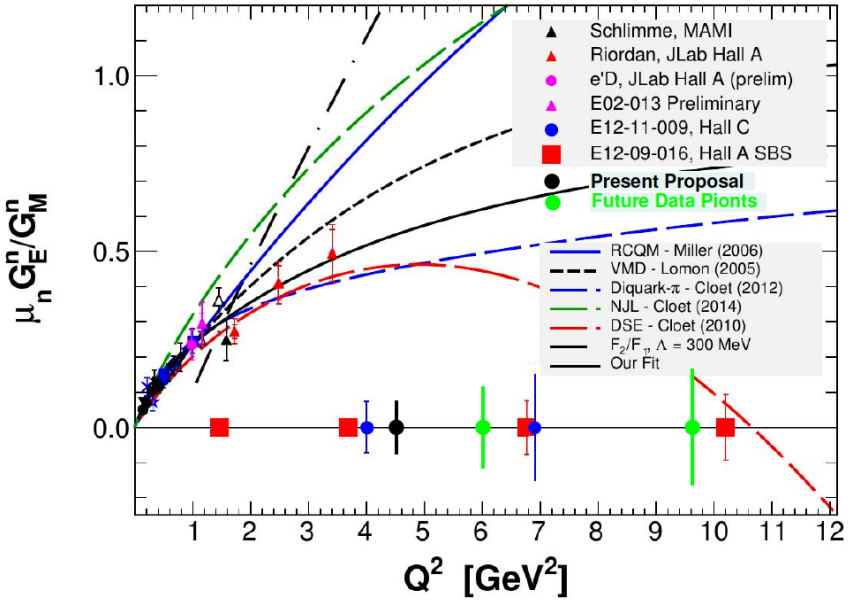

- E12-17-004 layout (above) and projected results (right):
  - First use of charge-exchange polarimetry in a FF experiment
- E12-20-008 approved as add-on to measure K_{LL} for $\gamma n \to \pi^- p$